Ⓓ LEVEL Ⅲ

NW

Special Technical Report 5   *December 1975*

ORBITAL, ATTITUDE, AND DEPLOYMENT CONSIDERATIONS FOR A PASSIVE SPACE ARRAY

By GERRY B. ANDEEN

D D C
RECEIVED
JAN 18 1979
B

Ⓢ **STANFORD RESEARCH INSTITUTE**
Menlo Park, California 94025 · U.S.A.

78 12 18 06
78 12 18 063

STANFORD RESEARCH INSTITUTE
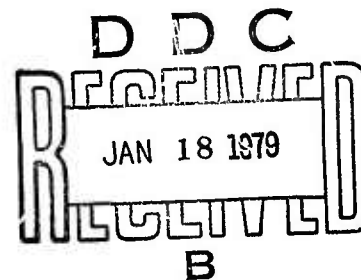Menlo Park, California 94025 · U.S.A.

Special Technical Report 5

December 1975

ORBITAL, ATTITUDE, AND DEPLOYMENT CONSIDERATIONS FOR A PASSIVE SPACE ARRAY

D D C
RECEIVED
JAN 18 1979
B

By: GERRY B. ANDEEN

Approved by:

DAVID A. JOHNSON, *Director*
Radio Physics Laboratory

RAY L. LEADABRAND, *Executive Director*
Electronics and Radio Sciences Division
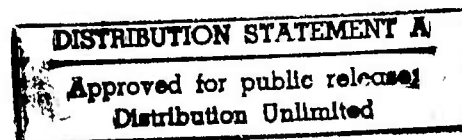
Copy No. ....39.

78 12 18 063

REPORT DOCUMENTATION PAGE		READ INSTRUCTIONS BEFORE COMPLETING FORM
1. REPORT NUMBER	2. GOVT ACCESSION NO.	3. RECIPIENT'S CATALOG NUMBER
4. TITLE (and Subtitle) ORBITAL, ATTITUDE, AND DEPLOYMENT CONSIDERATIONS FOR A PASSIVE SPACE ARRAY		5. TYPE OF REPORT & PERIOD COVERED Special Technical Report 5, covering the period 1 April 1975 to 30 November 1975
		6. PERFORMING ORG. REPORT NUMBER SRI Project 3323
7. AUTHOR(s) Gerry B. Andeen, with contributions from Clarence M. Ablow, Michael S. Frankel, Raymond A. Nelson, Samuel Schechter, and Arthur R. Tobey		8. CONTRACT OR GRANT NUMBER(s) Contract DCA100-74-C-0035
9. PERFORMING ORGANIZATION NAME AND ADDRESS Stanford Research Institute Menlo Park, California 94025		10. PROGRAM ELEMENT, PROJECT, TASK AREA & WORK UNIT NUMBERS ARPA Order No. 2645
11. CONTROLLING OFFICE NAME AND ADDRESS Defense Communications Agency Washington, D.C. 20305		12. REPORT DATE December 1975
		13. NO. OF PAGES 186
14. MONITORING AGENCY NAME & ADDRESS (if diff. from Controlling Office)		15. SECURITY CLASS. (of this report) UNCLASSIFIED
		15a. DECLASSIFICATION/DOWNGRADING SCHEDULE N/A

16. DISTRIBUTION STATEMENT (of this report)

Approved for public release;
distribution unlimited.

17. DISTRIBUTION STATEMENT (of the abstract entered In Block 20, if different from report)

19. KEY WORDS (Continue on reverse side if necessary and identify by block number)

Passive space array	Attitude dynamics
Geostationary satellite	Cable dynamics
Gravity-gradient stabilization	Libration damping
Orbital dynamics	Deployment

20. ABSTRACT (Continue on reverse side if necessary and identify by block number)

SRI is presently in the second year of a project to demonstrate the feasibility of long-distance, jam-resistant satellite communication by means of a completely passive array of scattering elements that is attitude-stabilized by the earth's gravity gradient. It is planned to launch a prototype of such a satellite into synchronous orbit in the fall of 1977. We here discuss the orbital, attitude, and deployment considerations for this array

(Abstract continued)

DD FORM 1473
1 JAN 73

EDITION OF 1 NOV 65 IS OBSOLETE

19. KEY WORDS (Continued)

(con +)

was developed

20 ABSTRACT (Continued)

Our work has resulted in a preliminary design for a passive space array that meets electromagnetic, orbital, attitude, deployment, and manufacturability requirements. The central portion of the prototype consists of 10,000 spherical aluminum scattering elements that are uniformly spaced along a straight vertical line to form an array that is 150 meters long. The spheres are one centimeter in diameter and are resonant over the frequency range 10 ± 0.5 GHz. They are supported by 75 segments of stiff wire 1 mm (40 mils) in diameter. These segments are connected by joints whose free motion is limited to 3°. We found that the stiff sections were needed to absorb transverse kinetic energy occurring during deployment.

To provide needed damping of librational motions, each end of the array will be extended by a coil of the same construction as the main array, but prestressed to assume a pigtail shape when released in space. Each coil will have a radius of 5 meters and will carry 2000 spheres. These coils provide damping by converting librational energy into flexural motion, which in turn is subject to viscous forces in the joints. A damping time constant of less than two months has been calculated.

The mechanical behavior of an array with libration-damping devices has been investigated by analytical and numerical techniques. Perturbing effects such as solar radiation pressure and thermal strain have been considered.

We also simulated the array behavior, using two different computer programs. One of them—the Flexible Spacecraft Dynamics Program—is a general code that has been used with considerable success in modeling other gravity-gradient satellites, and that we have modified to include libration damping using tip configurations. In addition, we have written a program specific to our tasks. The two programs work by entirely different mathematical procedures and give different insights into the array behavior. The results are mutually consistent, and agree with analytical results. Simulation has made it possible to consider a great many variables concurrently—a procedure not possible in a tractable mathematical analysis.

We have designed a deployment mechanism that will constrain the array within a circularly cylindrical storage locked during launch and, at the appropriate time, will eject the array along the local vertical. Capture by gravity gradient is expected even if the array initially tumbles after deployment.

DD FORM 1 JAN 73 **1473** (BACK)

EDITION OF 1 NOV 65 IS OBSOLETE

CONTENTS

v

ILLUSTRATIONS

TABLES

I   INTRODUCTION

This report examines the orbital and attitude mechanics of a passive space array and describes a mechanism for its deployment. Such an array, first proposed by Joseph C. Yater in the mid-60s, consists of an ordered set of scattering elements. Incident electromagnetic radiation scattered from these elements is reinforced at certain angles to provide a powerful return signal (see Figure 1).

SRI is conducting a program to demonstrate the feasibility of this array concept. The concept will be implemented by attachment of the scattering elements to a semiflexible cable. The cable is to be placed in a geostationary orbit, where it will be maintained in a vertical attitude by the gravity gradient.

This program to develop and demonstrate the passive-space-array concept is in its second year. Work done during the first year, covered in Summary Report--Phase I, dated April 1975, concentrated on feasibility. Several factors affecting orbit and array stability were considered. These included collapse of the array due to solar pressure, distortion of the orbit due to solar pressure, and libration pumping due to orbital eccentricity. Elementary models were used to study these effects. In addition, extensive use was made of the Flexible Spacecraft Dynamics Program (FSDP), a program designed to deal with gravity-gradient satellites having flexible appendages.

Various configurations involving supported arrays were considered and rejected because of difficulties in meeting straightness requirements, especially for arrays on the order of a kilometer in length that may be useful in communications systems. An array consisting of relatively

1
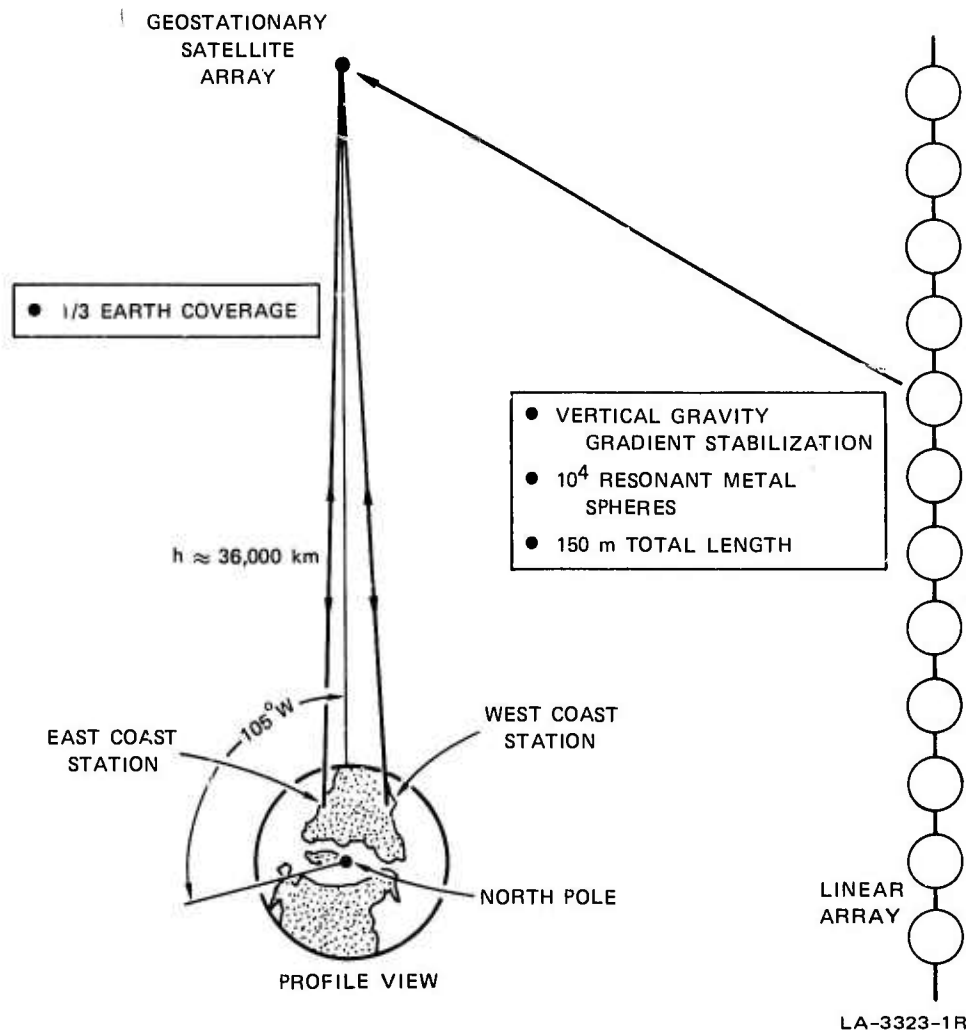
FIGURE 1   CONFIGURATION OF FEASIBILITY DEMONSTRATION

massive balls supported on a thin cable evolved as a means of satisfying
diverse requirements. This configuration is a departure from the light
ribbon that was originally considered, and that was found to collapse
and to be blown out of orbit due to solar pressure. The substantially
higher mass-to-area ratio of the beads than that of the ribbon provides
the needed margin for feasibility. The conclusions drawn from the first
year of work are that it is feasible to put this array into synchronous
orbit, and that it will remain stable there.

2

During the first year we found that the lowest normal vibration mode of the cable, the libration mode, is straight (unlike that of a cable hanging in a gravity environment). Therefore, a flexible cable could become straight and thereafter librate as a rigid body without internal relative motion. Such a libration would persist unless some mechanism for damping was provided. Two mechanisms for damping libration were identified and studied. Both involved adding structures to the ends of the array in order to introduce flexure into the lowest libration mode. Flexure of the cable that supports the array will dissipate energy through internal friction, ultimately leaving the structure in the desired stable gravity-gradient equilibrium position.

The FSDP simulation was unable to deal with the complexities of the proposed tip arrangements. Hence, evaluation of the two libration-damping methods remained as a part of the task being reported here.

The first year of work also identified several deployment mechanisms. This work was important because the array configuration is intimately related to the deployment scheme selected.

The work being reported herein is a continuation and elaboration of the work discussed in our first summary report. Most of the subsequent effort has been directed toward the design of a test array 150 m long, consisting of 10,000 scattering elements. This array length was selected for a feasibility demonstration purpose. A much longer array (1500 meters), with 100,000 scattering elements, is considered more appropriate for later systems application. The theories that have been developed are applicable to arrays of any length, but most of the calculations presented are concerned with the shorter test array.

3

II APPROACH

A. General

We have investigated a large number of combinations of array configurations and deployment mechanisms. The approach has been to examine each candidate combination to evaluate its feasibility in terms of the various constraints that are imposed by the deployment process and the subsequent requirements of capture by gravity gradient, attitude stability, and orbital stability. We found that many combinations meet several of these requirements. However, the configuration described in the following sections seems best to meet the overall system requirements.

Many of the requirements are actually or seemingly in conflict. For example, a very light array is attractive from the standpoint of launch requirements. In contrast, a heavy array having a large ratio of mass to surface area is desirable to minimize the effects of solar radiation pressure. A very flexible array is desirable in the interest of obtaining straightness under the weak forces of gravity gradient. On the other hand, an array having considerable stiffness is desirable to minimize the risk of tangling during deployment.

To avoid distortion by solar radiation pressure, it is desirable to make the array homogeneous--i.e., to make each section exactly like every other section. Also, the deployment process is greatly simplified if the array is essentially homogeneous. In contrast, libration damping requires that the ends of the array have a configuration that is in some way significantly different from that of the rest of the array.

5

The deployment process would be greatly simplified if the launch vehicle were perfectly stationary in orbital space for a time fully adequate for the deployment process. Actually, the transtage of the TITAN III-C maintains approximate stability by a cycling process that produces accelerations and motions that are inconveniently large for the planned deployment process. The time available for deployment is limited by this cycling process and by the small amount of fuel and battery energy that will be available after both prime payloads are discharged.

The array must remain straight to within a few centimeters and stationary in space to properly serve its communication function. However, prior to deployment it must be stored in some reasonably compact container. This pair of requirements leads to the choice of a stiff but highly elastic wire as the supporting element. The apparent conflict between flexibility and stiffness is resolved by the use of limited-motion joints that are quite free for small motions but that prevent larger motions.

We have investigated the candidate array structures in two supplementary ways. First we have treated the individual effects that influence the orbital and attitude dynamics of each configuration. This approach provides for tractable analysis and makes it possible to check special cases. Secondly, we have used an overall simulation modeling all of the essential effects on orbital and attitude dynamics simultaneously in specific cases.

B. Analysis

By limiting our attention to small-amplitude cable motions we were able to use linearized theoretical models so that each effect on orbital and attitude dynamics could be investigated individually. By this method we have determined the normal modes of vibration for the cable.

The importance of these modes is that, once identified, they can be introduced as initial conditions into the more complex simulation models in order to permit investigation of the damping of the lower-order modes. This procedure makes it unnecessary to wait for higher-order modes to damp out. The higher modes would be introduced into the simulation only if an arbitrary cable shape were used as an initial condition.

C. Simulation

Two types of simulations were used--the Flexible Spacecraft Dynamics Program at Computer Sciences Corporation and an SRI-developed, finite-segment model. The Flexible Spacecraft Dynamics Program uses model analysis. For specified initial mode shapes this program calculates the time behavior of the amplitudes of these modes. A summation of the individual modes gives the shape of the cable. At SRI we chose to pursue a finite-element approach--that is, the cable was considered to be composed of a finite number of rigid links. In the limit of a large number of modes and a large number of links, the two techniques become identical. At the other extreme, where only a few modes and a few elements are used, the two techniques yield different results. The Flexible Spacecraft Dynamics Program uses three modes on each of two limbs, or six independent variables, while the SRI program has modeled arrays of up to ten segments.[*]

D. Array Configurations Modeled

We set out to examine the orbital and attitude dynamics of four array configurations.

   (1) A free cable

   (2) A cable with tip masses

---

[*] A much larger number of links can be modeled in the SRI program with increased computer run time.

(3)   A cable with tip masses attached by means of hys-
teretic springs ("bouncing tip mass" arrangement)

(4)   A cable with tip masses having large moments of
inertia.

Cases 3 and 4 are of primary interest because they correspond to
systems in which the lowest normal mode includes curvature, which may be
used to damp libration. Cases 1 and 2 are more tractable problems that
were used to develop our intuition and to provide a basis on which to
formulate the more complex problems.

The spring-mass arrangement shown in Figure 2 corresponds to the
third configuration. It is patterned after the Applied Physics Laboratory
TRAAC satellites, also illustrated in the figure. Libration causes
extension and contraction of the spring. Coriolis forces associated with
outward and inward motions of the tip mass cause that mass to lag or lead
the natural libration motion of the array. Libration energy is dissipated
in flexing both the cable and the spring. The energy required to extend
the spring is greater than that recovered when the extension is reduced.
This hysteresis of the spring mechanism, augmented by coatings on the
spring, was the energy dissipation mechanism used in the TRAAC
satellites.

We have determined that the affect of the spring-mass damper on the
satellite motion is considerably different for in-plane than for out-of-
plane motions. Specifically, for small-amplitude libration, the damping
effect disappears in the out-of-plane direction. Figure 3 demonstrates
this result. For the in-plane case, the libration rate is added to
the orbital rate, n. The increment in $\dot{\theta}$ about the orbital rate makes
a significant difference in the centrifugal acceleration of the mass,
causing the spring to extend.
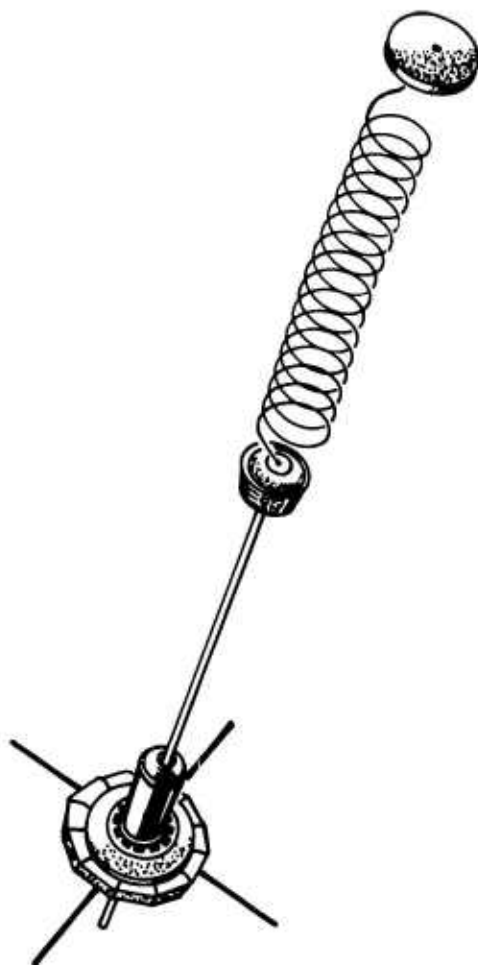
(a) TRAAC SATELLITE   (b) THE SPACE ARRAY

LA-3323-58

FIGURE 2   BOUNCING-TIP-MASS CONCEPT
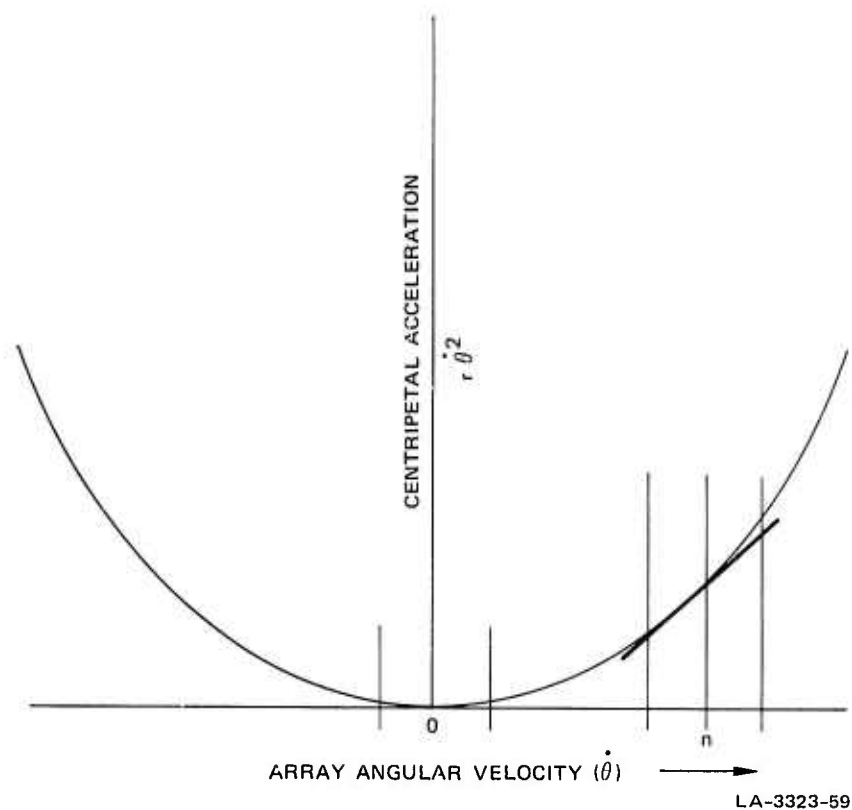
FIGURE 3   FORCE ON SPRING DUE TO LIBRATION

In the out-of-plane direction, the rate of the libration is added
to zero. As shown, a small change in $\dot{\theta}$ from zero gives no significant
change in the centrifugal acceleration and therefore no spring extension
(and damping). Our concern with this phenomenon is that out-of-plane
damping will decrease as the libration amplitude decreases. The approach
to alleviating this difficulty is to transfer energy from the out-of-
plane motion to the in-plane motion. This can be accomplished by tuning
one of the in-plane modes to a frequency at which this mode can be
excited by forces at twice the natural frequency of the out-of-plane
libration. This tuning increases damping for small libration, out-of-plane
amplitudes.

10

The natural frequency required of the spring-mass arrangement corresponds to a period an order of magnitude greater than the one-hour period of the TRAAC satellite. To achieve this frequency, the spring must be very "soft"--i.e., 8.5×10^{-8} N/m for a tip mass of one kilogram. Our concern is whether such a spring can be built without excessive length or fragility, both of which contribute to softness. Additional concerns are whether the exact tuning frequency could actually be established and whether the mechanism could be successfully deployed.

The tip-inertia concept is similar to that of the bouncing tip mass in that the basic idea is to make the natural behavior of the tip mass different from that of the rest of the array. A tip mass with large inertia would tend to travel back and forth without rotating. Attachment of this tip at a position other than the center of gravity of the array would give rise to a set of rocking frequencies that interact with the modal frequencies of the cable itself.

We envision the tip body as an extension of the cable. In the gravity environment on earth the tip would be indistinguishable from the rest of the array, but in space the wire would assume a preset curvature. If the natural frequency of this wire were well above the libration frequencies of concern, the tip would appear as a rigid body. Figure 4 illustrates the concept.

The viscous magnetic damper has also been investigated but appears to offer no advantages. The magnetic field gives a reference against which damping of relative motion can take place. A magnet tends to align with the field and is viscously coupled to the housing, either by fluid or eddy current. This device is space-proven and is an accepted means of libration-damping for conventional gravity-gradient satellites at synchronous altitude. However, it is not clear how the damper could be attached to the space array so as to take advantage of the magnetic

11
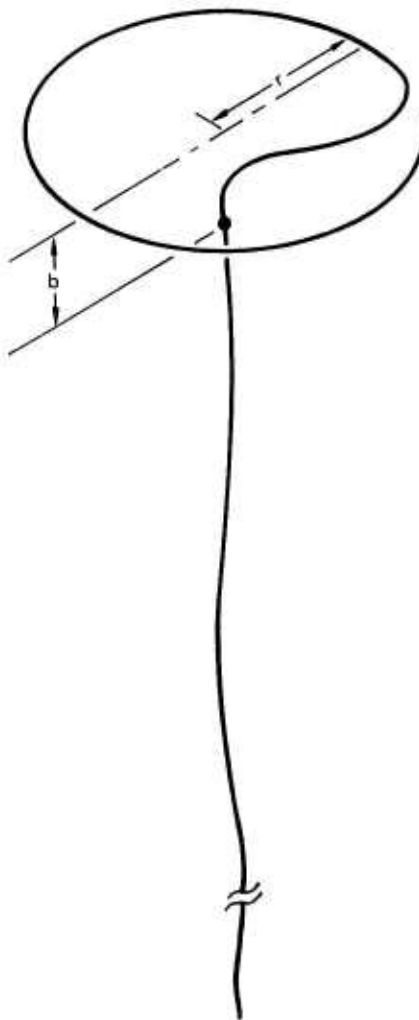
LA-3323-60

FIGURE 4   TIP-INERTIA CONCEPT

field. Furthermore, additional discouraging factors are: (1) The smallest available damper is about the size of a fist—i.e., much larger than the array beads; (2) the magnetic field at synchronous altitude is distorted by the solar wind so that, depending on the orbital relationships and the intensity of solar activity, the magnetic field may be perturbed by many degrees and thereby give rise to an unwanted periodic disturbance;

12

(3) in the steady state, the viscous magnetic damper applies a constant torque to the array which increases the problem of designing a flexible structure. Because this approach has no demonstrable advantage over the tip-inertia concept, and has a host of discouraging features, it was not pursued further.

E.   Deployment Method

The approach to finding a deployment method has been to compare various proposed schemes against the attitude requirements, keeping in mind the most likely configuration of the array. Probably the most severe criteria are that the deployment mechanism be simple, that it be able to fit aboard the launch vehicle as a secondary package, and that it be capable of using the attitude-control system of the transtage. These criteria have strongly affected the design of the array as well as the deployment method.

F.   Other Considerations

A variety of secondary factors have been evaluated in the course of the work, usually to ensure that a particular effect is not important. Our approach has been that of a design engineer; we first identify the dominant considerations, and then check and continue to check on the other concerns that were at first ignored. There is no way to ensure that every relevant factor has been considered short of the actual experiment. However, we have made a diligent effort to avoid overlooking any important detail and have supplemented our own efforts by exposing our concepts to a variety of people, both in and out of the satellite business, and have followed up the suggestions given.

III   ANALYSIS RESULTS

A.   General

The equations of motion of the array have been formulated with
respect to an orbiting reference system.   The local vertical has been
chosen as one of the coordinates, and the orthogonals for the in-orbit
and out-of-orbit planes are the other two coordinates.   We have assumed
a linearized gravity gradient and small-amplitude deflections of the
array.   Equations for the first four array configurations mentioned
above, as well as analytical or numerical solutions, are given in
Appendices A and B.   Our results are summarized in this section.   The
reader should note that the small-amplitude assumptions apply only to
the analysis.   The computer simulations, discussed in Section IV, are
not so restricted.

B.   Free Cable

As reported in Summary Report--Phase I, the shapes of the normal
modes of the free array are Legendre polynomials in both the in-plane
and out-of-plane directions.   The first several of these polynomial
shape functions (eigenfunctions) of the free array are shown in
Figure 5.   Also shown are the harmonic frequencies (eigenvalues) for
both the in-plane and out-of-plane modes.   As noted earlier, the first
mode is straight--i.e., its motion is similar to the librational motion
of a rigid body.   As noted in Appendix A, n is the orbital frequency,
which, for a geostationary satellite, is one cycle in 24 hours.

15

| MODE | FREQUENCY | |
	in plane	out of plane
1	1.73 n	2.0 n
2	3.00 n	3.16 n
3	4.24 n	4.36 n
4	5.48 n	5.57 n
5	6.71 n	6.78 n

$$n\sqrt{\frac{3}{2}\,i(i+1)} \qquad n\sqrt{1+\frac{3}{2}\,i(i+1)}$$

n — ORBITAL RATE
i — MODE NUMBER
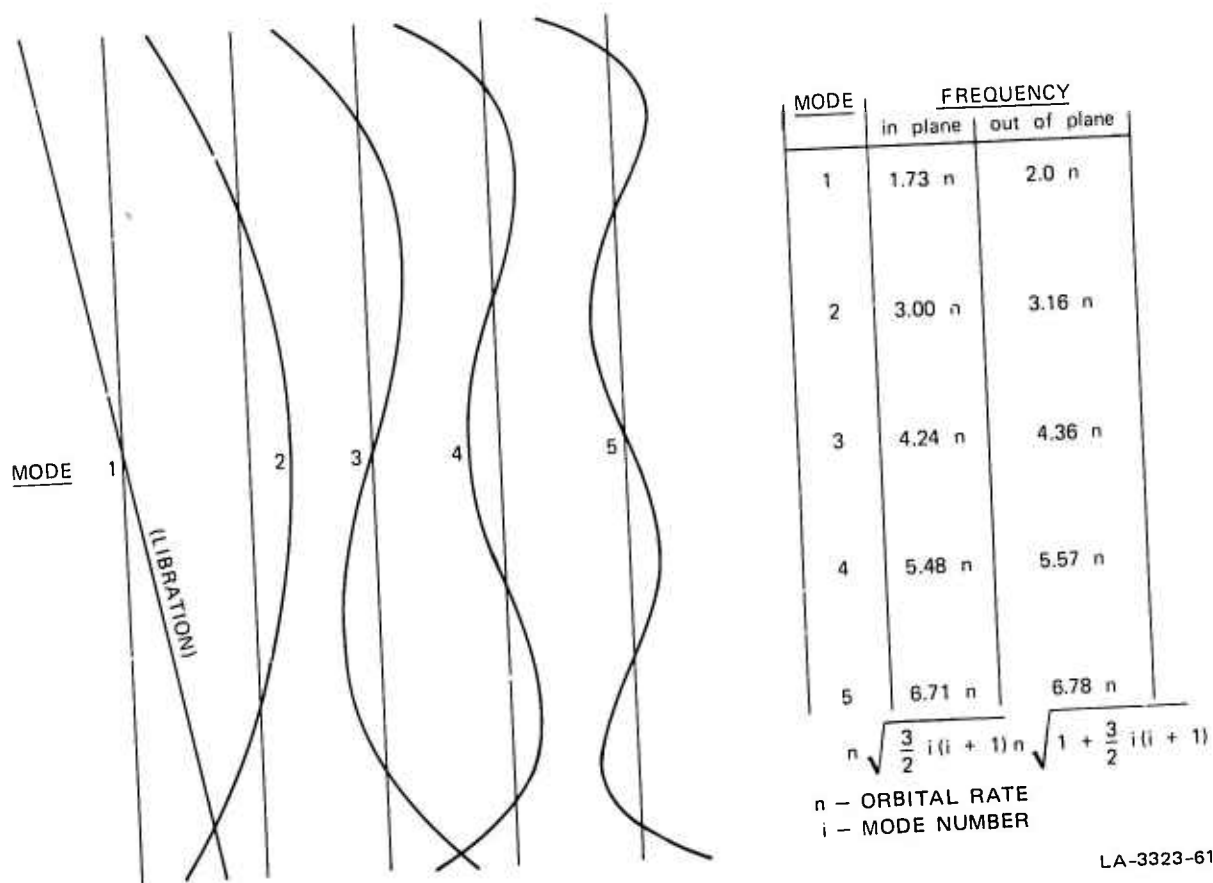
LA-3323-61

FIGURE 5   GRAVITY-GRADIENT NORMAL MODES FOR FREE CABLE

C.   Cable with Tip Masses

The shapes of the normal modes of a cable with tip masses tend toward sinusoids with increasing tip mass. For small tip masses the primary difference is that the cable becomes straight at the tip. Except for the straight modes, the modal frequencies (eigenvalues) increase with increasing tip mass. The effect of the tip masses is an increase of tension in the array and a tendency toward string-type vibrations. Figures 6 and 7 show how these frequencies change with

16

ω = FREQUENCY
n = ORBITAL RATE
m = TIP MASS
σ = CABLE LINEAR DENSITY
l. = CABLE LENGTH
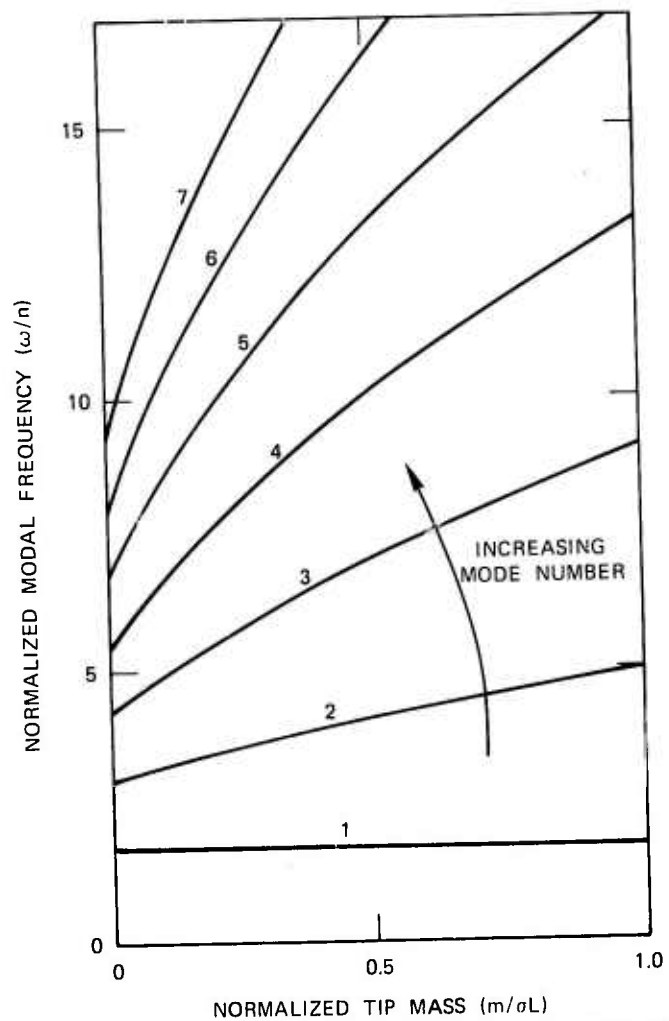
LA-3323-62

FIGURE 6   MODAL FREQUENCIES OF CABLE WITH TIP MASSES (in-plane)
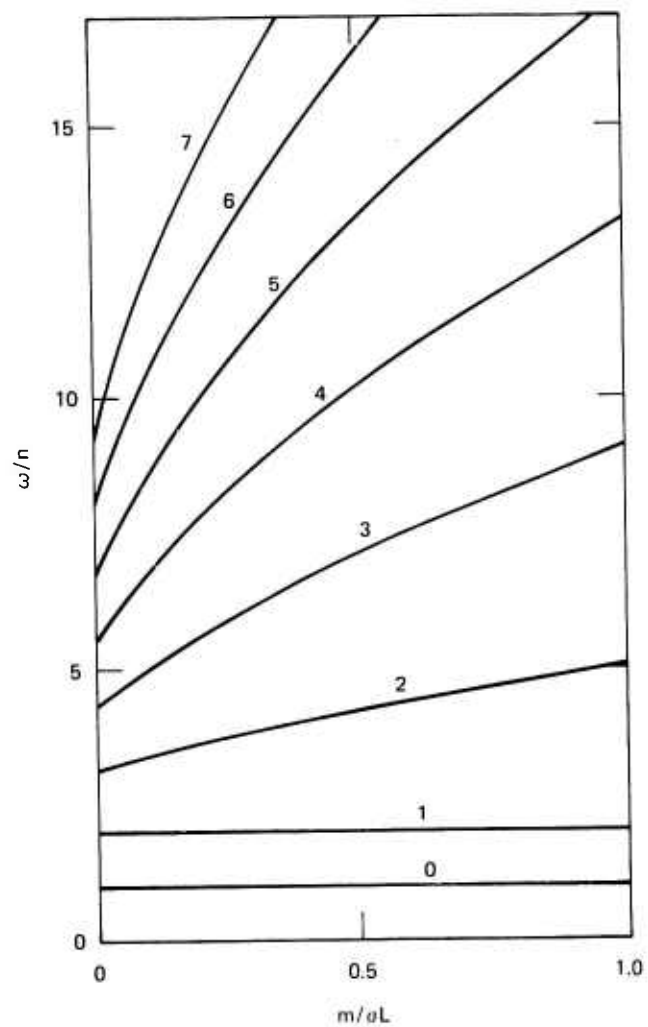
LA-3323-63

FIGURE 7   MODAL FREQUENCIES OF CABLE WITH
TIP MASSES (out-of-plane)

18

increasing tip mass. The ordinates give the frequency compared with the orbital frequency, and the abscissas show the value of the tip mass, m, normalized to the total mass of the active portion of the array.

Several important conclusions may be drawn from these figures. First, for all the modes above the first, the frequency increases as m increases, and the difference between frequencies for the in-plane and out-of-plane modes becomes smaller. Second, there are three modes that do not change frequency as the tip mass increases. Two of these are out-of-plane modes and one is an in-plane mode. The in-plane mode is the familiar libration mode. Once again, attention is called to the fact that this libration mode remains straight and has a fixed frequency for any array displacement regardless of the mass distribution or the array length. In the out-of-plane case, the higher of the two modes that do not change in frequency is the out-of-plane libration mode. The lowest frequency mode, whose frequency is exactly that of the orbital rate, actually corresponds to an orbit with a slight inclination from the reference orbit. The two orbits then move with respect to one another with a frequency of one cycle per orbit.

In order to prvent distortion of the array shape by solar pressure, the tip masses must have a projected area-to-mass ratio that is the same as that of the cable.

D. Bouncing Tip Mass

The small effect of the bouncing tip masses on out-of-plane libration can be increased if one of the in-plane modes is tuned to a frequency four times the orbital rate. This "parametric" tuning causes the in-plane mode to be excited by the out-of-plane libration. Figure 8 shows how a spring-and-tip-mass combination could be selected to accomplish this. We note that for each value of the tip mass there are two in-plane modes that can be tuned to the desired frequency--one odd and the other even.

19
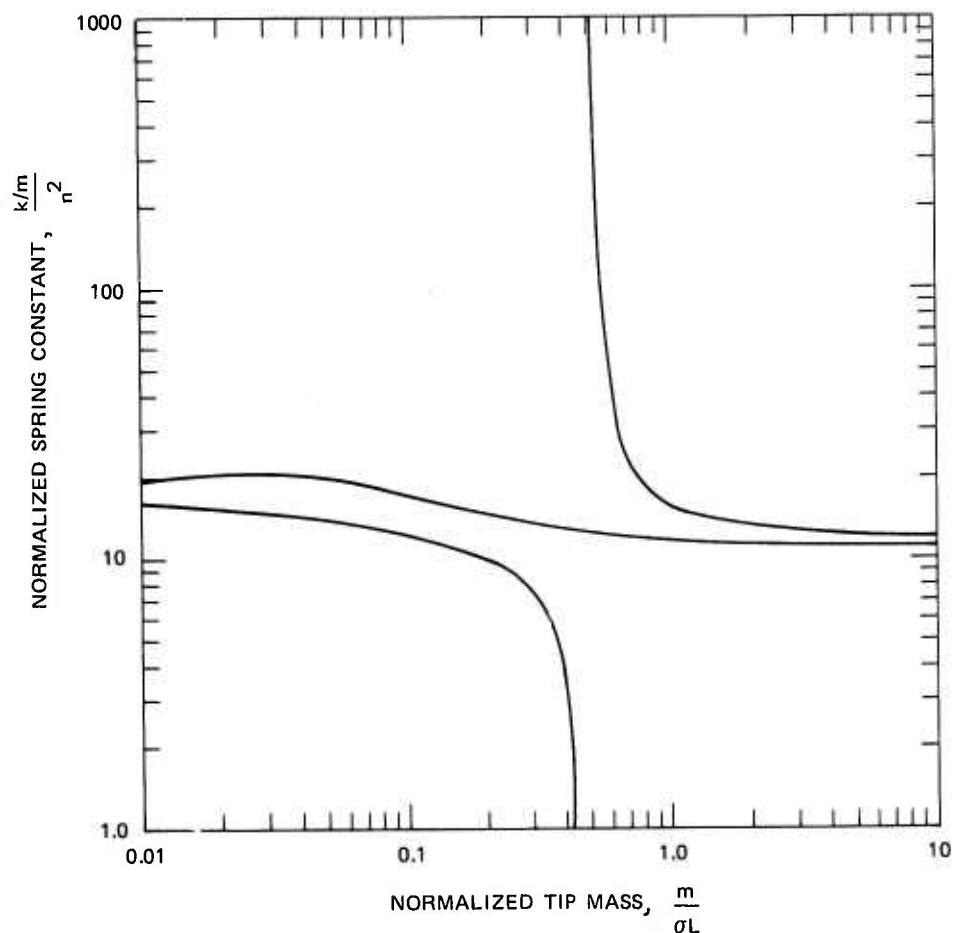
FIGURE 8   MASS AND SPRING VALUES TO PRODUCE IN-PLANE MODE WITH A
FREQUENCY OF 4 n

We have examined the bouncing-tip-mass configuration for the special case in which one of the in-plane normal modes had a natural frequency of four times the orbital rate. For this tuned system, the spring extension is 90° out of phase with the angular deflection of the cable. That is, when the cable is at its maximum deflection and stationary, the tip mass is at its equilibrium position and moving with maximum speed.

20

Even when the spring-mass is selected to give an in-plane natural frequency of four times orbital rate, the out-of-plane damping goes to zero as the libration angle goes to zero. This is not a serious concern, however, because damping down to a few degrees of libration is adequate. The decision to use the bouncing-tip-mass depends on several practical questions of implementation; in theory, the method can be made to work.

The practical questions are (1) whether a spring-mass can be built with a natural frequency an order of magnitude lower than that of the TRAAC satellites (which took considerable development); (2) whether the frequency of that system can be controlled to sufficient accuracy to give the tuning required to augment the out-of-plane damping; and (3) whether the system could be deployed. Because of these practical concerns, and because of the early positive results on the tip-inertia scheme discussed in the following section, effort was focused on the latter method. Were the bouncing tip mass to be pursued further, the next analytic step would be to determine the sensitivity of the out-of-plane damping to tuning.

E.   Large Tip Inertia

Solutions have also been achieved for the motions of the array with the large tip moments of inertia shown in Figure 4. The solutions are very similar, except for minor perturbations, to those of the tip-mass cases. These perturbations are of the kind anticipated--that is, there is distortion of the mode shape from those associated with the cable and tip masses. This distortion is the greatest at the tips of the cable and can either be toward the local vertical or away from it, depending on the parameters chosen for the tip body. This interdependence of mode-shape distortion and tip-body parameters is shown in Figure 9 for the lowest mode. When the distance from the center of mass to the point of attachment of the tip body is small, resulting in an

21
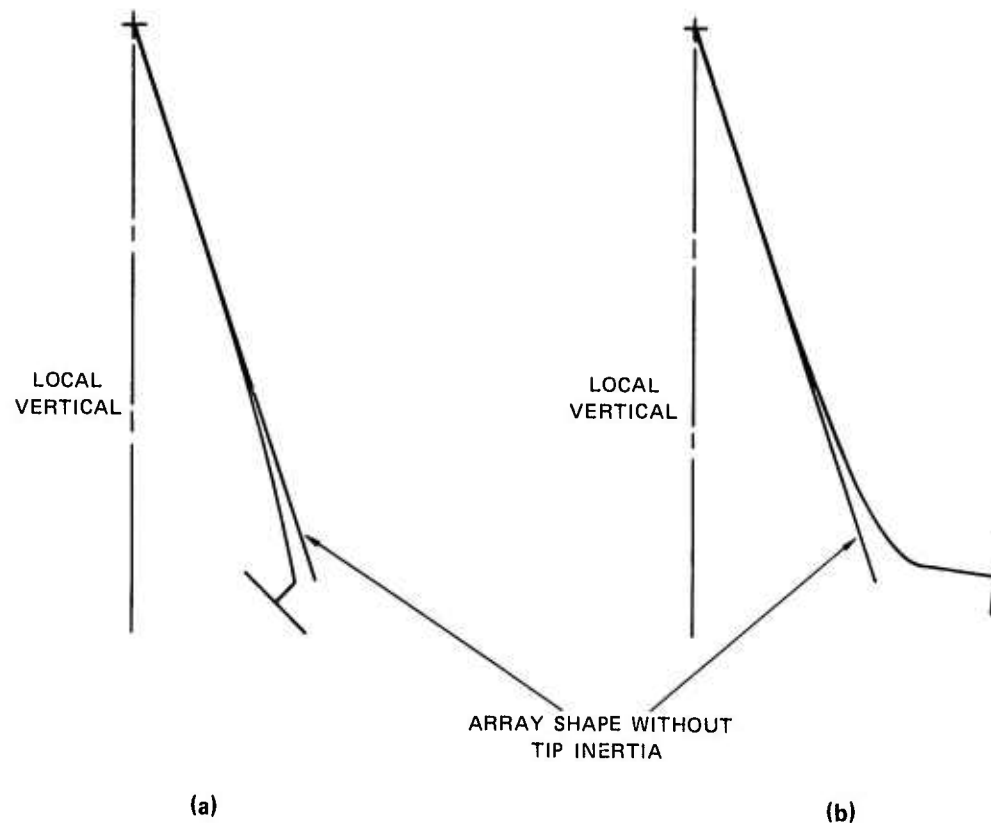
FIGURE 9   FIRST MODE SHAPE WITH TIP INERTIA

oscillating frequency of the tip body less than the libration frequency, the array departs from straightness toward the local vertical as shown in Figure 9(a). In this case, the angle made by the tip body is out of phase with the libration angle.

When the distance from the attachment point to the center of mass of the tip body is large, the oscillation frequency of the tip body is greater than the libration frequency. Consequently, the array libration mode departs from straightness away from the local vertical as shown in Figure 9(b). In this case the angle of the tip body is in phase

22

with the libration angle. The greatest amount of damping can be achieved when the length of the tip body is chosen to achieve resonance--that is, when the tip body rocks back and forth at the same frequency as that of the array libration.

It should be noted that there exists a minimum value for the distance b (see Figure 4) between the point of attachment and the center of gravity of the tip body for which the tip body will be stable. The tip body tends to line up in the gravity gradient with its longest axis in the local vertical. In order to put the axis of the largest moment of inertia in the direction of the local vertical, it is necessary to apply a restoring torque greater than any gravity-gradient destabilizing torque. This implies that the distance from the center of gravity of the tip body to the point of attachment to the array is great enough so that the moment arm generated an angular deflection of the attachment joint times the body force gives a sufficient torque to counter the natural tendency of the loop to be upset.

It is practically impossible to make a tip body that is radially symmetric, and this fact was included in the analytic considerations. With such a lack of symmetry, there will be a tendency for the longer axis to lie in the orbital plane.

F.   Summary

Analytical and numerical results have been generated to examine the behavior of the array with the candidate libration-damping schemes. The validity of the analyses is supported by internal consistency and by conformity to known results. For example,

(1)   The numerical solutions for the frequencies of the cable with tip masses degenerate to give the frequencies for the free cable when the magnitude of the tip masses goes to zero.

(2) The tip mass, called for when an infinitely stiff spring is required to achieve tuning in the bouncing-tip-mass case, corresponds to the mass of a simple tip mass.

(3) The tip-inertia solutions are similar to the tip-mass solutions.

(4) Numerical solutions for the tip inertia agree with approximate analytic solutions.

(5) The frequency of straight modes is independent of linear density.

IV COMPUTER SIMULATIONS

A.   General

The Flexible Spacecraft Dynamics (FSD) Program that was used in the first phase of this project has been further modified for use in Phase II. In addition, during the current phase of the project we have written our own program which is described in Appendix C. A side-by-side description of the two programs is presented here in Table 1 to show how they complement each other.

Table 1

COMPARISON OF SIMULATION PROGRAMS

FSD Program	SRI Program
Origin and Location:	Origin and Location:
The Flexible Spacecraft Dynamics Program was written in the 1960s by Mr. Edward Lawler of the AVCO Corporation, Waltham, Mass. The program was resident at the Goddard Spacecraft Center, Greenbelt, Md., in the care of AVCO representatives. In 1974, this group became a part of the Computer Sciences Corporation, Silver Spring, Md., where the program is currently located. The program was developed under Government contract and is government property.	The SRI Program was written by Dr. Arthur R. Tobey under this contract. The program is resident at SRI; the code is a deliverable to the government.

Table 1 (continued)

<table>
<tr><td>

Purpose:

  This program was developed to
deal with the IMP class of satel-
lites. Specifically, the program
is able to model satellites with
a central body and up to a dozen
flexible booms, plus momentum
wheels and magnetic dampers. The
program was used to study and de-
sign the Radio Astronomy Explorer
(RAE) satellites and most recently
it has been used in the planning
studies for the GEOS-C spacecraft.

Code and Machine:

  The FSDP is written in FORTRAN
for IBM equipment.

Method of Analysis:

  The FSDP uses modal analysis.
The amplitudes of assumed modes,
taken to be the generalized co-
ordinates, are computed by the
program. Up to 3 modes in each
of two directions can be con-
sidered for each of the booms.
Major revision of the program
would be required to accommodate
additional variables.

Orbit:

  This program calculates orbital
position and is capable of using
simple or sophisticated gravita-
tional models.

</td><td>

Purpose:

  This program was written specifi-
cally to study the gravity-
gradient dynamics of the space
array.

Code and Machine:

  The SRI program is written in
FORTRAN for CDC equipment.

Method of Analysis:

  The SRI program uses a finite-
element analysis--that is, the
array is considered to be composed
of straight links with joints in
between. No assumption needs to
be made as to plausible mode
shapes. This program has been
written to accommodate up to 10
links of individually specified
lengths in the array. A greater
number of links can be modeled
by increasing memory allocated
to link positions.

Orbit:

  This program assumes an orbit
based on a simple earth gravita-
tional model. Eccentricity can be
included. The effect of solar pres-
sure on the orbit is not calculated,
and the effect of earth oblateness
is not considered.

</td></tr>
</table>

Table 1 (continued)

Damping:	Damping:
The FSDP calculates damping for each mode on the basis of the gradient change of curvature and adjusts the corresponding modal amplitude accordingly.	The SRI program explicitly considers viscosity in the joints. Resistance to motion is provided in proportion to the rate of change of the angle of the joint. Nonlinear viscous properties can also be used. Individual joint behavior can be specified.
Effect of Solar Pressure on Shape:	Effect of Solar Pressure on Shape:
The FSDP considers that the array is a uniform cylindrical cable.	The SRI program considers that the array is made up of spheres and that these spheres can shadow each other.
Coordinate System:	Coordinate System:
The FSDP is written primarily for spacecraft with large central bodies. The coordinate systems chosen to express the satellite attitude and configuration are the Eulerian angle of the central body and the amplitudes of the modes of flexures for the beams. The central angle and the three generalized coordinates allowed for each of two booms gives a description of the cable in one plane in terms of seven variables.	The SRI program is written to give the position and orientation of each link in terms of the coordinate system defined by the local vertical and the in-plane and out-of-plane directions. Ten variables are needed to describe the complete position of the array in one plane.
Other Features:	Other Features:
This program calculates a relative Hamiltonian which is a measure of the energy of the configuration.	This program calculates relative energy so that the amount of damping can be determined.
Other features are also available, such as a fast Fourier analysis to determine the frequency of various satellite motions.	

B.   Simulation Results

   1.   Test Cases

        Both computer programs have been run for a variety of test
cases in order to verify that the programs are working properly.   These
cases included observing that the lowest mode remains straight for the
free cable and for the array with tip masses.   Furthermore, the programs
were used to verify the small-amplitude analytical solutions.   In par-
ticular, we have verified most of the analytically predicted normal
modes for the bouncing tip mass and for the tip-inertia configurations.
When the correct mode shapes are used as inputs for simulations,
oscillations occur at the predicted frequencies.   In addition, the two
programs have been checked against each other; the same input conditions
yield similar results.

   2.   Comprehension Runs

        Several different runs have been made to reinforce our under-
standing of the array attitude dynamics.   A number of those runs are
discussed in the following paragraphs.

        We have studied the effects of varying the distance from the center
of mass to the point of attachment of the tip body with inertia, and
the overall array behavior.   In this study, which used the SRI program,
the array was considered to be composed of two components.   The first
component is a long, rigid member of length equal to that of the active
portion of the array.   A tip mass is attached to one end of the rigid
member.   The second component is a tip body with inertia attached to the
opposite end of the rigid member.   The mass of the "tip inertia" is equal
to the tip mass at the opposite end.   The initial condition chosen was
an in-plane libration angle of 10° with no initial velocity.   We
expected that the results of this simple model would not differ

28

significantly from those of a symmetric array with many links, because the shape of the libration mode is nearly straight. This expectation was verified by running one simulation of an eight-link array with symmetrical tip inertias. The resulting tip-body angles in one orbit were within 5% of those obtained from the simple model. Thus the simple model allows exploration of variables with a minimum of computer time.

Figure 10 shows our results. The ordinate is the angle of the tip body, and the abscissa shows the array's orbital position. One can see that when the length, b, between the center of mass of the tip and the attachment point is large, the tip body tends to librate at frequencies considerably higher than those of the array. As b is shortened,
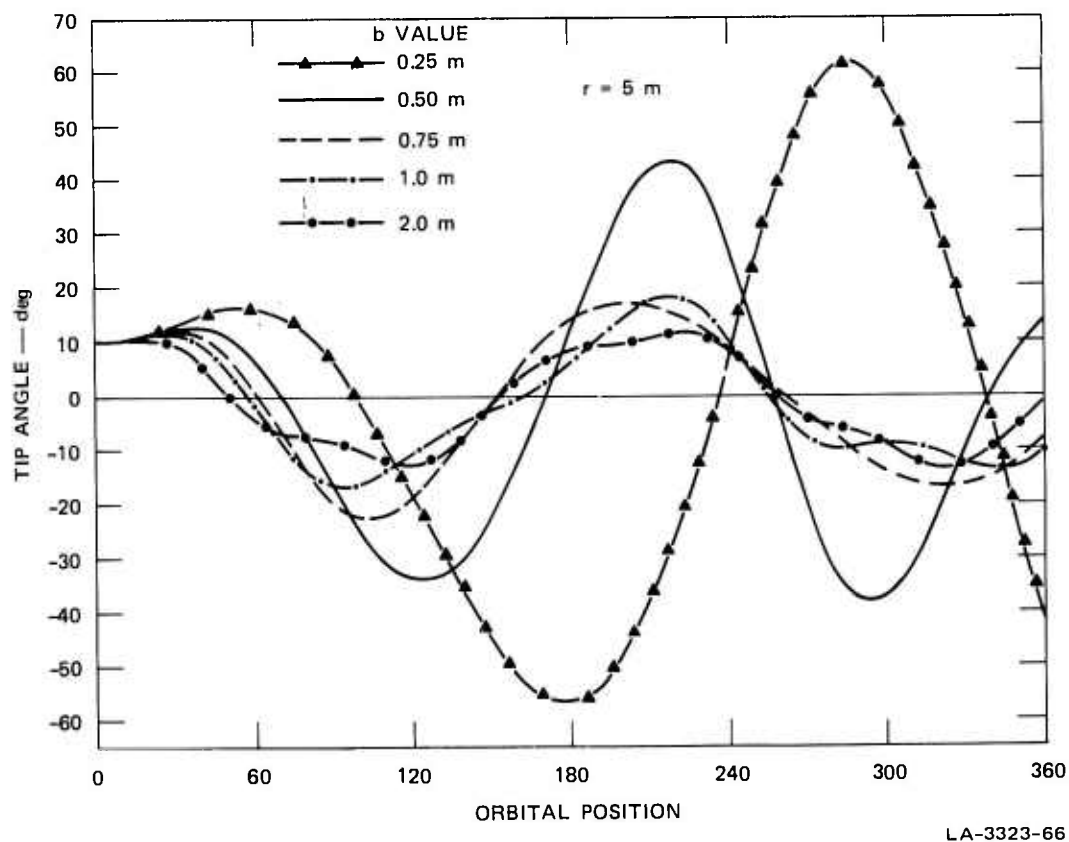
FIGURE 10   SIMULATION RESULTS WITH TIP INERTIA AND NO DAMPING, r = 5 m

29

a resonance condition is passed through and the tip-body motion becomes 180° out of phase with respect to the libration. For the case shown, the value of b to achieve the resonance is one-third of a meter. Where there is no damping, the shape is independent of the linear density.

Figure 11 shows the results of test runs with different amounts of linear damping at the joints. The lower curves show the percentage of the initial energy remaining as a function of time. As the viscosity in the joint is increased, the rate of energy dissipation increases up a maximum and then decreases as the joint becomes so stiff that the tip inertia tends to oscillate with the array as a rigid body. Although there is an optimum joint viscosity, substantial departures from the optimum degrade the damping performance only slightly. Figure 11 shows that the three values of viscosity that give the greatest damping range over a factor of 6.

The joint damping is given as a ratio of the torque applied in a joint (N·m) to the angular rate of change of the joint (s^{-1}). The units of the joint damping coefficient, γ, are thus N-m-s. When damping is involved, the array behavior is not independent of the linear density, σ, but is similar only when the dimensionless grouping $\dfrac{\gamma n}{\sigma L^2}$ has the same value. If we find that the optimum damping for a 50-kg array is in the neighborhood of $\gamma = 0.005$ N-m-s, we can infer that similar behavior would be achieved from a 20-kg array (constructed from aluminum rather than steel) with $\gamma = 0.002$ N-m-s.

Runs have also been made starting with greater and lesser amplitudes, and, as expected, the period of oscillation decreases with increasing amplitude. We have also simulated cases starting with kinetic energy but no initial displacement of the array.
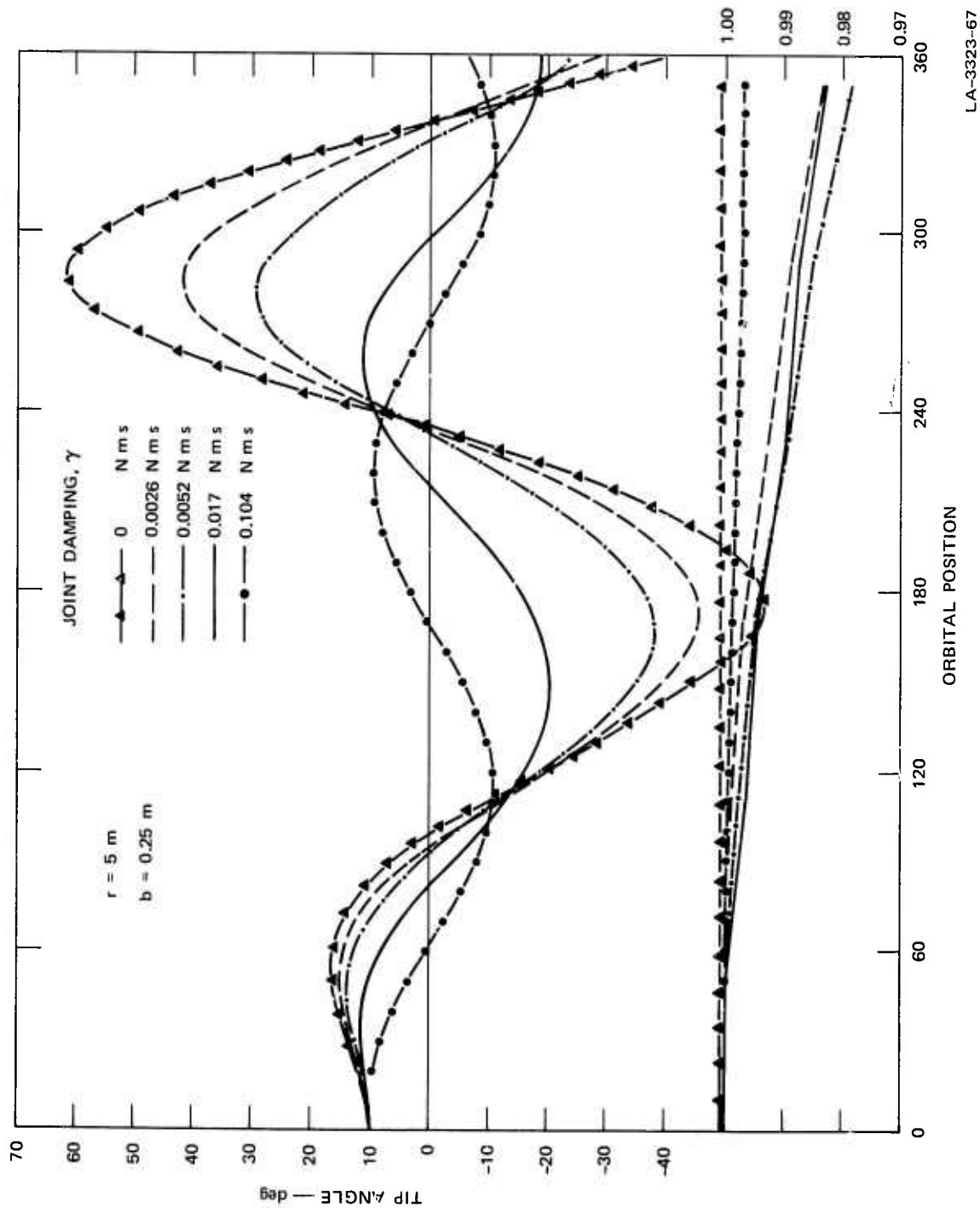
FIGURE 11   SIMULATION RESULTS WITH TIP INERTIA FOR VARIOUS ViSCOSITIES

LA-3323-67

31

One of the interesting features that is expected and appears in
our simulations (but is absent in the small-amplitude analysis), is
that out-of-plane libration transfers energy to in-plane libration.
Figure 12 shows the result of a simulation of the motion of a rigid
body beginning with 20° of out-of-plane libration angle. Some of the
energy from this libration mode is transferred, giving rise to in-plane
libration. Also shown in this figure are data for the same body with
an initial angular displacement of 40°. As can be seen by comparing
the data, the larger initial libration produces disproportionally
greater coupling between out-of-plane and in-plane motion. At very
small angles the coupling disappears.
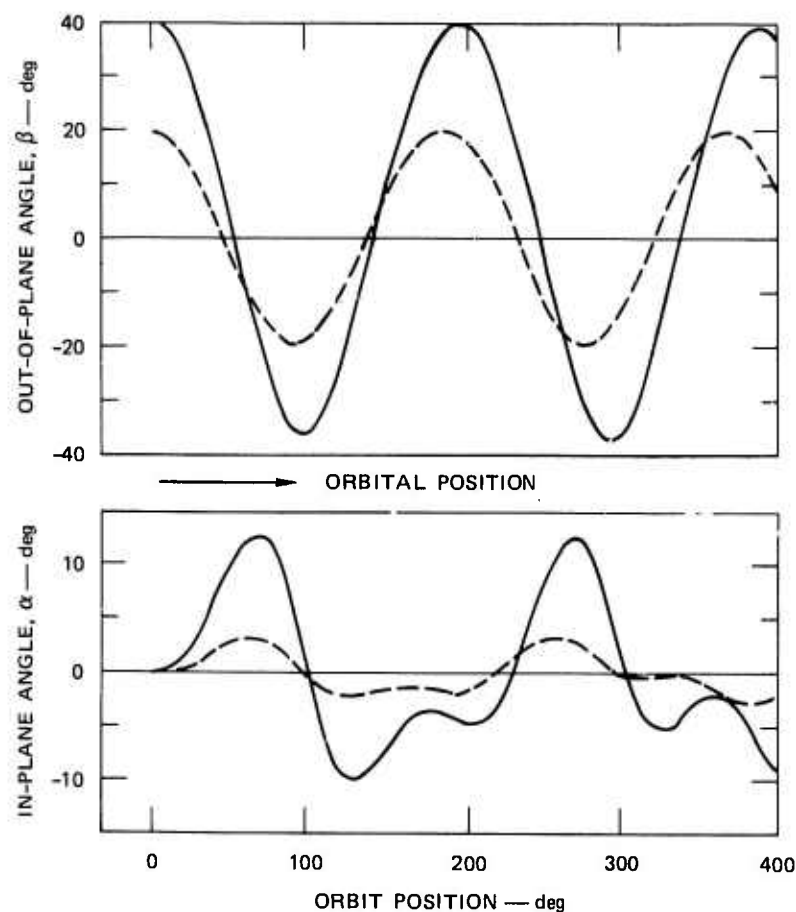
LA-3323-68

FIGURE 12   OUT-OF-PLANE-TO-IN-PLANE COUPLING FOR RIGID BAR

32

V DEPLOYMENT

A. General

Deployment is integral to orbital and attitude considerations, because the deployment provides the initial conditions. In the case of a completely passive satellite, such as the space array, the deployment is the last phase in which the behavior of the array can be affected.

The requirements of the deployment and several candidate mechanisms were examined in Summary Report--Phase I. The desired function of the deployment is to put the array into its stable equilibrium condition. That is, the array should be (1) straight, (2) pointed toward earth, (3) rotating at the orbital rate so that it will continue to be earth-pointing, and (4) tranquil and at low stress. It should be possible to stow the array on the transtage so that it is not damaged by the launch environment.

B. Method

Several deployment mechanisms have been considered. They can generally be classified as mechanically assisted, naturally assisted, or inertial. The use of booms or of rockets to position the array fall in the category of mechanically assisted deployments. Although booms could conceivably be used to deploy the 150-m test array, booms to deploy the 1.5-km array lengths being considered for systems applications are out of the question. The rocket-assist concept becomes applicable for very long arrays where the gravity-gradient strength is sufficient to tolerate the turbulent forces involved. This may be possible with the 1.5-km arrays and larger. The deployment mechanism most frequently conceived

33

for long tethered bodies takes advantage of the gravity gradient to separate the bodies. This type of deployment would be a naturally assisted deployment. Note that other forces such as the solar pressure, which is normally considered to be a difficulty, could conceivably be used to assist the deployment. In order to take advantage of the gravity gradient, however, initial separation must be achieved by other means. These other means generally are to give an initial velocity to a part or parts of the array. When these initial velocities dominate the deployment, then the deployment is what we call a quick inertial deployment. Gravity-gradient-assisted deployments are most desirable where very large (several kilometers) arrays are being deployed. For arrays of shorter length, and in particular the 150-m test array, the gravity-gradient forces are too small to assist the deployment. Thus, we have focused on quick inertial deployments.

The basic strategy of our selected deployment is to launch each subsequent bead into the identical trajectory. In this way the string of beads would be projected into a straight line with zero tension from bead to bead, and it would make no difference how the beads were interconnected. In order to get the one rotation per orbit, a linearly increasing transverse velocity can be added to each subsequent trajectory. Such a linearly varying transverse velocity could be provided either by uniformly accelerating the deployment mechanism in the transverse direction or by slowly changing the direction of the trajectory. The angular rate at which the trajectory should be changed corresponds to a negative orbital rate with respect to the fixed stars, or a negative twice-orbital rate with respect to the rotating frame of reference. This would require a control system comparable to that required for making telescopic time exposures. The existence of such systems allows us to infer that an attitude-control system could be constructed that would give a nearly perfect deployment. However, the actual system will have

34

to function in a more adverse environment since it must tolerate the control system of the transtage selected. For the test satellite this will be the TITAN III-C launch vehicle.

Figure 13 shows an artist's concept of the deployment mechanism and storage canister. The array is shown coiled, similar to a spool of twine, and resting in a canister. Constraint means will be provided for support in the launch environment; an elastic diaphragm for this purpose is shown in Figure 13. The canister will be bolted to the transtage and the driving drums solidly affixed to the canister. Only the lightweight guide tube will be pivoted to provide the directional correction, should that be needed.

The entire mechanism will be launched with the end of the array led through the drive sprockets and the guide tube and with the constraint mechanism in place. The deployment sequence consists in removing the constraint and then quickly accelerating the drive sprockets to the deployment velocity.

C. Transtage Detail

The TITAN III-C transtage, now regarded as the designated launch vehicle, has a statistically described limit-cycle attitude-control system. The transtage cycles from +1/2° to -1/2° from its set position in all three axes. This cycling of position together with the fact that the pitch and yaw attitude control jets also accelerate the transtage creates special problems that are considered in detail in Appendix D. Our tentative conclusion is that the deployment must take place at a few feet per second in order to overcome the acceleration effect, and that the attitude-control system will not support a deployment sufficiently quiescent so that the attitude can be maintained by the gravity-gradient forces alone. It has been noted that if the array is

35

GUIDE TUBE

ELECTRICALLY DRIVEN
DEPLOYING SPROCKETS

FAIRING COVER

COILED ANTENNA

CANNISTER

ELASTIC
DIAPHRAGM

BASE PLATE

GAS TUBE
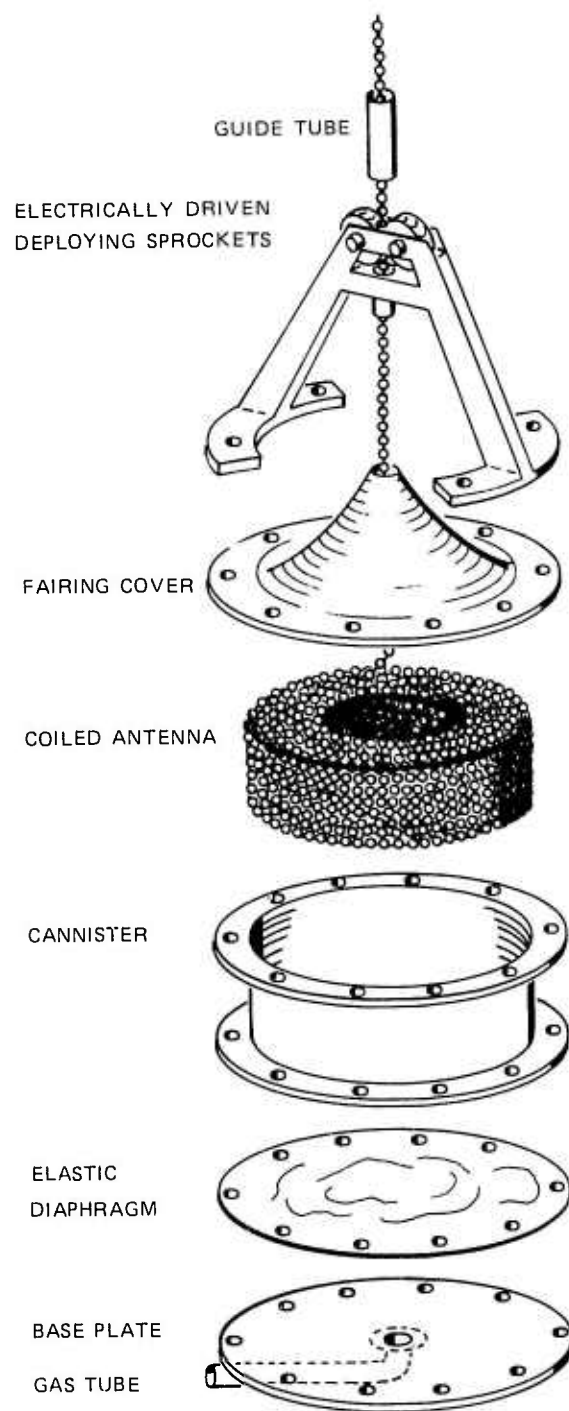
LA-3323-78

FIGURE 13   BLOWUP OF DEPLOYMENT MECHANISM

36

made up of stiff sections of wire instead of being completely flexible, then sufficient energy can be absorbed in the flexing of this wire to give a stable deployment. As noted in Appendix D, the guide tube can significantly reduce spurious transverse velocities, but a complete elimination of them would also require motion of the deployment mechanism relative to the transtage.

A deployment with no average rotation will be achieved if the forward and backward rocking motions of the transtage cancel each other. In this case, the deployed array would start with an initial libration of 36°, which would have to be damped out by the tip-inertia process. By initiating the deployment on a forward angular motion in the orbit plane, one can ensure that the transverse velocity will never give rise to a negative average in-plane rate. If the deployment is completed during a reverse motion of the transtage, the average angular rate of the array may be near one revolution per orbit. Thus, the anticipated libration values resulting from this deployment technique are 36° or less.

D. Orbital Distortion

Figure 14 shows the eccentricity of the orbit generated as a function of the deployment velocity when the array is deployed from a transtage in a perfectly circular, synchronous orbit. A deployment velocity of 5 m/s would generate an orbital eccentricity of 0.0027, a value that is somewhat greater than the tolerance limits we have selected for the array orbit. This difficulty could be overcome by making an adjustment of the velocity of the transtage just prior to deployment, or making the deployment at a chosen time in an imperfect orbit of the transtage so that a nearly perfect array orbit results.

37
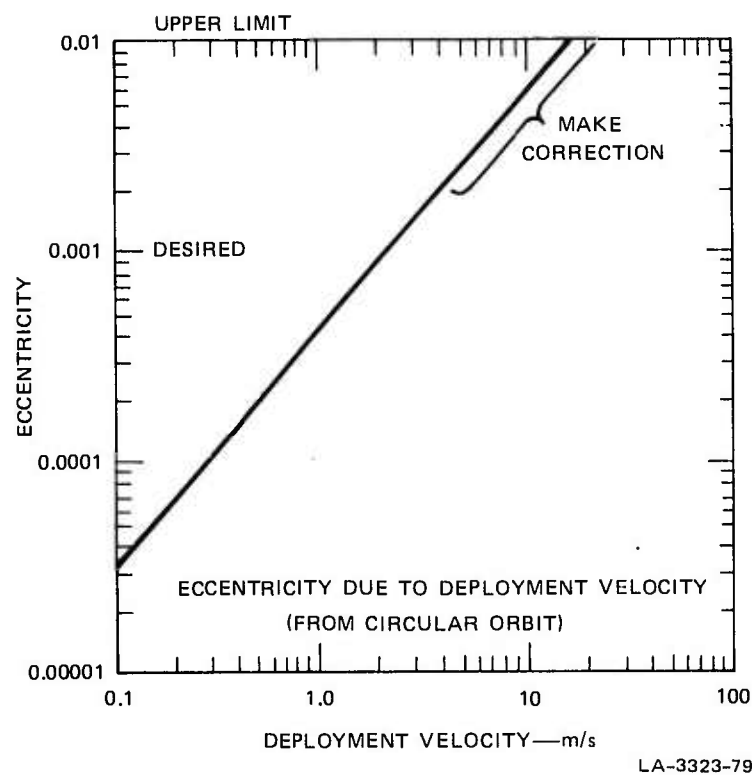
FIGURE 14 ECCENTRICITY DUE TO DEPLOYMENT VELOCITY

E. Tests

Various parts of the deployment mechanism have been built and
tested. Arrays having bead densities from aluminum to lead, and with
stiffness parameters ranging from completely flexible to that provided
by a 1-mm-diameter steel wire have been driven out from between a
drive wheel and a mating flexible roller. The consistency of the bead
trajectores has been examined as a function of the deployment variables.
The beads appear to be deliverable without a guide tube within a total
angle of one degree, where the spectrum of disturbance is at high
frequency (i.e., there is no correlation between the delivery angle of
beads spaced a meter or more apart).

The concept of accelerating a stiff section of the bead array to
5 m/s within one meter has been experimentally verified. An analysis
of the acceleration behavior remains to be completed.

38

A complete model is presently being prepared for testing. This model will confirm parameters for the design of the prototype package.

The tension of 2.34 newtons involved in the deployment at 5 m/s dominates the array behavior within the deployment mechanism. It seems likely, therefore, that testing of the concept and the mechanisms developed can be accomplished in the earth's gravity environment.

VI ARRAY STIFFNESS CONSIDERATIONS

A. General

There are several reasons why it would be desirable for the array to have considerable stiffness instead of being completely flexible. This section presents the advantages and disadvantages of such stiffness.

B. Reasons for Stiffness

1. Prevention of Collapse During Deployment

As explained in Section V, the array is to be spun or fired out of its storage chamber. Ideally, each bead would follow the preceding bead in exactly the same trajectory. In a perfect deployment of this kind the desired equilibrium conditions would be attained immediately.

For economic reasons, the deployment mechanism will be bolted directly to the launch vehicle. Consequently, the deployment will be perturbed by any motion resulting from vehicle station-keeping. In particular, since the launch vehicle uses a limit cycle in its attitude control, successive beads will be subjected to different deployment conditions--i.e., the station-keeping process will impart to the beads velocities that are transverse to the intended direction. These transverse velocities carry with them undesired kinetic energy, which might exceed the gravity-gradient potential energy and hence might collapse a flexible array.

If the array has stiffness, some of this kinetic energy will be expended in bending the array, in addition to overcoming the gravitational potential. Hence, stiffness would provide another sink for spurious kinetic energy introduced during the deployment, consequently increasing the probability of deployment success.

2.   Tolerance to Compressional Forces

When the array is in its stable equilibrium position, all portions of the array are under tension. However, under some circumstances the forces within the array are compressional. In the worst case the magnitude of the compressional force is one-third the value of the tension in the stable position. If we assume that the array might sometimes approach this unstable equilibrium position, either as a consequence of large-amplitude librations or through the necessity of capturing from tumbling, then stiffness would help to avoid collapse of the array. Furthermore, sufficient stiffness will prevent buckling and help ensure straightness during deployment.

The motion of a thin, long, rigid body with large-amplitude motion is considered in Appendix E. The principal result is contained in the phase-plane plot of Figure 15. Demarkated regions in this figure include forward and backward tumble of the array, and gravity-gradient capture of the array. The indicated regions of compression intersect other regions of behavior. As shown, capture from backward tumble (that is, tumble opposed to the rotation direction) could take the array through the point of maximum compression. Capture from a forward tumble, on the other hand, would never subject the array to a compression of more than half the maximum value. Also indicated is the fact that the array would never be subject to compressional forces if the amplitude of libration can be limited to a maximum of 66°.
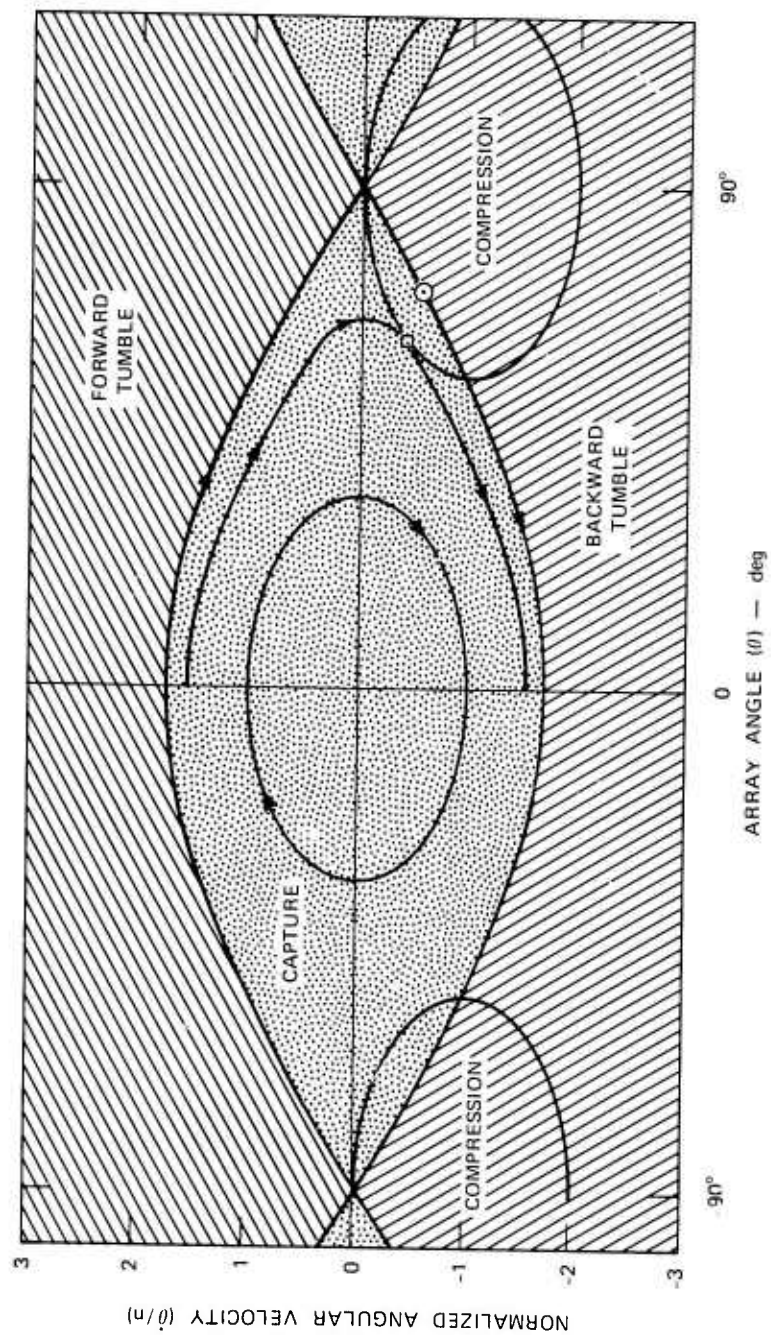
FIGURE 15   PHASE-PLANE PLOT FOR THE IN-PLANE MOTION OF A RIGID ROD

LA-3323-69

43

3. Increased Damping Rate

As has been shown, all the motions of the array under the gravity-gradient forces are slow--i.e., comparable with the orbital rate--even if large tip masses are added. If the array were given some stiffness it would vibrate as a beam as well as a gravity-gradient controlled cable. This beam behavior results in faster relative motion, with a period measured in seconds, which could be used to accelerate the dissipation of energy.

4. Avoidance of the Collapsed State

As shown in Appendix F, the mutual gravitational effect of the balls is small but is not entirely negligible. For example, an array consisting of half a dozen balls would collapse on itself even if it were initially extended along the local vertical. More generally, the collapsed state is a stable equilibrium state for any completely flexible array. Addition of only a very small amount of stiffness completely avoids the possibility of entering this state.

C. Reasons for Avoiding Stiffness

We rely entirely on gravity-gradient forces to straighten the cable, as required for reinforcement of electromagnetic scattering. There is no way that stiffness can improve upon the straightness resulting from those forces, but there are at least two ways in which stiffness could degrade it.

1. Residual Shape

The residual shape of wire produced on earth is an important factor affecting the array performance in space. For example, if the wire had a residual radius of curvature of one kilometer, a 150-m length

would have a displacement at the center of the array of nearly 3 m.
This displacement is two orders of magnitude larger than that which
gives tolerable electromagnetic performance.

2. Thermal Strain and Excitation

Even if all residual strain were removed, a stiff array would
be distorted by thermal strains resulting from solar heating. The
deflection due to these strains is important in itself. However, there
is an additional concern that the periodic nature of the thermal
strains might excite orbital or attitude perturbations. Several
satellites with extended booms appear to have experienced such
excitation.

Appendix G shows a calculation of the temperature distribution
in a wire exposed broadside to the sun. The thermal gradient that
causes strain (or bending) is a function of the surface radiation
properties and the thermal conductivity of the wire. Curiously, the
amount of bending is independent of the size of the wire. Calculations
of the thermal strain, given in Appendix G for a beryllium copper wire,
indicate that thermal effects will produce a radius of curvature near
50 km. Although this degree of curvature is small, it produces a
deflection of several centimeters at the midpoint of the array. Con-
sequently, thermal excitation is of concern. It is noted that the
actual deflection of the array would probably be less than that cal-
culated because approximately two-thirds of the wire is constrained
within the beads of the array.

D. The Chosen Array Structure

Certain advantages result from making the array stiff, whereas
other advantages result from making it very flexible. Fortunately,

a compromise is available that preserves all the advantages of both choices. This compromise is to make the array of stiff sections joined by hinges that permit only a limited amount of deflection, on the order of 3° of motion. Since only small motions are permitted, the array appears stiff to greater deflections. Hence, during deployment, a large amount of energy can be accommodated by the flexing of the relatively stiff sections of wire. Then, when the energy is dissipated and the array quiets down, the structure is flexible so that residual stresses and thermal excitation do not disturb its shape. The joints provide this needed flexibility.

Measurements are currently under way to determine how much curvature can be expected in various kinds of wires manufactured by different techniques. This information together with simulations of the electromagnetic performance of arrays constructed with these wires will set an upper limit on the length of array segments that can be used for the array. It is reasonable at this point to suppose that the array will be composed of sections of between one meter and ten meters long.

It should be noted that the flexible-cable analysis and the calculations of energy during deployment assuming beads on a wire are both still valid, but only in a limited range. The flexible-cable analysis applies only when the joints do not go to their stops, and the energy calculations apply only when the joints do go to their stops. The in-between region is of interest, but the details are not crucial. We are assured by these separate analyses that deployment will not collapse the array, and that the array will achieve the desired straight, earth-pointing position.

VII   ORBITAL CONSIDERATIONS

A.   Interference with Other Satellites

It is planned that the array will be carried as a piggyback
package on a launch vehicle whose primary mission is to deploy other
satellites. It is therefore necessary to demonstrate that there will be
no interference between the array and the other satellites.

The envisioned deployment sequence is shown in Figure 16. This
figure is a modification of a figure from a TITAN III-C handbook. The

TERMINATE
TRANSTAGE
SECOND BURN
(t = 0)

RELEASE FIRST
777
(t = 2.85 min)

5 ft/s ΔV

RELEASE SECOND
777
(t = 13.2 min)

5 ft/s ΔV

DEPLOY
SPACE
ARRAY
TOWARD
NADIR
≈ 22 min

REORIENT
AND BURN
TO PROPELLANT
DEPLETION
(t = 29 min)
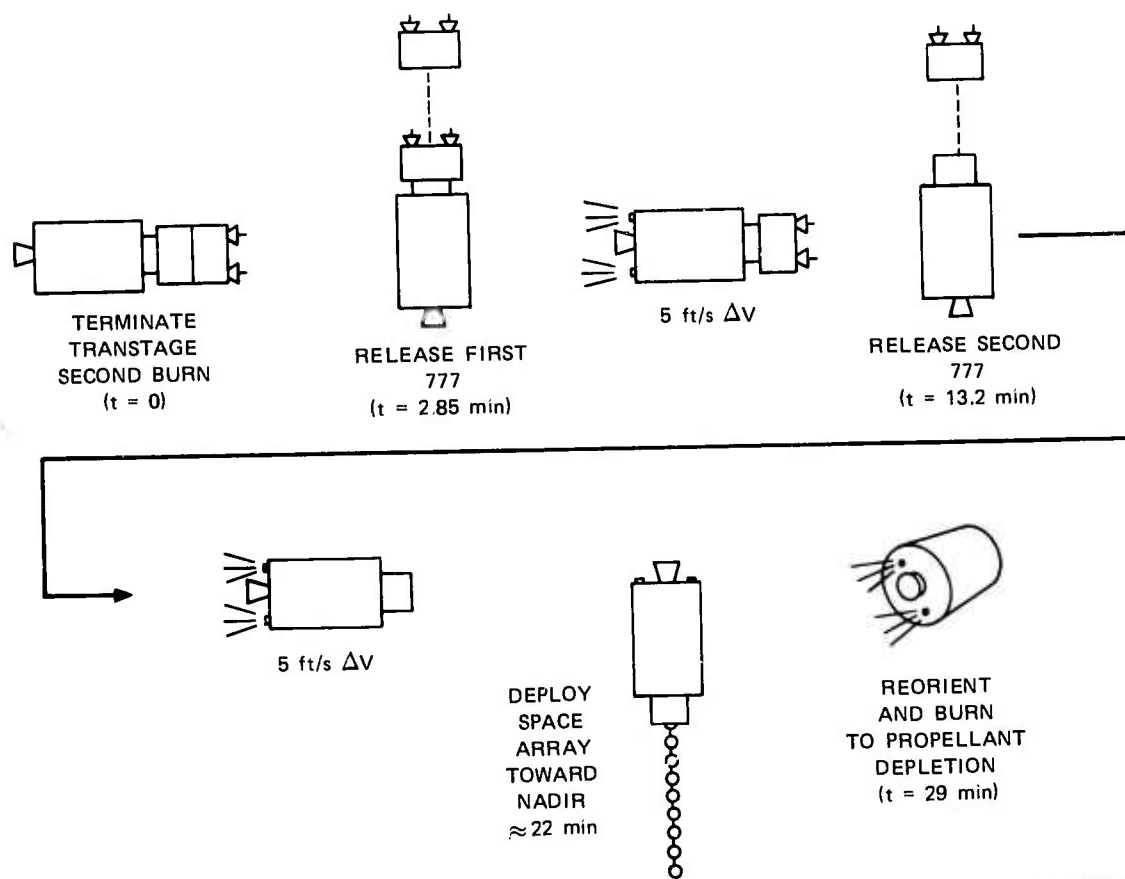
LA-3323-70

FIGURE 16   REPRESENTATIVE DEPLOYMENT SEQUENCE

deployment sequence proceeds as follows. After the first satellite is released, the transtage is rotated by 90° and accelerated an additional five feet per second. This procedure is repeated after the release of the second satellite. Finally, the deployment of the space array takes place along an earth radial. It might be desirable to make a slight upward or downward adjustment to the velocity of the transtage before deployment of the array, in order to avoid introducing eccentricity to the orbit of the array.

The Euler-Hill equations have been written to describe the relative motion of the three bodies in the local reference frame of one of the prime satellites. Solution to these equations shows that the closest point of approach of an upwardly deployed array to the second satellite should be about 20 km after the first day. This distance increases thereafter. If the array is deployed downward, the corresponding distance of closest approach is 50 km.

The satellites that are to be deployed before the space array contains thrusters to move them into test positions and subsequently into operational positions. The calculations that we have performed, of course, do not consider the possibility of collision during these movements, although they could easily be performed were the data available. However, the calculations do give assurance that there will be large separations and that it is possible to achieve the transfer of these satellites from their test position to their operation positions without any interference from the array.

3. Inclination of Orbit and Earth Oblateness

Because the ecliptic plane is not aligned with the equatorial plane, and because the moon does not lie exactly in the ecliptic, forces will be exerted by the sun and the moon that will tend to change the

inclination of the array orbit. The calculations shown in Appendix I indicate that, starting with an equatorial orbit, the inclination will increase to 17° and return to zero during a 50-year period. This inclination of the array orbit decreases the possibility of interference with station-kept satellites that remain in the equatorial plane.

Although the sun and the moon have a significant effect on the inclination of the orbit, their effect on the gravity-gradient environment of the satellite is negligible. This is shown in the following comparison of the gravity gradients from the earth, the sun, and the moon. The gravity gradient of the earth is used as a reference.

Earth	Sun	Moon
1.0	7.36×10^{-6}	1.604×10^{-5}

As shown in an earlier report, orbital eccentricity excites libration in a uniform cable array. We therefore were concerned that eccentricity might have some pumping effect on the normal modes of the more complex array structure. Furthermore, if other than circular synchronous equatorial orbits are considered, it becomes necessary to evaluate secondary perturbations of the earth's gravitational field. In particular, for inclined orbits, the oblateness of the earth is important because it can pump array libration as does orbital eccentricity.

Our analysis of forced libration due to eccentricity and to oblateness of the earth is summarized in the following equations:

$$\ddot{\varphi} + 3n^2\varphi = 6.5J_2 \left(\frac{R_\oplus}{r}\right)^2 \sin i \sin 2nt + 2\epsilon n^2 \sin \theta \tag{1}$$

$$\ddot{\psi} + 4n^2\psi = 7.5J_2 \left(\frac{R_\oplus}{r}\right)^2 \sin 2i \sin nt \tag{2}$$

where

φ = In-plane libration angle

ψ = Out-of-plane libration angle

i = Inclination of orbit

θ = Orbital angle from perigee

J_2 = Orbital constant due to oblateness (1.08×10^{-3})

$R_\oplus$ = Earth radius

r = Orbital radius.

From these equations, we conclude that the in-plane, forced, steady-state oscillation amplitude is equal to the eccentricity. This conclusion is a well-known result.

For oblateness we find

$$\text{Amplitude of } \varphi = 6.5 J_2 \left(\frac{R_\oplus}{r}\right)^2 \sin i \qquad (3)$$

$$\text{Amplitude of } \psi = 2.5 J_2 \left(\frac{R_\oplus}{r}\right)^2 \sin 2i \qquad . \qquad (4)$$

The worst case for in-plane oscillation is the polar orbit; oblateness will cause an amplitude of $0.01°$. The worst case for out-of-plane oscillation due to oblateness is the 45° inclined orbit where an amplitude of less than $0.004°$ results. Thus, the effect due to oblateness is negligible for all synchronous orbits.

A possible parametric excitation of the out-of-plane libration due to eccentricity was considered. Our result showed stability with a

50

limit-cycle amplitude proportional to the fourth power of eccentricity. As long as nearly circular orbits are involved (i.e., $\epsilon < 0.01$), this effect is negligible.

C. Effects of the Sun

The sun has several additional effects on the array and on altitude and orbital dynamics. These effects result from solar pressure and solar heating of the array.

Solar pressure tends to distort the orbit, and to collapse the array. Both of these considerations apply to completely uniform cables as well as to irregular structures, and both are discussed in the Summary Report for Phase I. We note that the orbital distortion and collapse of the array can be prevented by a design that satisfies straightforward criteria previously developed.

An additional distortion of the array can result if the array has a nonuniform area exposed to the solar pressure and a nonuniform area-to-mass ratio, and if the beads have nonuniform optical properties. This last consideration is probably the most serious, since the optical properties may change with time. Calculations of deflection due to inhomogeneities in area-to-mass ratio were given in Summary Report-- Phase I, leading to the conclusion that uniformity was an essential consideration. Appendix J gives calculations to show how differences in optical behavior for a few selected beads affect the array. Once again the conclusion is that uniformity is an essential consideration for the final design. However, the numbers that have been obtained for deflections in simple cases lend confidence to the assertion that sufficient, long-term uniformity can be achieved.

The identified thermal effects are bending, lengthwise straining, and possible change in the behavior of the joints. The bending is a

51

differential temperature problem and has been dealt with in this report (see Appendix G). These stresses are one of the principal reasons for making a segmented array. Lengthwise strain is important because it changes the moment of inertia of the array (and could be a parametric or pumped excitation), and because, if it happens fast enough, it could accelerate the array more than the gravity gradient. These average temperature effects have been considered and reported in the Summary Report for Phase I. The daily temperature variation will not exceed 100°C for the worst-case orbit, where the array sometimes points directly toward the sun and sometimes is broadside to the sun. In this same orbit, when the array is eclipsed, the temperature will drop an additional 80°C. Appropriate coatings can reduce these values. In the earlier report we have discounted the possibility of a pumped instability, or of the ends of the array snapping together due to rapid shortening. The libration amplitude will vary somewhat as the moment of inertia is changed by thermal extension of the array. The joints will have to be designed and lubricant selected to give the desired joint behavior (i.e., the viscosity must remain within about six, as discussed in Section IV) over a temperature range of -80°C to +20°C.

VIII   STATUS AND CONCLUSIONS

The orbital and attitude behavior of the passive-communication space array has been studied through analysis and computer simulations. We have examined alternative tip configurations that provide libration damping. These studies, together with manufacturing and deployment considerations, have led us to the selection of an array design that promises to be readily deployable and stable in orbit. This array will have inertial tips and it will be made from sections of stiff wire on which the scattering elements will be placed. These sections will be hinged together through viscous joints that are limited in their motion. This construction technique results in an array that is flexible for small deflections and relatively stiff for large deflections. This type of array can be captured from tumble and can be made to have a libration-damping time constant of less than two months.

Deployment of the entire array including the tip bodies can be accomplished from a driving device on the transtage. The deployment rate will be about 5 m/s in order to minimize the effect of acceleration of the transtage due to the attitude-control system. Orbital corrections of the transtage are recommended to give the most nearly circular orbit for the array. Deployment will be initiated on a forward-tilting motion of the transtage. Depending on the attitude behavior of the transtage, the array will be deployed with a maximum libration of 36°.

The preliminary design parameters for the 150-m test array are as follows. The main array will be made up of 75 two-meter sections of steel wire approximately 1 mm in diameter. Attached to this wire will

be 10^4 one-centimeter aluminum spheres with center-to-center spacings of 1.51 cm. Twenty percent additional length, preformed into the pigtail tip-inertia arrangement, will be provided at each end. This inertial tip arrangement will be 5 m in radius (when deployed) and have a drop of one-third of a meter from its point of attachment to its center of mass. The joint connecting the end of the array to the tip inertia will be capable of large excursions; the other joints will be limited to $1°$ to $3°$ of deflection.

The test array has been designed so that it will capture from tumble without collapse. Although such design is not realistic for much longer arrays, the possibility of their tumbling is also remote.

Considerable effort is now going into the design and testing of joints that produce the desired kind of behavior. This effort will lend support to the analysis and simulation described herein.

The reasons for the present array design are summarized as follows:

1-cm beads	Resonant at the electromagnetic transmission frequency.[*]
150-m test length	Sized to test concept with available ground facilities.[*]
1.51-cm spacing	Electromagnetic requirement for diffraction pattern.[*]
5-m tip-body radius	Large enough to give less than two-month damping time constant; greater size would give more damping but would begin to effect the array shape during libration. Sized primarily not to be excessively large; already adds 40% to the mass of the array.

---

[*] Not covered in this report.

54

0.33-m drop to center of mass	Gives resonant excitation of tip-inertia by array.
2-m sections	Selected to give straightness to within 0.001 m assuming a radius of curvature of 100 m. Should the residual curvature prove to be sufficiently better, this length may be increased. Residual rather than thermal strain will be the dominant consideration.
$1°$-to-$3°$ included angle in limited-motion joints	Must be small so that wire is bent to absorb energy. An included angle less than $9.6°$ will prevent the 2-m sections from wrapping around on themselves without stress. The smaller angles ensure that the array cannot find a non-straight equilibrium position.
Aluminum beads	Minimum kinetic energy relative to bending energy.
1-mm-diam steel wire	Gives sufficient bending stiffness to ensure deployment from TITAN III-C limit-cycling transtage. Ensuring stability from buckling is a second consideration.

Appendix A

ANALYTICAL FORMULATIONS

Appendix A

ANALYTICAL FORMULATIONS

1. Coordinates and the Equation of Motion

We use a reference frame attached to the center of mass of the cable. This reference frame moves in a circular orbit of radius r as shown in Figure A-1. The x-axis (with unit vector $\vec{i}$) is defined by the direction of the radius vector from the center of the earth, the y-axis (with unit vector $\vec{j}$) lies in the orbital plane, and the z-axis (with unit vector $\vec{k}$) is perpendicular to the orbit plane.

We consider the motion of a uniform, perfectly flexible cable or chain. The equation of motion for an array element, ds, located at position $\vec{\rho}$ with respect to the origin of the chosen reference system, can be written as

$$\sigma ds \; [\ddot{\vec{\rho}} + 2(n\vec{k} \times \dot{\vec{\rho}}) + n\vec{k} \times (n\vec{k} \times \vec{\rho})]$$

$$= \sigma ds \; n^2[3(\vec{i} \cdot \vec{\rho})\vec{i} - \vec{\rho}] + [\text{string tension terms}] \qquad (A-1)$$

where

    s = Length along the array

    σ = Linear density

    n = Orbital rate

    $\vec{\rho}$ = Position vector
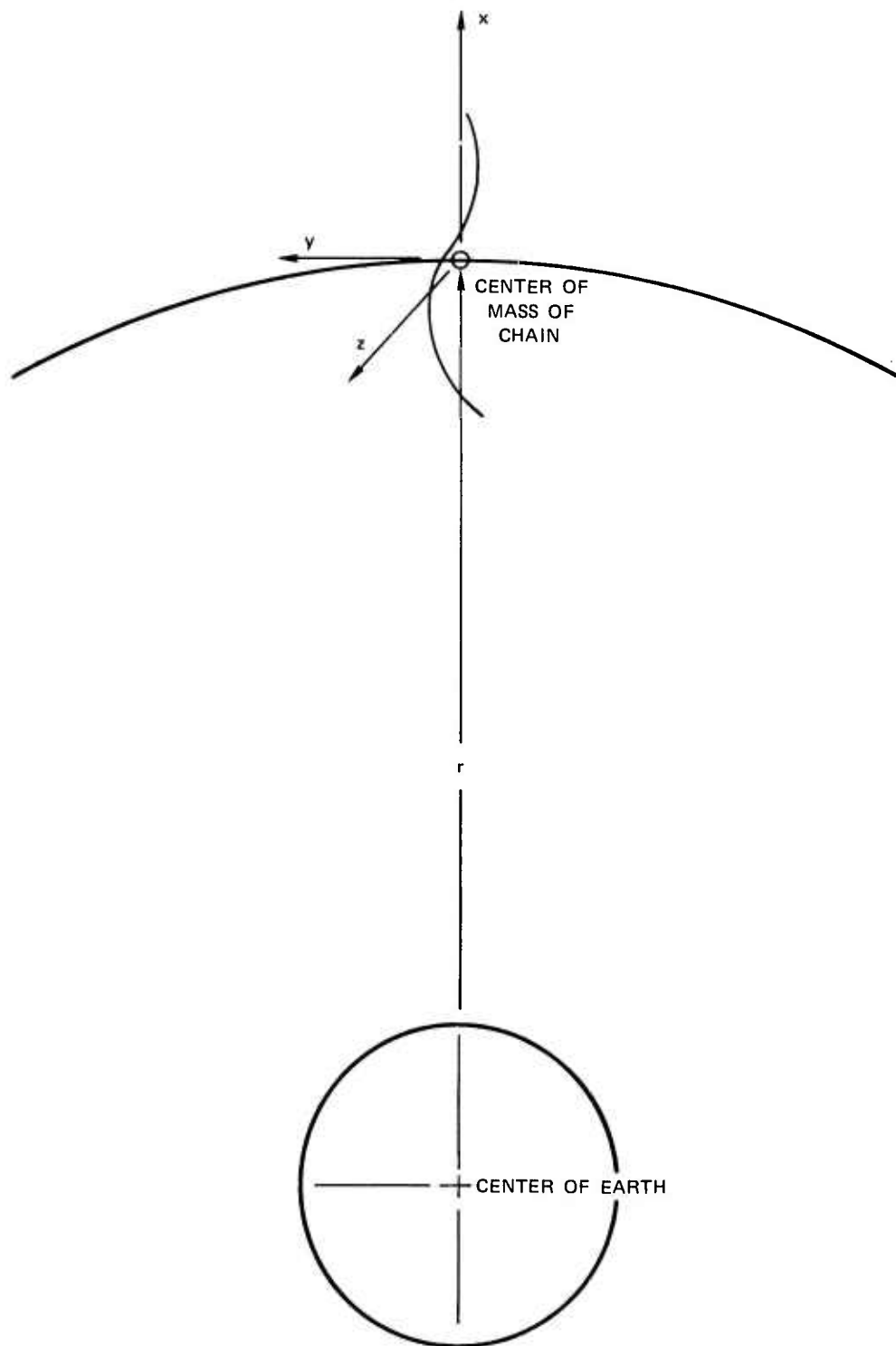
FIGURE A-1   COORDINATE SYSTEM

LA-3323-71

60

2. Small-Amplitude Approximations

If the cable is nearly straight and in a nearly vertical position $dx \cong ds$, and the position vector can be approximated by

$$\vec{\rho} \cong x\vec{i} + y(x,t)\,\vec{j} + z(x,t)\,\vec{k} \tag{A-2}$$

then the bracket, noted previously as string-tension terms, can be written as

$$-\frac{dT}{dx}\vec{i} + \frac{d}{dx}\left(T\,\frac{dy}{dx}\right)\vec{j} + \frac{d}{dx}\left(T\,\frac{dz}{dx}\right)\vec{k} \tag{A-3}$$

where T is the cable tension. Furthermore, we can assume that the cable tension is near its equilibrium value and that this tension is nearly independent of the cable displacement. Thus a linearized differential equation for the equilibrium tension, T_e, can be written as

$$\frac{dT_e}{dx} = 3n^2 x\sigma \quad . \tag{A-4}$$

The solution of this equation depends on boundary conditions, which for the free cable are zero tension at its ends. Hence, we obtain

$$T_e = \frac{3}{2}\sigma n^2 \left[\left(\frac{L}{2}\right) - x^2\right] \tag{A-5}$$

where L is the total length of the array.

The components of the vector equation (A-1) can now be written explicitly to give the desired equations of motion for the cable. The equation for the component in the $\vec{i}$ direction is not solved identically

61

but has an unsatisfied term that depends on $\dot{y}$; however, for small deflections this term is small, and our approximations are valid. The $\vec{j}$ and $\vec{k}$ components are

$$\ddot{y} = \frac{3}{2} n^2 \left[\left(\frac{L}{2} \right)^2 - x^2 \right] \frac{d^2 y}{dx^2} - 3n^2 x \frac{dy}{dx} \tag{A-6}$$

$$\ddot{z} = \frac{3}{2} n^2 \left[\left(\frac{L}{2} \right)^2 - x^2 \right] \frac{d^2 z}{dx^2} - 3n^2 x \frac{dz}{dx} - n^2 z \quad . \tag{A-7}$$

Equations (A-6) and (A-7) are separable in the independent variables x and t. The following harmonic forms are obtained:

$$y(x, t) = \sum_{j=1}^{\infty} e^{i\omega_j t} y_i(x) \tag{A-8}$$

$$z(x, t) = \sum_{j=1}^{\infty} e^{i\omega_j t} z_i(x) \quad . \tag{A-9}$$

3. Normalization of the Equations of Motion

The equations of motion of the cable depend on its tension, which is a function of the tip arrangement. Therefore, it would be advantageous to normalize these equations in such a way that the tip arrangement affects only the boundary conditions. This approach suggests a normalization based on the variable ξ, given by

$$\xi = \frac{x}{a} \tag{A-10}$$

where "a" is the distance to a zero-tension point, which may be outside the array.

Using this variable, the differential equations for the shape functions of the harmonic solution can be written as

$$(1 - \xi^2) \frac{d^2 y}{d\xi^2} - 2\xi \frac{dy}{d\xi} + \frac{2}{3} \frac{\omega^2}{n^2} y = 0 \qquad (A-11)$$

$$(1 - \xi^2) \frac{d^2 z}{d\xi^2} - 2\xi \frac{dz}{d\xi} + \frac{2}{3} \left(\frac{\omega^2}{n^2} - 1 \right) z = 0 . \qquad (A-12)$$

The cable tension and normalization variable for three cases--no tip masses, a single tip mass, and two equal tip masses--are shown in Figure A-2. In the case of the free cable,

$$a = L/2 \qquad (A-13)$$

and the boundary conditions are applied at $\xi = \pm 1$. For one tip mass at the upper end of the array,

$$a = \frac{L}{2} \left[\frac{1 + \frac{2m}{\sigma L}}{1 + \frac{m}{\sigma L}} \right] \qquad (A-14)$$

and the boundary conditions are applied at $\xi = -1$ and $\xi = \dfrac{1}{1 + \dfrac{2m}{\sigma L}}$.

For two equal tip masses,

$$a = \frac{L}{2} \sqrt{1 + \frac{4m}{\sigma L}} \qquad (A-15)$$

and the boundary conditions are applied at $\xi = \pm \dfrac{1}{\sqrt{1 + \dfrac{4m}{\sigma L}}}$.

63

$$\xi = \frac{x}{(L/2)}$$

$$\xi = \frac{x}{L/2} \; \frac{1 + \dfrac{m}{\sigma L}}{1 + \dfrac{2m}{\sigma L}}$$

$$\frac{1}{\dfrac{2m}{\sigma L} + 1}$$
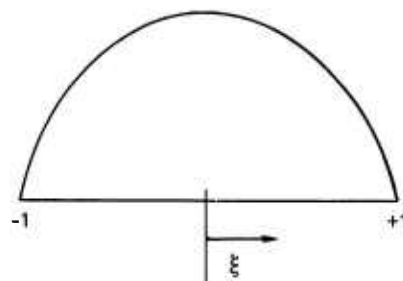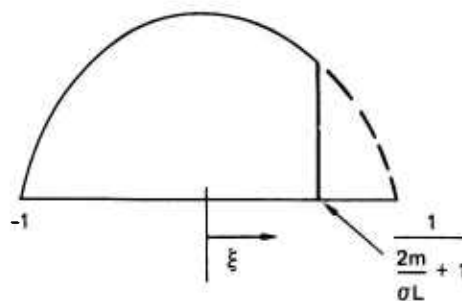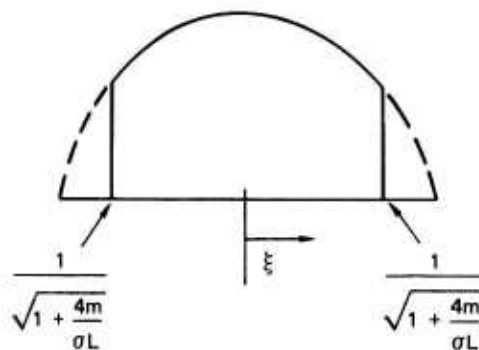
$$\xi = \frac{x}{L/2} \; \frac{1}{\sqrt{1 + \dfrac{4m}{\sigma L}}}$$

$$\frac{1}{\sqrt{1 + \dfrac{4m}{\sigma L}}} \qquad \frac{1}{\sqrt{1 + \dfrac{4m}{\sigma L}}}$$

LA-3323-72

FIGURE A-2   ARRAY TENSION FOR VARIOUS CONFIGURATIONS

64

The solutions for the tip-mass cases considered above are consistent with the assumption that the equilibrium tension exists in the cable when the cable swings through small amplitudes. An additional approximation must be made, however, when dealing with the bouncing tip masses or with tip inertia configurations. For these cases, the tension will change with the bouncing or rotating of these devices. The approximation of constant cable tension with time is still justified if we also assume either that the tip masses are small (compared to the array) or that small array motions are involved. Provided either of these assumptions is satisfied, the normalization factor for a pair of bouncing tip masses is

$$a = \frac{L}{2} \sqrt{1 + \frac{4m}{\sigma L} \left(1 + \frac{2\ell_e}{L}\right)} \qquad (A-16)$$

where ℓ_e is the equilibrium length of the spring (the distance between the end of the array and the bouncing tip mass at equilibrium). For the case in which large inertial tips are connected to the ends of the array using a rigid link of length ℓ_1, and b as shown in Figure 4,

$$a = \frac{L}{2} \sqrt{1 + \frac{4m}{\sigma L} \left(1 + \frac{2(b + \ell_1)}{L}\right)} . \qquad (A-17)$$

In the last two cases, the boundary conditions are applied at

$$\xi = \pm \frac{L}{2a} . \qquad (A-18)$$

The problem can also be solved for a single tip attachment or any combination of the tip arrangements described.

4.   Boundary Conditions

The boundary conditions to be used with Eq. (A-11) or Eq. (A-12) are given in this section.

    a.   Cable with Free End

The boundary condition at a free end is that the cable deflection must remain finite.

    b.   Cable with Tip Mass

The cable is straight at the point of attachment to a tip mass--i.e.,

$$\frac{\partial^2 y}{\partial \xi^2} = \frac{\partial^2 z}{\partial \xi^2} = 0 \, . \qquad (A-19)$$

    c.   Cable with Bouncing Tip Mass

To establish the boundary conditions for this case, we balance the components of force at the tip in the x-direction and in the direction of interest.

As we have noted earlier, the bouncing tip masses provide no linear damping for out-of-plane libration if the cable is undergoing small-amplitude motions. To achieve damping we need to mechanically tune the natural frequency of the composite structure so that it is parametrically excited by the out-of-plane motion. This means tuning one of the in-plane normal modes to a frequency of 4n. We have determined the boundary conditions for such a tuned array in the following manner.

66

The x-direction force balance gives[*]

$$\ddot{x}_s + \frac{K}{m} x_s + \frac{K'}{m} \dot{x}_s - 2n\dot{y} = 0 \qquad (A\text{-}20)$$

where

x_s = Spring stretched length

K = Spring constant

K' = Damping constant

The y-direction force balance gives

$$2n \dot{x}_s + \ddot{y} \pm \frac{T}{m} \frac{dy}{dx} = 0 \quad \left\{ \begin{array}{l} + \text{ upper end} \\ \\ - \text{ lower end} \end{array} \right\} \qquad (A\text{-}21)$$

where T at the tip is

$$T = m \, 3n^2 \left| x_{end} \right| \qquad (A\text{-}22)$$

Eliminating the spring-length variable, x_s, between Eqs. (A-20) and (A-21) and making the harmonic substitution results in the following boundary condition:

$$\frac{\xi \frac{dy}{d\xi}}{y} = \frac{\omega^2}{3n^2} \left(1 + \frac{4n^2}{\frac{K}{m} + \frac{K'}{m} j\omega - \omega^2} \right) \qquad (A\text{-}23)$$

_____

[*] The equilibrium length of the spring has been taken to be zero, and the equilibrium position of the mass is taken to be at the tip.

67

d. Cable with Tips Having Large Values of Inertia

The in-plane inertial tip boundary condition can be obtained from the equations governing the rotation of the tip inertia and the displacement of the end of the cable. These equations are

$$I_z \ddot{\theta} = -3n^2 \left(I_y - I_x\right)\theta - \left(bT + K'\frac{d}{dt}\right)\left(\theta - \frac{dy}{dx}\bigg|_{end}\right) \quad (A\text{-}24)$$

$$m(\ddot{y} \pm b\ddot{\theta}) = \mp T\frac{dy}{dx}\bigg|_{end} \quad \begin{Bmatrix} \text{upper end} \\ \\ \text{lower end} \end{Bmatrix} \quad (A\text{-}25)$$

where

θ = In-plane angle of tip mass from local vertical

b = Distance from the center of mass of the tip inertia to its attachment point

$I_{x,y,z}$ = Moment of inertia about respective axis

and the tension T at the tip is

$$T = m\,3n^2\,(|x_{end}| + b) \ . \quad (A\text{-}26)$$

Eliminating θ from these equations results in an in-plane boundary condition of

$$\frac{\xi\,\dfrac{dy}{d\xi}}{y} = \frac{1}{3}\left(\frac{\omega}{n}\right)^2\frac{1}{\left(1 + 2\dfrac{b}{L}\right)\left[1 - \dfrac{\left(2\,\dfrac{b}{L}\right)\left(\dfrac{\omega}{n}\right)^2}{1 + \dfrac{I_y - I_x - \dfrac{1}{3}\left(\dfrac{\omega}{n}\right)^2 I_z}{mb(b + L/2) + \dfrac{K'\,j\omega}{3n^2}}}\right]} \ .$$

$$(A\text{-}27)$$

The out-of-plane boundary condition must include yaw because out-of-plane tipping (roll) is coupled to yaw. Thus we must write an equation for roll, φ, an equation for yaw, ψ, and an equation for the out-of-plane cable displacement, z. The cable is assumed to have no torsional inertia, but its stiffness and damping are included. We have

$$I_x \ddot{\psi} + (I_z - I_y) n^2 \psi + (I_z - I_y - I_x) n \dot{\varphi} = Q \qquad (A-28)$$

$$Q = \begin{cases} -k_Q \psi - k'_Q \dot{\psi} & \text{even modes} \\ \\ 0 & \text{odd modes} \end{cases} \qquad (A-29)$$

$$(I_x + I_y - I_z) n \dot{\psi} + I_y \ddot{\varphi} + 4(I_z - I_x) n^2 \psi = -\left(bT + K' \frac{d}{dt}\right)\left(\varphi + \frac{dz}{dx}\right)$$
$$(A-30)$$

$$m\left(\ddot{z} + n^2 z \mp b\ddot{\varphi}\right) = \mp T \frac{dz}{dx} \begin{Bmatrix} \text{top end} \\ \\ \text{lower end} \end{Bmatrix} \qquad (A-31)$$

For simplicity, we have ignored torsional effects. The above equations can be combined to eliminate the variables ψ and φ. This manipulation yields the following out-of-plane boundary condition:

$$\frac{\xi \dfrac{dz}{d\xi}}{z} = \frac{(\omega^2 - n^2)}{3n^2} \frac{1}{\left(1 + 2\dfrac{b}{L}\right)\left[1 - \dfrac{m(\omega^2 - n^2) b^2}{C - B^2/A}\right]} \qquad (A-32)$$

where

$$A = \omega^2 I_x + n^2 (I_z - I_y) + k + j\omega k' \qquad (A-32a)$$

$$B = \omega n (I_z - I_y - I_x) \qquad (A-32b)$$

$$C = -\omega^2 I_y + 4n^2 (I_z - I_x) + 3bn^2 m\left(b + \frac{L}{2}\right) . \qquad (A-32c)$$

69

5.   Solutions to the Equations of Motion

Solutions have been obtained by both analytical methods and numerical methods on the computer. Cases have been studied both ways to provide cross checks.

a.   Free Cable

The oscillations of a free cable can be decomposed into normal modes whose shapes are Legendre polynomials for motions both in the orbital plane and out of it. These Legendre shapes and their corresponding eigenvalues (frequencies) are shown in Figure 5. The requirement that the amplitude be finite at the tip limits the selection to series that terminate (e.g., to the Legendre polynomials).

b.   Cable with Tip Masses

The numerical method described in Appendix B was used to obtain the appropriate eigenfunctions (normal mode shapes) and eigenvalues (frequencies) for the cable with tip masses. The values of the parameter $m/\sigma L$ examined were 0.0, 0.1, 0.2, 0.3, 0.5, and 1.0 These values cover the realistic range of tip mass to cable mass ratios.

For $m/\sigma L = 0$, which corresponds to the free-end case whose solution we know analytically, the numerical technique yielded the same eigenvalues and eigenfunctions for the lowest even and odd modes as obtained by the analytical approach. This concurrence of results gives credence to our solutions.

Numerical solutions were written out for 5, 10, and 31 joints in the half cable--i.e., matrices of the orders of 5, 10, and 31 were solved-- for the in-plane case. This was done in order to refine the analysis. However, we are primarily concerned with the lower-order modes (four even and four odd); hence the matrix of the order of 10 is sufficient. This is true because the higher-order modes are readily and rapidly

70

damped by friction in the joints. The numerical results for the tenth-order matrix are given in Table A-1. The eigenvalues for the modes are shown in Figures 6 and 7 of the main text. One should note in reading the table that the last value given in the eigenfunctions corresponds to a point 95% of the way to the end of the cable.

c. Bouncing Tip Mass

Because we are interested only in the case where the tip mass is designed to provide a normal mode with an in-plane frequency of 4n, the solution strategy is simplified. All one does is integrate the differential equation for the shape function with ω set equal to 4n, and check at each point to see whether the boundary condition has been satisfied. This is what we have done.

Figure A-3 shows the spacewise integration starting with odd and even cable-center conditions. The odd shape shows no reversals in curvature; hence there is only one mode to be dealt with. The even shape shows a reversal in curvature; hence, depending on the parameters, one of two different even modes is involved. Figure 8, in the main text gives a design curve to produce the normal modes of the desired frequency. This figure specifies the required value of spring constant for a given value of tip mass. We note that for a given tip mass, we can select the spring to tune either the odd or the even mode to the 4n value.

A check on the results is provided by the tip mass value at which the even mode calls for an infinite spring constant. This value should, and does, correspond to the cable-with-tip-mass case that gives $\omega = 4n$.

71

Table A-1

CALCULATED NORMAL-MODE SHAPES AND FREQUENCIES

FOR A CABLE WITH TIP MASSES IN A GRAVITY-GRADIENT ENVIRONMENT

Normalized Tip Mass $m/\sigma L = 0$

$\left(\dfrac{\omega}{n}\right)^2$ RPAC*	0	3	9	18	30	45	63	84
0	.3244428	.0000000	.3642590	.0000000	.3702283	.0000000	.3770221	.0000000
1	.3244428	.0592349	.3521171	.1347704	.3290918	.2084068	.2890503	.2781913
2	.3244428	.1184698	.3156912	.2542259	.2122268	.3505023	.0611233	.3856743
3	.3244428	.1777047	.2549813	.3430519	.0392666	.3741849	-.2082190	.2411594
4	.3244428	.2369396	.1699876	.3859334	-.1570666	.2557720	-.3861620	-.0876122
5	.3244428	.2961744	.0607098	.3675556	-.3309617	.0142096	-.3527441	-.3838679
6	.3244428	.3554093	-.0728518	.2726037	-.4235188	-.2747180	-.0668357	-.3712228
7	.3244428	.4146442	-.2306974	.0857630	-.3627490	-.4641788	.3490310	.0776768
8	.3244428	.4738791	-.4128269	-.2082815	-.0635746	-.3220832	.5049811	.5834792
9	.3244428	.5331140	-.6192404	-.6248445	.5721711	.4831248	-.3787358	-.2763849

*Relative Position Along Cable.

Notes: a. The value of $(\omega/n)^2$ is given for motion in the plane of the orbit.
For out-of-plane motion, the value of $(\omega/n)^2$ is greater than the
listed value by 1.0.

b. In each sub-table, nine equally spaced values are given plus the
center value (zero for the odd modes).
The nine-and-one-half position corresponds to the end of the cable.

72

Table A-1 (Continued)

m/σL = 0.1

$\left(\dfrac{\omega}{n}\right)^2$ RPAC*	.0000000	3.0583394	10.3899278	23.9724690	44.7194978	72.4466698	106.4186356	145.6079507
0	.2961744	.0000000	.3770928	.0000000	.4147087	.0000000	.4208772	.0000000
1	.2961744	.0479625	.3667360	.1432608	.3656853	.2485797	.3024813	.3321381
2	.2961744	.0959100	.3357430	.2703813	.2280219	.4044221	.0092541	.4098280
3	.2961744	.1438262	.2843542	.3657561	.0291705	.4028181	-.2992057	.1588580
4	.2961744	.1916920	.2130010	.4149158	-.1877594	.2306195	-.4378442	-.2404597
5	.2961744	.2394832	.1223621	.4052842	-.3682875	-.0595433	-.2941634	-.4498872
6	.2961744	.2871666	.0134720	.3272507	-.4533477	-.3499748	.0816346	-.2266699
7	.2961744	.3346917	-.1120649	.1758949	-.3898355	-.4808601	.4421882	.2900301
8	.2961744	.3819737	-.2516002	-.0457901	-.1478449	-.3065803	.4272264	.5082994
9	.2961744	.4288436	-.4001896	-.3195112	.2471873	.1929422	-.1524172	-.1209233

m/σL = 0.2

$\left(\dfrac{\omega}{n}\right)^2$ RPAC*	.0000000	3.0864325	11.9383442	30.3180805	59.3380071	98.4765507	146.6027733	202.2363283
0	.2742042	.0000000	.3900405	.0000000	.4310980	.0000000	.4359733	.0000000
1	.2742042	.0412915	.3804711	.1477618	.3785281	.2636968	.3046233	.3539548
2	.2742042	.0825681	.3518802	.2787256	.2318308	.4226210	-.0142118	.4144375
3	.2742042	.1238141	.3046276	.3769765	.0226643	.4079869	-.3323193	.1187432
4	.2742042	.1650116	.2393456	.4284233	-.2008270	.2144409	-.4468939	-.2953517
5	.2742042	.2061391	.1569948	.4218691	-.3810235	-.0899971	-.2607607	-.4527083
6	.2742042	.2471691	.0589632	.3503196	-.4608356	-.3711917	.1322321	-.1602685
7	.2742042	.2880642	-.0527595	.2127196	-.3969513	-.4788207	.4569402	.3411361
8	.2742042	.3287692	-.1752563	.0164953	-.1767841	-.3046393	.4039344	.4755520
9	.2742042	.3691947	-.3040181	-.2182323	.1599686	.1221672	-.0961523	-.0770156

*Relative Position Along Cable.

73

Table A-1 (Continued)

$m/\sigma L = 0.3$

$\left(\dfrac{m}{\pi\sigma}\right)^2$ RPAC*	.0000000	3.1029655	13.5323194	36.7557721	73.9155110	124.1780301	186.0556725	257.6526054
0	.2564946	.0000000	.4003055	.0000000	.4399964	.0000000	.4439451	.0000000
1	.2564946	.0367817	.3911996	.1504750	.3853274	.2720856	.3051008	.3658658
2	.2564946	.0735506	.3640223	.2836996	.2333731	.4321971	-.0279438	.4153156
3	.2564946	.1102930	.3192019	.3835449	.0184560	.4095777	-.3498917	.0948211
4	.2564946	.1469942	.2574808	.4361586	-.2082645	.2042275	-.4492531	-.3234203
5	.2564946	.1836366	.1799624	.4311914	-.3875991	-.1051600	-.2405428	-.4488548
6	.2564946	.2201990	.0881914	.3631493	-.4641032	-.3812033	.1578486	-.1236374
7	.2564946	.2566543	-.0157158	.2329507	-.4001623	-.4765330	.4615606	.3624221
8	.2564946	.2929650	-.1288494	.0498269	-.1913585	-.3040107	.3928294	.4588271
9	.2564946	.3290773	-.2471113	-.1661587	.1185571	.0896358	-.0704001	-.0565614

$m/\sigma L = 0.5$

$\left(\dfrac{m}{\pi\sigma}\right)^2$ RPAC*	.0000000	3.1215646	16.7693642	49.7238342	103.0137069	175.2352523	264.2183573	367.2482840
0	.2294157	.0000000	.4148795	.0000000	.4495445	.0000000	.4523760	.0000000
1	.2294157	.0309268	.4063061	.1535697	.3924783	.2812588	.3050857	.3786880
2	.2294157	.0618444	.3807515	.2893235	.2346005	.4422379	-.0434488	.4148895
3	.2294157	.0927428	.3387173	.3908700	.0134226	.4103252	-.3683191	.0675995
4	.2294157	.1236119	.2810586	.4446495	-.2164550	.1922342	-.4497521	-.3517767
5	.2294157	.1544399	.2090151	.4413051	-.3943318	-.1224724	-.2175309	-.4407287
6	.2294157	.1852133	.1242600	.3769945	-.4670016	-.3907732	.1836688	-.0847117
7	.2294157	.2159160	.0289744	.2546147	-.4031302	-.4733765	.4643518	.3807686
8	.2294157	.2465279	-.0740404	.0848989	-.2060210	-.3035553	.3820327	.4420172
9	.2294157	.2770227	-.1811888	-.1126749	.0782539	.0586061	-.0459311	-.0369863

*Relative Position Along Cable.

74

Table A-1 (Concluded)

m/σL = 1.0

$\left(\dfrac{\omega}{n}\right)^2$ RPAC*	.0000000	3.1406012	24.9450282	82.2932502	175.6446073	302.2907418	458.3970799	639.2163398
0	.1873172	.0000000	.4341819	.0000000	.4589444	.0000000	.4605904	.0000000
1	.1873172	.0234823	.4261769	.1567770	.3993648	.2904800	.3045421	.3913607
2	.1873172	.0469598	.4023517	.2950962	.2353681	.4518762	.0594785	.4130257
3	.1873172	.0704273	.3632760	.3532775	.0079629	.4100819	-.3859251	.0393607
4	.1873172	.0938797	.3099048	.4530960	-.2246743	.1794644	-.4481820	-.3776194
5	.1873172	.1173113	.2435853	.4512572	-.4005889	-.1393478	-.1938137	-.4289742
6	.1873172	.1407161	.1660687	.3905697	-.4692627	-.3990287	.2072833	-.0473330
7	.1873172	.1640872	.0795253	.2757116	-.4056018	-.4697147	.4652698	.3948227
8	.1873172	.1874169	-.0134335	.1184886	-.2194452	-.3032597	.3724366	.4266967
9	.1873172	.2106961	-.1097273	-.0625236	.0423702	.0314759	-.0246214	-.0198576

*Relative Position Along Cable.

75
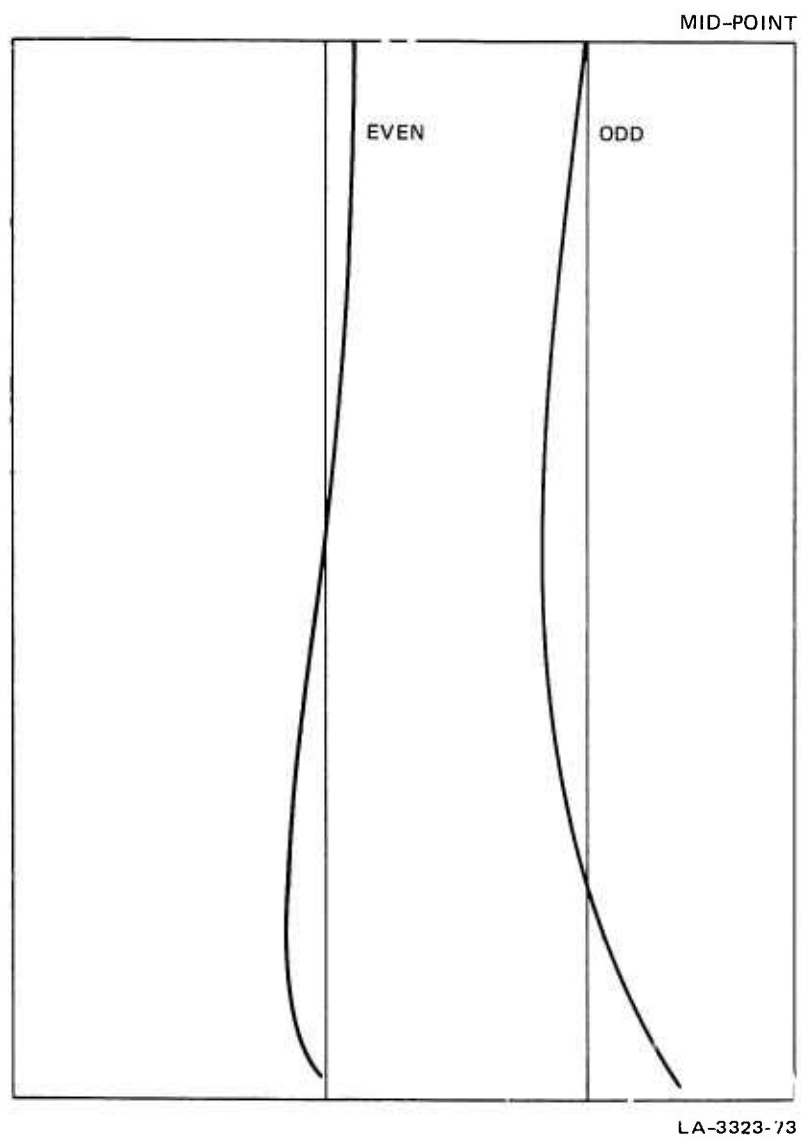
FIGURE A-3   ARRAY SHAPE WITH BOUNCING TIP MASS

d. Large Tip Inertias

(1) Numerical Solution

A solution for the eigenfunctions and eigenvalues of cables with large inertial tips is obtained by a numerical technique that is an elaboration of that already used for the tip masses. This more complicated numerical method is also described in Appendix B. We note that a complete numerical solution of the bouncing-tip-mass problem could be obtained by this method if it were needed.

For the numerical calculations we have taken the inertial tip to be a circular loop of wire with radius, r, and a linear density equal to that of the cable. For this configuration,

$$I_x = m r^2 \tag{A-33}$$

$$I_y = I_z = \frac{1}{2} m r^2 \tag{A-34}$$

where

$$m = 2\pi r\sigma . \tag{A-35}$$

In addition to the radius, the other important variable to be specified for the tip is the distance, b, between its center of mass and its point of attachment to the array. If b is too short, the loop will not be stable in a horizontal orientation but will instead tend to orient its axis of largest moment of inertia in that direction. For this "instability" not to occur, the following condition must be satisfied:

$$I_z - I_x + mb \frac{L}{2} > 0 . \tag{A-36}$$

77

Another consideration in selecting b is to make the natural frequency of the tip mass, when alone in a gravity-gradient field, equal to that of the cable libration. With this matching, one would expect large-amplitude motions for the tip mass and consequently faster damping of the cable libration. The matching condition is

$$I_x = mb \frac{L}{2} .$$

(A-37)

For the case of the circular inertial tip, Condition (A-36) can be put in the form [using Eqs. (A-33) and (A-34)]

$$\frac{b}{L} = 2k \left(\frac{r}{L} \right)^2$$

(A-38)

where

$$k \geq \frac{1}{2} .$$

Note that in this equation when the constant $k = 1.0$, we have the desired match (resonance), and when $k = \frac{1}{2}$ we reach the stability limit of expression (A-36).

In computing the eigenfunctions for this array configuration, all permutations of $r/L = 0.04$, $0.033\overline{3}$, 0.03, and 0.02, and of $k = 2.5$, 1.5, 1.0, 0.75, and 0.5 were examined. The results of the first four even and odd modes are printed in Table A-2. Again, the value of the eigenfunction is not given at the tip but at a distance within 5% of the tip; however, an extrapolated tip value is also given. The amplitude of the modes has been normalized to give a maximum deflection of unity. The tip angle, also printed in a dimensionless form, can be found from either Eq. (A-24) or Eq. (A-25).

78

Table A-2

CALCULATED NORMAL-MODE SHAPES AND FREQUENCIES

FOR A CABLE WITH TIP MASSES IN A GRAVITY-GRADIENT ENVIRONMENT

(a) $r/L = 0.04$

$\left(\dfrac{w}{n}\right)^2$	.0000000	3.0115774	11.79867	30.3108450	59.6964180	99.4729699	149.5790861	$k = 0.5$ 705.60688
y^+	.0024000	.5516051	.50160	-.5011420	-.3601787	-.2754724	-.2237044	-.18797
θ_R	2.5592442	-1.0025392	-.25529	-.0993227	-.0504232	-.0302584	-.0202572	-.01463
RPAC*								
0	.0024000	0.0000000	-.65542	0.0000000	-.9588621	0.0000000	.9037127	0.00000
1	.0024000	.0528478	-.64118	.3259111	-.8534580	-.5382580	.6564598	.68477
2	.0024000	.1056932	-.59861	.6186753	-.5571450	-.9831392	.0432209	.85288
3	.0024000	.1585340	-.52816	.8467001	-.1273710	-.9012790	-.6084942	.35687
4	.0024000	.2113674	-.43053	.985918	.3476504	-.5664432	-.9267407	-.44616
5	.0024000	.2641903	-.30722	1.0000000	.7603473	.0183160	-.6907052	-.90929
6	.0024000	.3169967	-.15964	.8858217	1.0000000	.6337530	-.0139888	-.57778
7	.0024000	.3697873	.00971	.6330288	.9740657	1.0000000	.7695440	.35203
8	.0024000	.4225488	.19742	.2496094	.6351518	.3768206	1.0000000	1.00000
9	.0024000	.4752720	.39843	-.2363478	.0146356	.2022033	.3557006	.48575

*Relative Position Along Cable.

Notes: a. The value of $(w/n)^2$ is given for motion in the plane of the orbit. For out-of-plane motion, the value of $(w/n)^2$ is greater than the listed value by 1.0. This applies only when the tip inertia is symmetrical ($I_{yy} = I_{zz}$).

b. Nine values are given plus the center value (zero for the odd modes). The nine-and-one-half position corresponds to the end of the cable. The value at this position is given as end deflection, y^+.

c. θ_R gives the ratio of the angle of the tip to the slope at the end of the cable.

Table A-2 (Continued)

k = 0.75, r/L = 0.04

$(c/m)^2$	-.0000000	3.0346529	11.83586	30.37189	59.7899111	99.6088140	148.7669689	205.8556419
θ_R	.3804000	-.3837256	.50413	-.50285	-.3614197	-.2764728	-.2246457	-.1886972
RPAC*	*015.2607479	-2.9683951	-.43838	-.15672	-.0775995	-.0460978	-.0307079	-.0221285
0	.3804000	0.0000000	-.65718	0.00000	-.9587285	0.0000000	.9040776	0.0000000
1	.3804000	-.0405003	-.64286	.32615	-.8532585	-.5383344	.6566106	.6849010
2	.3804000	-.0809954	-.60008	.61909	-.5567812	-.8831492	.0429003	.8528250
3	.3804000	-.1214797	-.52929	.84716	-.1268343	-.9010314	-.6091014	.3564169
4	.3804000	-.1619472	-.43129	.98192	.3482479	-.5658465	-.9271336	-.4467459
5	.3804000	-.2023904	-.30732	1.00000	.7607824	.0191264	-.6904104	-.9093576
6	.3804000	-.2428005	-.15911	.88532	1.0000000	.6343949	-.0149457	-.5769988
7	.3804000	-.2831653	.01090	.63195	.9734222	1.0000000	.7704724	.3530255
8	.3804000	-.3234681	.19925	.24801	.6338757	.8759510	1.0000000	1.0000000
9	.3804000	-.3636333	.40080	-.23820	.0131119	.2008716	.3546519	.4846435

k = 1.0, r/L = 0.04

$(c/m)^2$	-.0000000	3.2923483	11.8913241	30.44735	59.8969773	99.7530629	148.96837	205.1182576
θ_R	-.5000000	-.0740226	.5085965	-.50545	-.3632261	-.2779028	-.22596	-.1897146
RPAC*	*009.1710262	-23.7780721	-.6820797	-.22030	-.1062003	-.0624320	-.04137	-.0297341
0	.5000000	0.0000000	-.6602000	0.00000	-.9585366	0.0000000	.90451	0.0000000
1	.5000000	-.0079702	-.6457668	.32650	-.8529935	-.5384148	.6567P	.6850219
2	.5000000	-.0159317	-.6026223	.61969	-.5562994	-.8831389	.04253	.8527242
3	.5000000	-.0238755	-.5312427	.84781	-.1261326	-.9007018	-.60982	.3558677
4	.5000000	-.0317912	-.4324593	.98237	.3490254	-.5650890	-.92760	-.4474192
5	.5000000	-.0396665	-.3075237	1.00000	.7613492	.0201450	-.69004	-.9094093
6	.5000000	-.0474877	-.1582191	.88463	1.0000000	.6352025	.01612	-.5760513
7	.5000000	-.0552340	.0129500	.63044	.9725712	1.0000000	.77162	.3542261
8	.5000000	-.0628782	.2024234	.24572	.6321579	.8748264	1.00000	1.0000000
9	.5000000	-.0703739	.4049500	-.24093	.0199975	.1990763	.35326	.4832092

* Relative Position Along Cable.

80

Table A-2 (Continued)

k = 1.5, r/L = 0.04

$\left(\dfrac{a}{m}\right)^2$	-.0000000	2.9670188	12.1080799	30.65173	60.1563414	100.0994214	149.41357	206.6864339
$y\dagger$	.5000000	.4863034	.5289548	-.51388	-.3687059	-.2821263	-.22977	-.1926600
θ_R	*981.5996113	2.9128854	-1.5089477	-.36988	-.1680490	-.0966504	-.06339	-.0452961
RPAC*								
0	.5000000	0.0000000	-.6737428	0.00000	-.9579658	0.0000000	.90559	0.0000000
1	.5000000	.0510603	-.6587690	.32754	-.8521882	-.5385911	.65723	.6852598
2	.5000000	.1021269	-.6140204	.62147	-.5549414	-.8830569	.04159	.8524128
3	.5000000	.1532064	-.5400269	.84977	-.1241940	-.8997864	-.61166	.3544973
4	.5000000	.2043061	-.4377134	.98377	.3511774	-.5630649	-.92870	-.4490429
5	.5000000	.2554347	-.3084707	1.00000	.7629200	-.0228442	-.68917	-.9094788
6	.5000000	.3066031	-.1542781	.88250	1.0000000	.6373458	.01915	-.5736518
7	.5000000	.3578257	-.0220896	.62573	.9701801	1.0000000	.77463	.3572599
8	.5000000	.4091226	.2166966	.23853	.6272572	.8717649	1.00000	1.0000000
9	.5000000	.4605243	.4237535	-.24966	.0047506	.1940125	.34941	.4793561

k = 2.5, r/L = 0.04

$\left(\dfrac{a}{m}\right)^2$	-.00000	2.9814330	14.2259922	31.38069	60.8933335	100.9737728	150.4868641	708.0045202
$y\dagger$	.50000	.4871192	-.7810179	-.54972	-.3884853	-.2965687	-.2424760	-.2023589
θ_R	*058.63725	1.6460431	-7.6737461	-.79620	-.3132365	-.1717497	-.1102376	-.0778486
RPAC*								
0	.50000	0.0000000	.8440699	0.00000	-.9560069	0.0000000	.9087796	0.0000000
1	.50000	.0512030	.8220996	.33180	-.8494929	-.5390458	.6585532	.6857665
2	.50000	.1024095	.7566134	.62876	-.5504020	-.8826867	.0388673	.8513695
3	.50000	.1536232	.6489111	.85780	-.1176971	-.8968693	-.6170205	.3506306
4	.50000	.2048483	.5012484	.98947	.3583394	-.5567910	-.9322894	-.4534697
5	.50000	.2560897	.3169900	1.00000	.7681616	-.0311678	-.6863970	-.9095036
6	.50000	.3073534	.1008688	.87374	1.0000000	.6439754	.0281565	-.5667496
7	.50000	.3586476	-.1405776	.60628	.9620905	1.0000000	.7837274	.3459853
8	.50000	.4099835	-.3982469	.20862	.6104462	.8620392	1.0000000	1.0000000
9	.50000	.4613782	-.6590539	-.28638	-.0171781	.1773748	.3371343	.4675195

*Relative Position Along Cable.

Table A-2 (Continued)

r/L = 0.033 k = 0.5

$\left(\frac{m}{n}\right)^2$ / y⁺ / θ_R	.0000000	3.0074421	11.21201	27.8994665	54.1791615	89.6813391	133.4656952	184.25602
θ_R	.0016667	.5011136	.50111	.5011114	-.4190437	-.3225574	-.2607244	-.22155
RPAC*	*C00.4816170	-1.0019632	-.26832	-.1077936	-.0555017	-.0335286	-.0225288	-.01631
0	.0016667	0.0000000	-.58817	0.0000000	-.9532935	0.0000000	.8869434	0.00000
1	.0016667	.0527834	-.57491	-.2837524	-.8494410	-.5306182	.6489179	.66995
2	.0016667	.1055652	-.53525	-.5387448	-.5569828	-.8740100	.0554373	.84547
3	.0016667	.1583437	-.46956	-.7374051	-.1312894	-.8989469	-.5837735	.37548
4	.0016667	.2111170	-.37847	-.8546253	.3418515	-.5753486	-.9101440	-.41278
5	.0016667	.2638827	-.26299	-.8692360	.7562558	.0019783	-.6989006	-.89647
6	.0016667	.3166381	-.12452	-.7658479	1.0000000	.6209543	-.0140922	-.60474
7	.0016667	.3693790	.03489	-.5373532	.4755614	1.0000000	.7472383	.31543
8	.0016667	.4220997	.21226	-.1886724	.6270175	.8827520	1.0000000	1.00000
9	.0016667	.4747910	.40297	.2569219	-.0225023	.1826924	.3470584	.49146

r/L = 0.033 k = 0.75

$\left(\frac{m}{n}\right)^2$ / y⁺ / θ_R	.0000000	3.0222921	11.2364512	27.93910	54.23849	89.7659358	133.5812023	184.40775R4
θ_R	-.3787500	-.3806009	.5028896	.50264	-.42000	-.3232750	-.2614790	-.2221286
RPAC*	*099.9999981	-2.9954380	-.4644368	-.17086	-.08563	-.0511609	-.0341874	-.0246866
0	.3787500	0.0000000	-.5894134	0.00000	-.95318	0.0000000	.8872084	0.0000000
1	.3787500	-.0401420	-.5761031	-.28414	-.84928	-.5306677	.6490265	.6699209
2	.3787500	-.0802803	-.5362934	-.53945	-.55670	-.8740050	.0552057	.8453900
3	.3787500	-.1204111	-.4703570	-.73829	-.13087	-.8987467	-.5842274	.3751223
4	.3787500	-.1605301	-.3789491	-.85552	.34231	-.5748845	-.9104448	-.4132276
5	.3787500	-.2006319	-.2630659	-.86992	.75659	.0026069	-.6996854	-.8965255
6	.3787500	-.2407100	-.1241483	-.76612	1.00000	.6214564	-.0133609	-.6041369
7	.3787500	-.2807554	.0357367	-.53705	.97505	1.0000000	.7479670	.3162232
8	.3787500	-.3207547	.2135598	-.18773	.62600	.8820526	1.0000000	1.0000000
9	.3787500	-.3606871	.4046517	.25837	-.02371	.1816115	.3461957	.4905268

* Relative Position Along Cable.

Table A-2 (Continued)

k = 1.0, r/L = 0.033

$\left(\frac{n}{m}\right)^2$	-.0000000	3.2295872	11.2736589	27.98899	54.3075603	89.8601866	133.70650	184.5696064
θ_R	.5000000	-.5579070	.5060756	.50498	-.4214112	-.3244735	-.26253	-.2229414
y^+ / RPAC*	*024.4085595	-29.6996331	-.7307715	-.24143	-.1175227	-.0694048	-.04611	-.0331969
0	.5000000	0.0000000	-.5915677	0.00000	-.9530313	0.0000000	.88752	0.0000000
1	.5000000	-.0062204	-.5781713	-.28471	-.8490667	-.5307188	.64915	.6699839
2	.5000000	-.0124350	-.5381060	-.54049	-.5563274	-.8739817	.05492	.8452910
3	.5000000	-.0186376	-.4717531	-.73962	-.1303361	-.8984800	-.58477	.3746909
4	.5000000	-.0248213	-.3797823	-.85685	.3429112	-.5742919	-.91080	-.4137395
5	.5000000	-.0309778	-.2632122	-.87097	.7570321	.0034014	-.69841	-.896560*
6	.5000000	-.0370965	-.1235152	-.76657	1.0000000	.6220908	-.01245	-.6033964
7	.5000000	-.0431632	.0371967	-.53666	.9743828	1.0000000	.74867	.317179*
8	.5000000	-.0491572	.2158306	-.18639	.6246342	.9811453	1.0000000	1.0000000
9	.5000000	-.0550454	.4076214	.26055	-.0254100	.1801519	.34505	.489325*

k = 1.5, r/L = 0.033

$\left(\frac{n}{m}\right)^2$	-.0000000	2.9784093	11.4270062	28.12761	54.4784300	90.0797377	133.98792	184.9247146
θ_R	.5000000	.4903349	.5212912	.51274	-.4257189	-.3278292	-.26560	-.2253038
y^+ / RPAC*	*030.5782013	2.9400401	-1.6880920	-.41055	-.1871188	-.1078318	-.07092	-.0506528
0	.5000000	0.0000000	-.6016709	0.00000	-.9525706	0.0000000	.88831	0.0000000
1	.5000000	.0515165	-.5878743	-.28656	-.8484348	-.5308279	.64947	.6700948
2	.5000000	.1030375	-.5466208	-.54387	-.5552659	-.8738798	.05421	.8449708
3	.5000000	.1545678	-.4783287	-.74391	-.1288191	-.8977356	-.58616	.3736033
4	.5000000	.2061128	-.3837333	-.86123	.3445887	-.5726969	-.91172	-.4149834
5	.5000000	.2576791	-.2639513	-.87444	.7582626	.0055217	-.69772	-.8966011
6	.5000000	.3092748	-.1205961	-.76815	1.0000000	.6237854	-.01011	-.6015067
7	.5000000	.3609113	.0440220	-.53552	.9724791	1.0000000	.75125	.3196106
8	.5000000	.4126048	.2265245	-.18212	.6206993	.8786640	1.00000	1.0000000
9	.5000000	.4643915	.4217181	.26764	-.0304230	.1760197	.3418*	.486096*

* Relative Position Along Cable.

83

Table A-2 (Continued)

r/L = 0.033   k = 2.5

$\left(\frac{a}{\pi}\right)^2$	-.00000	2.9879002	13.4661746	28.6514R	54.9818859	90.6593303	134.6846256	185.7684181
$y+$	.50000	.4909577	-.5119072	.54827	-.4415876	-.3394383	-.2758885	-.2331303
θ_R	*046.06980	1.6523644	-11.6710840	-.92003	-.3542354	-.1932240	-.1237914	-.0873647
RPAC*								
0	.50000	0.0000000	.5094847	0.00000	-.9509519	0.0000000	.9906499	0.0000000
1	.50000	.0516251	.4957450	-.29491	-.8462441	-.5310977	.6504199	.6702755
2	.50000	.1032526	.4547748	-.55916	-.5516392	-.8734600	.0521350	.8439183
3	.50000	.1548855	.3873374	-.76342	-.1236668	-.8953312	-.5902411	.3704906
4	.50000	.2065265	.2947657	-.88121	.3502810	-.5676848	-.9144296	-.4184108
5	.50000	.2581795	.1790676	-.89050	.7624469	.0121456	-.6956744	-.8965725
6	.50000	.3098490	.0431086	-.77580	1.0000000	.6290908	-.0030968	-.5960115
7	.50000	.3615412	-.1090701	-.53098	.9659214	1.0000000	.7584976	.3266591
8	.50000	.4132654	-.2716731	-.16329	.6069502	.8707014	1.0000000	1.0000000
9	.50000	.4650361	-.4359989	.29971	-.0483687	.1623146	.3317326	.4761482

r/L = 0.03   k = 0.5

$\left(\frac{a}{\pi}\right)^2$	-.0000000	3.0057441	10.92534	26.7074158	51.4317448	84.78616	125.8915839	173.5354589
$y+$	.0013500	.5009016	.50090	.5009002	-.4565666	-.35290	-.2846396	-.2437204
θ_R	*998.7518749	-1.0016851	-.27522	-.1125533	-.0534409	-.03544	-.0238739	-.0173192
RPAC*								
0	.0013500	0.0000000	-.55448	0.0000000	-.9500370	0.00000	.8771363	0.0000000
1	.0013500	.0527552	-.54171	-.2625463	-.8470628	-.52622	.6444236	.6613741
2	.0013500	.1055092	-.50352	-.4985219	-.5567928	-.86872	.0624079	.8412721
3	.0013500	.1582604	-.44022	-.6823698	-.1334322	-.89753	-.5693275	.3863023
4	.0013500	.2110074	-.35238	-.7906446	.3386066	-.58044	-.9000973	-.3930941
5	.0013500	.2637483	-.24089	-.8033035	.7539485	-.00754	-.7032750	-.8884768
6	.0013500	.3164807	-.10700	-.7053573	1.0000000	.61339	-.0305798	-.6205389
7	.0013500	.3692011	.04741	-.4891855	.9763143	1.00000	.7336967	-.2930561
8	.0013500	.4219045	.21962	-.1581424	.6217339	.88635	1.0000000	1.0000000
9	.0013500	.4745928	.40523	.2670455	-.0460805	.17019	.3417652	.4956179

*Relative Position Along Cable.

84

Table A-2 (Continued)

k = 0.75, r/L = 0.03

$\left(\frac{r}{m}\right)^2$	-.0000000	3.0172114	10.9444879	26.73837	51.4775728	84.8508228	125.97921	173.6500645
y^+	.3780375	-.3793203	.5023496	.50214	-.4573889	-.3536794	-.28530	-.2442214
θ_R	033.5034847	-2.9979841	-.4783703	-.17886	-.0903055	-.0541423	-.03625	-.0262124
RPAC*								
0	.3780375	0.0000000	-.5554918	0.00000	-.9499423	0.0000000	.87735	0.0000000
1	.3780375	-.0399937	-.5426844	-.26286	-.8469266	-.5262602	.64451	.6614194
2	.3780375	-.0799844	-.5043684	-.49910	-.5565521	-.8687116	.06221	.8411950
3	.3780375	-.1199691	-.4408716	-.68310	-.1330304	-.8973576	-.56970	.3859914
4	.3780375	-.1599441	-.3527717	-.79138	.3399990	-.5800492	-.90035	-.3934683
5	.3780375	-.1999052	-.2409525	-.80387	.7542367	-.0070069	-.70309	-.8885131
6	.3780375	-.2398469	-.1067029	-.70559	1.0000000	.6138147	-.02995	-.6200134
7	.3780375	-.2797616	.0481053	-.48895	.9758756	1.0000000	.73432	.2937457
8	.3780375	-.3196378	.2206804	-.15739	.6208501	.8857421	1.00000	1.0000000
9	.3780375	-.3594568	.4066039	.26823	-.0471381	.1692377	.34099	.4947747

k = 1.0, r/L = 0.03

$\left(\frac{r}{m}\right)^2$	-.0000000	3.1996528	10.9739681	26.77772	51.5314213	84.9234797	126.07500	173.7731274
y^+	.5000000	-.0502726	.5049679	.50405	-.4595995	-.3546596	-.28623	-.2449323
θ_R	*993.9029865	-33.8191828	-.7572084	-.25347	-.1241316	-.0735221	-.04893	-.0352653
RPAC*								
0	.5000000	0.0000000	-.5572619	0.00000	-.9498072	0.0000000	.87761	0.0000000
1	.5000000	-.0053933	-.5443840	-.26333	-.8467383	-.5262985	.54461	.6614574
2	.5000000	-.0107821	-.5058589	-.49995	-.5562302	-.8686838	.06197	.8410849
3	.5000000	-.0161613	-.4420209	-.68419	-.1326163	-.8971222	-.57017	.3856152
4	.5000000	-.0215256	-.3534594	-.79249	.3395144	-.5795364	-.90066	-.3939043
5	.5000000	-.0268681	-.2410759	-.80475	.7546155	-.0063208	-.70287	-.8885396
6	.5000000	-.0321803	-.1061847	-.70599	1.0000000	.6143647	-.02918	-.6193709
7	.5000000	-.0374504	.0493058	-.48866	.9752911	1.0000000	.73511	.2945839
8	.5000000	-.0426608	.2225509	-.15630	.619653.	.8849429	1.00000	1.0000000
9	.5000000	-.0477828	.4090505	.27000	-.0486208	.1679456	.33997	.4936902

* Relative Position Along Cable.

85

Table A-2 (Continued)

k = 1.5   r/L = 0.03

$\left(\dfrac{n}{\omega}\right)^2$	-.0000000	2.9832085	11.0991244	26.98870	51.6663047	85.0946089	126.29226	174.0455633
y	.5000000	.4921172	.5178007	.51045	-.4623224	-.3575826	-.28893	-.2470042
θ_R	*990.8380775	2.9518579	-1.7916159	-.43419	-.1983572	-.1144726	-.07525	-.0538617
RPAC* 0	.5000000	0.0000000	-.5657741	0.00000	-.9494028	0.0000000	.87827	0.0000000
1	.5000000	.0517196	-.5525606	-.26485	-.8461880	-.5263783	.64487	.6615127
2	.5000000	.1034429	-.5130385	-.50274	-.5553133	-.8685756	.06137	.8407644
3	.5000000	.1551739	-.4475722	-.68774	-.1313092	-.8964635	-.57134	.3846612
4	.5000000	.2069169	-.3568039	-.79613	.3409611	-.5781502	-.90144	-.3949690
5	.5000000	.2586776	-.2417152	-.80767	.7556798	-.0044817	-.70229	-.8885642
6	.5000000	.3104627	-.1037363	-.70736	1.0000000	.6158398	-.02717	-.6177238
7	.5000000	.3622819	.0550591	-.48779	.9736289	1.0000000	.73719	.2967211
8	.5000000	.4141496	.2315833	-.15283	.6162000	.8827510	1.00000	1.0000000
9	.5000000	.4660892	.4209629	.27585	-.0530218	.1642799	.33715	.4907730

k = 2.5   r/L = 0.03

$\left(\dfrac{n}{\omega}\right)^2$	-.00000	2.9906079	9.9675878	27.32257	52.0722151	85.5545506	126.8389115	174.7025687
y	.50000	.4926415	.3965260	.54047	-.4762093	-.3677670	-.2580048	-.2538962
θ_R	*030.64907	1.6551127	6.9829817	-.99653	-.3789698	-.2061440	-.1319484	-.0930997
RPAC* 0	.50000	0.0000000	-.4884855	0.00000	-.9479638	0.0000000	.8802092	0.0000000
1	.50000	.0518111	-.4782560	-.27190	-.8442561	-.5265686	.6456505	.6615525
2	.50000	.1036242	-.4476096	-.51566	-.5521421	-.8681471	.0595975	.8397195
3	.50000	.1554416	-.3966763	-.70428	-.1268167	-.8943198	-.5748229	.3819077
4	.50000	.2072658	-.3256861	-.81315	.3459273	-.5737588	-.9037728	-.3979229
5	.50000	.2590998	-.2349920	-.82147	.7593399	-.0013080	-.7005496	-.8885064
6	.50000	.3109475	-.1251118	-.71415	1.0000000	.6204918	-.0211059	-.6129032
7	.50000	.3628143	.0031976	-.48427	.9678410	1.0000000	.7435267	.3029496
8	.50000	.4147081	.1487980	-.13712	.6040157	.8756742	1.0000000	1.0000000
9	.50000	.4666421	.3099710	.30294	-.0689454	.1520536	.3280601	.4817677

*Relative Position Along Cable.

Table A-2 (Continued)

		r/L = 0.02					k = 0.5
$\left(\frac{n\pi}{L}\right)^2$	-.0000000	3.0020872	10.10364	23.2131015	43.2547380	70.0889774	103.0218779	141.01008
y+	.0006000	.5004003	.50040	.5004000	.5004000	.4489003	.3565687	.28819
θR	*997.1618710	-1.0009110	-.29723	-.1193541	-.0694159	-.0428384	-.0291440	-.02129
RPAC*								
0	.0006000	0.0000000	-.45297	0.0000000	.7489325	0.0000000	-.7537101	0.00000
1	.0006000	.0526872	-.44171	-.1990308	.6691819	.4619436	-.5625528	-.51435
2	.0006000	.1053739	-.40797	-.3779567	.4435826	.7690090	-.0789000	-.67396
3	.0006000	.1580595	-.35195	-.5172126	.1121589	.8078812	.4615805	-.34888
4	.0006000	.2107432	-.27599	-.5983770	-.2615887	.5427377	.7714383	.25778
5	.0006000	.2634243	-.17464	-.6049250	-.5958798	.0394582	.6436523	.69651
6	.0006000	.3161016	-.05471	-.5232766	-.7988610	-.5290628	.0843263	.55565
7	.0006000	.3687734	.08458	-.3444375	-.7812815	-.9059505	-.6088695	-.16256
8	.0006000	.4214370	.24125	-.0669338	-.4768597	-.8161557	-.897621	-.81494
9	.0006000	.4740874	.41184	.2969391	.1212758	-.1021994	-.2968637	-.42361

*Relative Position Along Cable.

87

Table A-2 (Continued)

k = 0.75, r/L = 0.02

$\left(\frac{n}{\omega}\right)^2$	-.0000000	3.0061995	10.1110235	23.2251752	43.27216	70.11278	103.0535584	141.0506787
$y^{\dagger}$	.3763500	-.3765524	.5010574	.5009624	.50093	.44917	.3568250	.2884239
θ_R	*998.4793892	-3.0020020	-.5235414	-.2074331	-.10787	-.06566	-.0443672	-.0322963
RPAC*								
0	.3763500	0.0000000	-.4534348	0.0000000	.74917	0.00000	-.7536092	0.0000000
1	.3763500	-.0396676	-.4421496	-.1391753	.66938	.46188	-.5624446	-.5143561
2	.3763500	-.0793340	-.4083566	-.3782218	.44365	.76888	-.0787916	-.6739042
3	.3763500	-.1189978	-.3522504	-.5175524	.11205	.80767	.4616365	-.3487356
4	.3763500	-.1586575	-.2741779	-.5987274	-.26185	.54246	.7713636	.2579450
5	.3763500	-.1983112	-.1746815	-.6052096	-.59623	.03918	.6434108	.6965243
6	.3763500	-.2379563	-.0545775	-.5234163	-.79916	-.52920	.0840057	.5554072
7	.3763500	-.2775891	.0848923	-.3443645	-.78138	-.90582	-.6090365	-.1628989
8	.3763500	-.3172034	.2417427	-.0666124	-.47653	-.81570	-.8073951	-.8149525
9	.3763500	-.3567850	.4124706	.2974776	.12180	-.10165	-.2863500	-.4231521

k = 1.0, r/L = 0.02

$\left(\frac{n}{\omega}\right)^2$	-.0000000	3.1162707	10.1228227	23.24108	43.2933954	70.1404937	103.08890	141.0956166
$y^{\dagger}$	.5000000	-.0291607	.5022770	.50183	.5017195	.4495442	.35717	.2887375
θ_R	*009.1272850	-56.3379674	-.8448491	-.29704	-.1491816	-.0895206	-.06604	-.0435207
RPAC*								
0	.5000000	0.0000000	-.4542577	0.00000	.7495336	0.0000000	-.75341	0.0000000
1	.5000000	-.0031143	-.4429404	-.19939	.6696691	.4617764	-.56226	-.5143085
2	.5000000	-.0062268	-.4090518	-.37861	.4437592	.7686540	-.07865	-.6737746
3	.5000000	-.0093355	-.3527890	-.51806	.1119173	.8073320	.46166	-.3485276
4	.5000000	-.0124382	-.2745037	-.59925	-.2622233	.5420574	.77120	.2581199
5	.5000000	-.0155321	-.1747454	-.60564	-.5967300	.0388268	.64305	.6964807
6	.5000000	-.0186133	-.0543411	-.52363	-.7996141	-.5293512	.08359	.5550657
7	.5000000	-.0216765	.0854514	-.34427	-.7815576	-.9055873	-.60919	-.1632994
8	.5000000	-.0247125	.2426214	-.06613	-.4763521	-.8150615	-.89703	-.8149012
9	.5000000	-.0277051	.4136221	.29829	.1225596	-.1009116	-.28565	-.4225249

*Relative Position Along Cable.

88

Table A-2 (Concluded)

k = 1.5, r/L = 0.02

$\left(\dfrac{a}{m\,\pi}\right)^2$	-.0000000	2.9938559	10.1783300	23.28837	43.3491034	70.2086826	103.17296	141.1091073
θ_R	.5000000	.4964403	.5088151	.50485	.5041807	.4506168	.35816	.2896201
RPAC*	*021.3140182	2.9796441	-2.1703599	-.52248	-.2416877	-.1405516	-.09286	-.0667389
0	.5000000	0.0000000	-.4585757	0.00000	.7506230	0.0000000	-.75274	0.0000000
1	.5000000	.0522171	-.4470912	-.20011	.6705610	.4613670	-.56165	-.5140734
2	.5000000	.1044358	-.4127053	-.37994	.4441108	.7678574	-.07826	-.6732974
3	.5000000	.1566578	-.3556277	-.51977	.1115359	.8062295	.46163	-.3479245
4	.5000000	.2038852	-.2762327	-.60104	-.2633053	.5408443	.77061	.2585073
5	.5000000	.2611204	-.1751051	-.60713	-.5982184	-.0378484	.64198	.6962203
6	.5000000	.3133668	-.0531242	-.52442	-.8009749	-.5296327	.08250	.5540720
7	.5000000	.3656293	.0883729	-.34378	-.7821217	-.9047587	-.60951	-.1643050
8	.5000000	.4179158	.2472506	-.06158	-.4755400	-.8131103	-.89591	-.8146190
9	.5000000	.4702413	.4197453	.30106	-.1249359	-.0987665	-.28367	-.4207599

k = 2.5, r/L = 0.02

$\left(\dfrac{a}{m\,\pi}\right)^2$	.00000	2.9965781	9.7671457	23.4989537	43.5306064	70.4051253	103.3987527	141.46490
θ_R	.50000	.4966938	.4574018	.5205429	.5138321	.4542842	.3614304	.29247
RPAC*	*030.49720	1.6616241	6.5682324	-1.3165540	-.4785418	-.2581193	-.1648807	-.11637
0	.50000	0.0000000	-.4255102	0.0000000	-.7548525	0.0000000	-.7501670	0.0000000
1	.50000	.0522614	-.4152897	-.2037830	-.6740456	-.4596987	-.5594168	-.51301
2	.50000	.1045237	-.3846676	-.3867126	-.4455541	-.7647139	-.0770555	-.67142
3	.50000	.1567879	-.3337652	-.5285254	-.1101962	.8020781	.4612015	-.34592
4	.50000	.2090550	-.2627998	-.6102070	-.2673330	.5365371	.7682716	.25944
5	.50000	.2613265	-.1721113	-.6148107	-.6038579	.0346606	.6382664	.69496
6	.50000	.3136042	-.0622124	-.5285957	-.8062332	.0790898	.6100973	.55076
7	.50000	.3658909	.0661145	-.3427982	-.7844548	-.9014601	-.6100973	-.16719
8	.50000	.4181910	.2116149	-.0567892	-.4726545	-.8061715	-.8918864	-.81328
9	.50000	.4705127	.3720664	.3152330	.1335060	-.0914316	-.2771393	-.41504

*Relative Position Along Cable.

89

2) Approximate Analytic Solution

Because of the similarity of the two configurations, one can reasonably assume that the solution to the tip inertia problem will be similar to that of the tip mass problem. That is, the solution for the lowest mode will be the straight libration mode plus a sm perturbation.

$$y = \xi + \epsilon\, y_o \tag{A-39}$$

Substitution of this equation into the differential Eq. (A-11) yields, after some manipulation,

$$(1 - \xi^2)\, \frac{d^2 y_o}{d\xi^2} - 2\xi\, \frac{dy_o}{d\xi} + 2y_o - \xi = 0 \tag{A-40}$$

whose solution is

$$y_o = -\frac{\xi}{6} \ln (1 - \xi^2) + \xi\, 0(\epsilon) \quad . \tag{A-41}$$

Hence,

$$y = A\xi \left[1 - \frac{\epsilon}{6} \ln (1 - \xi^2) + 0(\epsilon^2) \right] \tag{A-42}$$

where

$$\left(\frac{\omega}{n}\right)^2 = \frac{3}{2} (2 - \epsilon) \quad . \tag{A-43}$$

90

The use of Eq. (A-42) and the boundary condition given in Eq. (A-27) allows us to arrive at an approximate relationship between ϵ and values of r/L and b/L (or k):

$$1 + \frac{\epsilon}{24\pi\left(\dfrac{r}{L}\right)\left(1 + 2\,\dfrac{b}{L}\right)} = \frac{1 - \dfrac{\epsilon}{6}}{\left(1 + \dfrac{2b}{L}\right)\left[1 - \dfrac{\left(\dfrac{2b}{L}\right)\left(1 - \dfrac{\epsilon}{6}\right)}{1 + \dfrac{2b}{L} - \dfrac{2 - \dfrac{\epsilon}{6}}{2k}}\right]} \, . \quad \text{(A-44)}$$

The values of ϵ found from the above equation are close to those that can be inferred from the ta' ation of our numerical results. In particular, we find that when $0.5 < k < 1.0$, the tip of the cable bends inward, and the natural frequency is slightly increased. When $k > 1.0$, the tip bends away from the local vertical, and the natural frequency is slightly decreased.

91

Appendix B

NUMERICAL METHODS USED IN THE SIMULATIONS OF THE OSCILLATING CABLE

by

Samuel Schechter

Appendix B

NUMERICAL METHODS USED IN THE SIMULATIONS OF
THE OSCILLATING CABLE

Numerical solutions are usually generated by writting the steady-state equations of motion of a system in finite-difference form. This procedure results in a matrix equation that can be manipulated by standard computer routines to yield the eigenvalues and eigenfunctions that correspond to the frequencies and modes of vibration of the system.

In the case of the tip inertia, however, the boundary conditions contain the natural frequency information. The matrix to be solved thus contains entries that are only known after the matrix itself is solved by the conventional means. An iterative procedure to obtain the eigenvalues could be used--that is, the eigenvalues could be estimated to give all the matrix entries and the matrix solved. If the eigenvalues so obtained matched the assumed values, the problem would be solved; otherwise a new eigenvalue would be assumed and the process repeated.

This appendix discusses a relatively new, expanded matrix method for generating the desired eigenvalues and eigenfunctions without iteration. One should note that because of the expanded matrix, this method generates spurious eigenvalues and eigenfunctions that are sometimes difficult to distinguish from the desired solutions.

1. The Eigenvalue Problem

We write Eqs. (A-11) and A-12) in the form

$$- (fy')' = \Omega y \qquad \qquad (B-1)$$

$$- (fz')' = \hat{\Omega} z \qquad \qquad (B-2)$$

where

$$f = 1 - \xi^2, \quad y' = \frac{dy}{d\xi}, \quad \Omega = \frac{2}{3}\left(\frac{\omega}{n}\right)^2, \quad \hat{\Omega} = \frac{2}{3}\left(\frac{\omega^2}{n^2} - 1\right) \qquad . \qquad (B-3)$$

The boundary conditions for y are of the form

$$\begin{cases} y(o) = 0 \qquad \text{odd case} \\ y'(o) = 0 \qquad \text{even case} \end{cases} \qquad (B-4)$$

$$(\overline{\xi}) = \Omega \cdot q \qquad \qquad (B-5)$$

where

$$\overline{\xi} = \frac{1}{\sqrt{1 + \frac{4m}{cL} b_1}} \qquad \qquad (B-6)$$

$$F(\xi) = 2\xi y'/y \qquad \qquad (B-7)$$

$$b_1 = 1 + b_o, \quad b_o = 2b/L \qquad \qquad (B-8)$$

and $q = Q(\Omega)$ = a given function of Ω, and b/L = a given constant. The boundary conditions for z are the same as for y except that Ω is replaced by $\hat{\Omega}$, and Q may be changed.

The problem is to determine the eigenvalues Ω (or $\hat{\Omega}$) and the corresponding eigenfunctions y (or z) that satisfy Eqs. (B-1) through (B-5). Because q is a function of Ω, the eigenvalue problem is in general nonlinear. For $q \equiv 1$, and $m = 0$, we obtain odd or even Legendre polynomials depending on the boundary condition at y(o).

96

2. Numerical Approximation

We will use a finite difference approximation to solve the differential equations over the interval $(0, \bar{\xi})$; we give the details only for the y function. We employ a standard centered difference technique over a uniform mesh given by $\xi_k = k \cdot h$, for $k = 0, 1, 2, \ldots, N$, and h is the mesh interval given by

$$h = \bar{\xi}/(N - 1/2) \qquad (B-9)$$

where

$$\bar{\xi} = \left(\xi_N + \xi_{N+1}\right)/2 = Nh + h/2 = \xi_N + h/2 \qquad . \qquad (B-10)$$

Our approach is to set $y(\xi_k) = y_k$ and obtain an approximation at ξ_k, with an error constrained to be on the order of h^2. That is,

$$-(fy')' = \left[- f_k^- y_{k-1} + \left(f_k^- + f_k^+\right)y_k - f_k^+ y_{k+1}\right]/h^2 + 0(h^2)$$

$$\qquad (B-11)$$

where

$$f_k^\pm = 1 - \left(\xi_k \pm \frac{h}{2}\right)^2 \quad , \quad 0 \le k \le N \quad . \qquad (B-12)$$

For example, with this equation and the symmetric (even) boundary condition at the origin ($y_1 = y_{-1}$), the first iteration at $\xi = 0$ becomes

$$af_o^+ y_o - 2f_o^+ y_1 = h^2 \, \Omega y_o \qquad (B-13)$$

since $f_o^+ = f_o^-$.

The other boundary condition--i.e., Eq. (B-5)-- at $\xi = \bar{\xi}$ can be written using

$$y(\bar{\xi}) = \bar{y} = (y_{N+1} + y_N)/2$$

97

$$y'(\overline{\xi}) = \overline{y}' = (y_{N+1} - y_N)/h \qquad ,$$

as

$$\overline{\xi}(y_{N+1} - y_N) = h\Omega q \cdot (y_N + y_{N+1})/2 \qquad (B-14)$$

again with an accuracy of the order of h^2. Elsewhere, for $1 \leq k \leq N$, we use Eq. (B-11) to get

$$e_k y_{k-1} + a_k y_k + e_{k+1} y_{k+1} = h^2 \Omega y_k \qquad (B-15)$$

where

$$e_k = -f_k^- = -\left[1 - \left(kh - \frac{h}{2}\right)^2\right] = -\left[1 - \left(2k - 1\right)^2 \left(\frac{h}{2}\right)^2\right] \qquad (B-16)$$

$$e_{k+1} = -f_k^+ = -\left[1 - \left(kh + \frac{h}{2}\right)^2\right] = -\left[1 - \left(2(k+1) - 1\right)^2 \left(\frac{h}{2}\right)^2\right] \qquad (B-17)$$

$$a_k = -\left[e_k + e_{k+1}\right] \qquad . \qquad (B-18)$$

Now, we let

$$\lambda = h^2 \Omega \qquad (B-19)$$

and rewrite Eq. (B-14) as

$$-y_N + y_{N+1} = \frac{\tau_0}{2} \lambda q(y_N + y_{N+1}) = q_o \lambda(y_N + y_{N+1}) \qquad (B-20)$$

where

$$q_o = \frac{\tau_o}{2} q \qquad \tau_o = 1/2 \ \xi^+ h \qquad .$$

Then Eqs. (B-15) and (B-20) can be written in matrix form as follows:

$$A_1 y = \lambda B_1 y \qquad (B-21)$$

98

where

$$y = (y_o, y, y_2, \ldots, y_N, y_{N+1})^T \qquad \text{(B-22)}$$

and

$$A_1 = \begin{bmatrix} & & & & & | & 0 \\ & & & & & | & . \\ & & A_o & & & | & . \\ & & & & & | & . \\ & & & & & | & e_{N+1} \\ - & - & - & - & - & - & | & - & - \\ 0 & . & . & . & 0 & -1 & | & 1 \end{bmatrix} \qquad \text{(B-23)}$$

and A_o is a tridiagonal square matrix of order N+1 with $(a_o, a_1, \ldots, a_N)$ as its main diagonal, $(2e_1, e_2, \ldots, e_N)$ as its superdiagonal, $(e_1, e_2, \ldots, e_N)$ as its subdiagonal, and zeroes elsewhere.

The matrix B_1 is given by

$$B_1 = \begin{bmatrix} & & & & & | & 0 \\ & & & & & | & . \\ & & I & & & | & . \\ & & & & & | & . \\ & & & & & | & 0 \\ - & - & - & - & - & - & | & - & - \\ 0 & . & . & . & 0 & q_o & | & q_o \end{bmatrix} \qquad \text{(B-24)}$$

where I is the unit matrix of order N+1. Since q is in general a function of λ, Eq. (B-21) represents a "nonlinear" eigenvalue problem. To solve this system for a general q would require special techniques; however, in our problem q is a continued fraction. This allows us to transform our problem into a generalized (but linear) eigenvalue problem:

$$Ay = \lambda By \qquad \text{(B-25)}$$

where B is independent of λ.

3. Solution of the Eigenvalue Problem

The function $q = Q(\Omega)$ often has the form

$$q = \frac{1}{b_1} \cdot \frac{1}{q_1} \qquad \text{(B-26)}$$

where

$$q_1 = 1 - \frac{b_2 \lambda}{b_3 + b_4 \lambda} = 1 - \frac{b_2 \lambda}{q_2} \qquad . \qquad \text{(B-27)}$$

We assume this is valid for our case. In order to reduce our problem to the form of Eq. (B-25), we introduce a new variable y_{N+2} defined by

$$y_{N+2} = \frac{1}{q_1} \left(y_N + y_{N+1} \right) \qquad . \qquad \text{(B-28)}$$

This allows us to reexpress Eq. (B-20) as

$$- y_N + y_{N+1} = \frac{\tau_o}{2b_1} \lambda \frac{1}{q_1} \left(y_N + y_{N+1} \right) = \frac{\tau}{2} \lambda y_{N+2} \qquad \text{(B-29)}$$

which is in a linear format, with $\tau = \tau_o/b_1$. Likewise the relation for q_1 yields

$$y_{N+2} - \frac{b_2 \lambda}{q_2} y_{N+2} = y_N + y_{N+1} \qquad \text{(B-30)}$$

$$q_2 = b_3 + b_4 \lambda \qquad . \qquad \text{(B-31)}$$

Now, we introduce another variable defined by

$$y_{N+3} = \frac{1}{q_2} y_{N+2} \qquad . \qquad \text{(B-32)}$$

Then Eq. (B-30) can be written in the form

$$- y_N - y_{N+1} + y_{N+2} = \lambda b_2 y_{N+3} \qquad \text{(B-33)}$$

100

which is also in a linear format. Finally, from Eq. (B-32) we get the
lin ar equation

$$b_3 y_{N+3} - y_{N+2} = - b_4 \lambda y_{N+3} \quad . \tag{B-34}$$

(This process is analogous to the evaluation of a polynomial by nesting
of variables.)

By combining Eq. (B-21) with Eqs. (B-29), (B-33), and (B-34) we
obtain the desired form for Eq. (B-25).

Since each of our equations, except (B-33), involves only three of
the variables and since the most efficient methods for solving Eq. (B-25)
will be applied to either tridiagonal or Hessenberg matrices, we will
change Eq. (B-33) by eliminating y_N. Thus if we subtract Eq. (B-33)
from Eq. (B-29) we get

$$2y_{N+1} - y_{N+2} = \lambda\left(\frac{\tau}{2} y_{N+2} - b_2 y_{N+3}\right) \tag{B-35}$$

which replaces Eq. (B-33) and which involves only three variables.

The final system can then be written as $AY = \lambda BY$ or

$$
\begin{bmatrix}
 & A_o & & 0 & 0 & 0 \\
 & & & \cdot & \cdot & \cdot \\
 & & & \cdot & \cdot & \cdot \\
 & & & \cdot & \cdot & \cdot \\
 & & & e_{N+1} & 0 & 0 \\
0\ldots0 & -1 & 1 & 0 & 0 \\
0\ldots0 & 0 & 2 & -1 & 0 \\
0\ldots0 & 0 & 0 & -1 & b_3
\end{bmatrix}
\begin{bmatrix}
y_o \\ \cdot \\ \cdot \\ \cdot \\ y_N \\ y_{N+1} \\ y_{N+2} \\ y_{N+3}
\end{bmatrix}
= \lambda
\begin{bmatrix}
 & I & & 0 & 0 & 0 \\
 & & & \cdot & \cdot & \cdot \\
 & & & \cdot & \cdot & \cdot \\
 & & & \cdot & \cdot & \cdot \\
 & & & 0 & 0 & 0 \\
0 & & & 0 & \tau/2 & 0 \\
 & & & 0 & \tau/2 & -b_2 \\
 & & & 0 & 0 & -b_4
\end{bmatrix}
\begin{bmatrix}
y_o \\ \cdot \\ \cdot \\ \cdot \\ y_N \\ y_{N+1} \\ y_{N+2} \\ y_{N+3}
\end{bmatrix}
$$

$$\tag{B-36}$$

101

4.   Particular Cases

Parameters for either in-plane or out-of-plane oscillation of the extended tip mass are given by

$$b_2 = (3/2)Kb_o/h^2$$
$$b_3 = 3b_1K - 3/2 \qquad\qquad (B\text{-}37)$$
$$b_4 = -3/4h^2 \qquad\qquad .$$

To get the case of free ends we let $b_o = 0$ (thus $b_2 = 0$), $b_3 = 1$, and $b_4 = 0$. A similar simple modification applies to the bouncing tip masses.

In all the cases, if we wish to obtain the odd cases, in which $y(0) = 0$, we merely set $a_o = 1$, $e_1 = 0$ in the A matrix, and made the first row of the matrix B all zero.

Note that the matrix A is tridiagonal (and thus Hessenberg), while B is an upper triangle in the general case. This allows us to directly use the method of Moler and Stewart.[1]

For the case of a constant q, as in the free-cable case, we may use $B = I$ and operate with Eq. (B-25) to get a standard tridiagonal eigenvalue problem. A simple transformation can be used to symmetrize A_1 so that much faster computational methods can be employed. We also have available for the latter case the choice of getting only the first few eigenvalues and vectors. This is not so in the Moler-Stewart algorithm. Thus in the extended-tip-mass case all the vectors and eigenvalues are computed, and a typical run takes about 1.5 min for $N = 10$. The symmetric free-cable case takes about half as much time. In the former computation

---

[1] C. B. Moler and G. W. Stewart, "An Algorithm for Generalized Matrix Eigenvalue Problems," SIAM J. Numer. Anal., Vol. 10, pp. 241-256 (1973).

we also compute the value

$$\theta_R(\bar{\xi}) = 3(b_1 F - 1)/b_o F \Omega_o$$

where

$$\Omega_o = 3/2 \ \Omega$$

$$F = 3\bar{\xi} \ \bar{y}' / \bar{y} \ \Omega_o$$

and the approximations for $\bar{y}$ and $\bar{y}'$ are used as in Eq. (B-14).

Appendix C

THE SRI SIMULATION PROGRAM

by

Arthur R. Tobey

Appendix C

THE SRI SIMULATION PROGRAM

1. Purpose of the Simulation

The behavior of a many-linked chain orbiting the earth with arbitrary initial conditions may be very complex. Analytical solutions to the many coupled differential equations describing the chain dynamics are very difficult to obtain, and have been generally restricted to motion in one plane, single modes of oscillation (simple shapes), and small displacements from the ideal vertical orientation. Such analysis is essential to understanding the problem but leaves many unanswered questions--for example, coupling between oscillations transverse to and in the orbital plane, effects of complex initial conditions, and large-displacement phenomena.

The purpose of developing the simulation is to extend our understanding of the dynamics of an orbiting chain or cable, and to investigate and evaluate various complex end devices designed to damp unwanted libration energy from the system. Simulations allow us to investigate the dynamics of the cable and its associated end devices by providing rigorous treatment of motion in three dimensions; such a treatment cannot be reasonably obtained through analytical solutions.

2. Design and Limitations of the Simulation Program

As currently envisioned, a 150-meter chain could be made up of as many as 10,000 individual ball-jointed links. If each of these were assigned two independent degrees of freedom, 20,000 simultaneous

107

equations would have to be solved for 20,000 accelerations during each
iterative step of simulation. Clearly, simulation is not without its
limitations. The SRI simulation accommodates up to ten straight sections
with distributed mass. These sections (links) are hinged together at
their ends. Two of these links may be end devices with additional
degrees of freedom--e.g., elongation in the case of springs and rotation
in the case of cylinders (also referred to as tip inertias). Some point
on the chain (we have chosen the top) must be selected as a reference
point and given three additional degrees of freedom to locate the chain
in space. Thus our 10-link approximation can require the solution of as
many as 25 simultaneous equations for as many accelerations during each
iterative step of simulation. For this many, or more, acceleration
variables, computation time and cost tend to increase with the square
of the number of links.

For up to ten links, the choice of segmentation is a simulation
option in our program. Many end-device tests have been run inexpensively
with only two links, the chain as one and the end device as the other.
In principle, minor programming changes could adapt the program to any
number of links, subject only to possible loss of precision in the
solution of an excessive number of simultaneous equations.

Ideally, we should like the chain to execute a circular orbit at
synchronous altitude, hanging perfectly vertical at all times. We have
chosen to describe the motions of the chain relative to a coordinate system
in which it would be at rest in the ideal case--namely, a coordinate
system centered at the center of mass of the chain, executing an earth
orbit, with the Z-axis always pointing toward the center of the earth.
This is a moving-reference system, with centripetal acceleration toward
the center of the earth and rotation in inertial space. Furthermore,
because we allow orbit ellipticity, this rotation is not necessarily

constant. Two axes of our reference frame lie in the orbital plane, the downward vertical Z axis, and the X axis, which we take perpendicular to the Z axis and pointed in the general direction of satellite travel. For a synchronous orbit, the X axis is directed to the East--i.e., toward the rising sun. Our Y axis is chosen to complete a right-handed cartesian coordinate set, thus being perpendicular to the orbit plane and pointing south. The vector orbital angular velocity $\vec{\Omega}$ has the direction of the negative y axis, and is parallel to and has the same sense as the earth's rotational velocity vector.

In order to confine our solution to the cable motions relative to the moving reference frame, we must include as body forces not only the gravitational force but also kinetic reaction terms resulting from the motion of the reference frame. Force per unit mass in our moving reference frame has the following cartesian components:

$$F_x = (\Omega^2 - \mu/R^3) + \dot{\Omega}z + 2\Omega\dot{z} \qquad (C-1)$$

$$F_y = - \mu/R^3 y \qquad (C-2)$$

$$F_z = (\Omega^2 + 2\mu/R^3)z - \dot{\Omega}x - 2\Omega\dot{x} \qquad (C-3)$$

where

Ω = Magnitude of the orbital angular velocity

μ = The gravitational constant multiplied by the mass of the earth

R = The distance from the center of the earth to the center of the moving coordinate system

x, y, & z = Cartesian coordinates measured in the moving reference frame

and dotted quantities are time derivatives.

109

These are gravity-gradient forces that vanish for a mass element at rest at the center of the coordinate system. Terms involving μ are due to earth gravitation, which is linearized in the region of the satellite. All other terms are exact. Terms involving Ω^2 arise from the centrifugal force, and those involving Ω represent the Cariolis force. The terms in $\dot{\Omega}$ are less familiar and will be nonzero only for elliptical orbits. All except the gravitational terms are kinetic reactions, which appear as explicit forces when we confine our attention to motion in the moving-axis system.

In applying Lagrange's method to the formulation of the differential equations for the motions of the links and end masses, we have chosen the following generalized coordinates. For each link, including end devices, the pitch angle, α, is measured in the orbital plane from the downward Z axis toward the forward-pointing X axis. Thus, positive pitch is "nose up" in aeronautical terms. Roll angle, β, is measured in the pitch plane from the orbital plane toward the positive Y axis. Positive roll is thus counterclockwise to one facing in the direction of travel. Fixed lengths of the links representing the segmented cable do not appear as coordinates; however, for a bouncing-tip-mass device the length of the spring enters as a generalized coordinate. In the case of a cylindrical end device, its angle of rotation about its axis also enters as an independent coordinate. Finally, the cartesian coordinates of the top of the cable-plus-end-device assembly fix the position of the chain in the coordinate system. (For a top-mounted end cylinder, the center of mass of the cylinder is so chosen.)

Since the forces, Eqs. (C-1) to (C-3), are nonconservative--i.e., not expressable as partial derivatives of a potential function--we use Lagrange's equation in the following form:

$$\frac{d}{dt} \frac{\partial T}{\partial \dot{q}_k} - \frac{\partial T}{\partial q_k} = Q_k + Q_k' \tag{C-4}$$

where

T = Total kinetic energy of the system in the moving coordinate system

q_k = One of the generalized coordinates

$\dot{q}_k$ = Corresponding generalized velocity

Q_k = Associated generalized external force

Q_k' = Associated generalized internal force due to hinge friction, spring damping, etc.

Since the mass of the chain is distributed along its length, computation of the total kinetic energy involves an integration over the total mass of the system:

$$T = \frac{1}{2} \int v^2 \, dm \tag{C-5}$$

where v is the velocity of the mass element, dm, in the moving reference frame. Ultimately, T must be expressed in terms of the generalized coordinates and velocities.

otaining the generalized external forces also requires integrations over the total mass of the chain and its end devices--i.e.,

$$Q_k = \int \vec{F} \cdot \frac{\partial \vec{r}_o}{\partial q_k} \, dm \tag{C-6}$$

where $\vec{F} \, dm$ is the vector force on the mass element dm, with the components of $\vec{F}$ given in Eqs. (C-1) through (C-3), and $\vec{r}_o$ is the vector

111

locating the element dm with respect to the origin of the coordinate system.

The generalized dissipative forces may be obtained by a technique attributed to Lord Rayleigh. With this technique,

$$Q_k' = -\frac{\partial \mathfrak{F}}{\partial \dot{q}_k} \tag{C-7}$$

where the Rayleigh dissipation, $\mathfrak{F}$, for hinge damping can be expressed as

$$\mathfrak{F} = \frac{1}{2} D \sum_{i=1}^{N-1} \left\{ \left(\dot{\beta}_i - \dot{\beta}_{i+1} \right)^2 + \cos \beta_i \cos \beta_{i+1} \left(\dot{\alpha}_i - \dot{\alpha}_{i=1} \right)^2 \right\} \tag{C-8}$$

for a chain with N links.

This brief outline of our approach to obtaining the differential equations of motion of the chain in space has an apparent simplicity that masks the very considerable labor required to actually evaluate the many terms that make up the final set of equations. The largest and most complicated subroutine of the simulation program is concerned almost entirely with the computation of matrix elements composed of these terms.

3. Run-Time Options

The simulation program is organized for parametric studies. Most parameters are initialized with realistic default values, minimizing the number of input cards required to initiate simulation. Parameter values entered for one case carry over to the next, so that only change cards plus a START card are required to initiate successive cases in the same run. Input cards are formatted with a ten-column alphanumeric

112

field for the card name, followed by up to seven ten-column floating-point fields for input parameter data. Descriptions of the input parameters are given in the following:

(1) Chain Parameters

- MASS (total mass of chain exclusive of end devices). Default value is 50 kilograms.

- LINKS (number and lengths of links into which chain is to be segmented). Maximum number is ten. Lengths of individual links may be specified. Default is one 150-meter link.

- ANG DAMP (hinge damping constants). Individual damping constants may be specified for each hinge. Default is no damping.

(2) End Devices. Prefixes T- and B- designate the top and bottom of the chain. Devices may be intermixed at opposite ends of the chain, but only one device may occupy a given end.

- T-MASS, B-MASS (end mass affixed directly to end of chain). These options do not add links to the chain. Defaults are zero end masses. Entered with zero-mass value, these cards will effectively remove end devices entered for a previous case.

- T-SPRING, B-SPRING (end mass, resonant frequency, spring damping time constant, equilibrium length, initial length, initial stretch rate). These options add a link to the top and/or bottom of the chain. Resonant frequency is for vertical motion in the gravity-gradient field. Equilibrium length is the length that would be assumed if the chain were straight and vertical, at "rest" in a circular orbit. The distributed mass of the spring is zero.

113

- T-CYLNDR, B-CYLNDR (mass of cylinder, diameter, height, drop to center of mass, initial spin rate). These options add a link to the top and/or bottom of the chain. Axis of the cylinder is the line joining the end of the chain and the center of mass of the cylinder.

- T-BOOM, B-BOOM (end mass, distributed mass, length). These options add a link to the top and/or bottom of the chain. This is a rigid beam attached to one end of the chain.

(3) Orbital Parameters. The simulation is currently written for an average synchronous orbit.

- EPSILON (eccentricity of orbit). Default is zero, circular orbit.

(4) Solar Pressure. Forces due to solar radiation pressure will be ignored unless this card is entered. Although provision is made for the entry of a reflection coefficient, the current status of the program is that solar radiation is assumed to be totally absorbed. In computing solar radiation forces on end devices, the assumption is made that they exhibit the same ratio of mass to projected area as that of the chain illuminated at right angles to its length. Self-shadowing by adjacent beads of each link is accounted for; however, shadowing of one link by another or by end devices is not. Radiation pressure is cut off in the earth's shadow. Orbit perturbation due to solar pressure is not computed.

- SOLAR (bead diameter, center-to-center bead spacing, reflection coefficient).

(5) Program Control

- STEP (orbit degrees per integration step). Third-order prediction algorithms preserve adequate precision under most circumstances if a step size of one orbit degree (the default value) is used, corresponding to about four minutes of real time.

- ORBITS (number of orbits to be completed in simulation). Default value is one orbit. The first orbit terminates at an orbital angle of 360°. If simulation is initiated at an orbital angle other

114

than zero (see START), this orbit will be a
partial one.

- PRINT (print interval in orbit degrees, diagnostic print
flag, centering print flag). Default values are
ten orbit degrees, no flags. The diagnostic print
option displays the numerical values of all the
array elements involved in the simultaneous solution
for all of the accelerations, along with those
solutions, at each iteration. It has been retained
beyond the debugging phase because it has proven
useful in understanding unexpected (though correct)
behavior as well as pinpointing the cause of
pathological behavior. In the absence of perturbing
forces, the center of mass of the chain and end-
device system should follow the center of our moving
reference frame, which travels in a synchronous
orbit. In order to prevent the accumulation of
roundoff and prediction errors, we recenter the
chain at each iteration. The centering printout
option displays the cartesian displacement and
velocity corrections. It is useful in determining
the adequacy of the STEP value selected for a given
situation, and it permits us to check the first-
order effects of solar radiation pressure.
(Modification of the shape of the chain resulting
from solar radiation pressure is due to selective
shadowing and appears as a second-order effect.)

(6) <u>Initial Conditions</u>. Except for the START parameters, initial
conditions, along with all the parameters listed for the
above-described input cards, are preserved from case to case
within a given computer run.

- ANGLES (link number, alpha, beta). Links are counted
from the bottom, including end devices. Initial
pitch angle (alpha) and roll angle (beta) are
assigned to the link whose number is entered and
to all higher-numbered links. Thus, for a
straight initial configuration at any angle, a
single card suffices. Curved initial configurations
are achieved by entering several cards in order of
increasing link number. Default values are zero
pitch and zero roll--i.e., the cable hangs
straight and vertical.

115

- TUMBLE (initial pitch rate, initial roll rate). These
  initial values apply to the whole chain and end
  device as a system and cannot be assigned to
  individual links selectively. Default values are
  zero pitch rate, zero roll rate.

- START (Julian date, hour, minute, initial orbit angle).
  Julian date and local time at initiation of
  simulation are required to position the sun for
  solar-pressure computation. The sun is directly
  overhead on Julian day 81 at 12 hours 0 minutes,
  moving 23.45° meridians with a period of 365.24
  days. Initial orbit angle is measured from perigee
  in the direction of satellite travel. A START card
  is required for the initiation of each case in a
  stacked run. Cards beyond it on the input file
  pertain to the following case.

4. Normal Output

Printout from a simulation run falls into three categories--
verified input, parameter summaries, and simulation results. Data in
the first two classes are headed by a print line identifying the
computer program, giving the compilation date of the version being run,
a job identifier, and the date and time of the run. Time advances from
case to case, so that the order of a sequence of cases can be
reconstructed.

a. Verified Input

Input data are displayed in a card-image format in order "as
entered." If data on a given input card are incomplete or unreasonable,
all data on that card may be zeroed out, essentially nullifying that
card. Printout will show the modified values. Cards entered for
previous cases are not repeated--only the additional cards required to
initiate the current case are displayed in the heading for that case.

116

b. Parameter Summaries

Values of all variable parameters and initial conditions not displayed elsewhere are summarized in a header to the simulation results of each case. Data are repeated here from case to case so that full information will be available if cases are separated. Additional derived information is displayed to assist in evaluation of results.

Included among these data is a computed value for the minimum energy of the system as measured in the moving coordinate frame. This value is a negative quantity representing the potential energy of the cable and end devices hanging straight and at rest in the ideal orbital configuration. (The zero reference corresponds to all of the mass of the system concentrated at the center of coordinates where all external forces vanish). The minimum energy represents the depth of the potential well corresponding to ideal deployment--i.e., it is a measure of the inherent stability of the ideal configuration.

c. Simulation Results

Each page of simulation results is headed by a print line identifying the computer program, giving a page number, and including two items of computed data. The first, EXCESS ENERGY, is the total energy of the chain and its end devices, measured in the moving reference frame, less the minimum energy. This is the amount of energy that must be removed from the system by one or more dissipative mechanisms in order to achieve the ideal configuration. The second item, RELATIVE ENERGY, displays, on page 1 of the printout, the ratio of the excess energy to the absolute value of the minimum energy, and is a measure of how far above the bottom of the potential well the initial energy level lies. On subsequent pages, RELATIVE ENERGY is the ratio of the excess energy at that point in the simulation to the initial excess energy--

117

i.e., to the value printed on page 1. These values provide a ready index as to how rapidly (or slowly) the system is approaching the ideal configuration. The current algorithm for computing excess energy fails for elliptical orbits.

Each page of simulation results consists of six records, each representing a snapshot of the chain and end-device configuration after successive print intervals. The first record on page 1 displays the initial configuration. The first line of each record contains the following data: orbit number, orbital angle, Julian date, local time in hours and minutes, stretch of end springs (if any), rotational velocity of end cylinders (if any), and tip-to-tip loss (length of ideally straight chain minus tip-to-tip distance in present configuration). The next three lines display the cartesian coordinates of the ends of each of the links of the chain and end devices. The last two lines are a printout of the pitch and roll angles for each of these links.

Using the default value of print interval (ten orbit degrees), each orbit yields six pages of printout, and excess energy is computed and printed every 60 orbit degrees.

5. Program Checkout and Verification

The current version of the simulation program has evolved through a large number of modifications. The initial version was a half-chain simulation, devoid of end devices, with lumped link masses. Starting with that relatively simple model, testing and verification have been done on each successive version, with the help of built-in diagnostics (many of which have since been removed). Periods of small librations in and transverse to the orbit plane have been checked against ell-established theory. Correct behavior of end devices has been confirmed for a number of limiting cases. All in all, several hundred test cases have been run and carefully analyzed. This step-by-step procedure, with

118

many test runs at each phase of modification, has built our confidence in the correctness of our simulation results.

All of the theory underlying this simulation has been derived from first principles and is well understood. We have not let unexpected results go unexplained. Thus we have developed a thorough understanding of the simulation. This understanding has made it relatively easy to spot and correct the inevitable logic errors and programming bugs that occur in the development of a program of this complexity. Furthermore, this understanding permits us to make major modifications to the program as required by the ongoing research, with confidence that we are maintaining the basic integrity of the simulation.

6. Current Modifications

The program is undergoing modifications of the following nature:

(1) to allow use of a larger number of links, e.g. as the 75 of the full test array

(2) to allow the length of links to be individually specified. Since most of the bending occurs at the ends of the array, these need to match the existing conditions more exactly.

(3) to allow the behavior of each joint to be individually specified

(4) to permit damping of the forms

$$Torque = A \left(\dot{\alpha}_i - \dot{\alpha}_{i+1} \right)^B \qquad (A \text{ and } B \text{ constants})$$

and

$$Torque = A \tan^{-1} B \left(\dot{\alpha}_i - \dot{\alpha}_{i+1} \right) \quad .$$

These allow the examination of nonlinear joint behaviors.

119

Appendix D

DEPLOYMENT CONSIDERATIONS

Appendix D

DEPLOYMENT CONSIDERATIONS

1.   Launch Vehicle

The prototype space array is to be carried into orbit as a secondary or tertiary package on the transport stage (transtage) of a Titan III-C vehicle. Two synchronous launches are scheduled in 1977 for the Air Force 777 Program. These are potential hosts for the test space array.

We have investigated the interface power and the telemetry specifications of the Titan III-C transtage, not only to gauge the feasibility of our concepts but also to structure some of our preliminary designs. Summary Report--Phase I includes a figure showing one of our early deployment concepts relative to this transtage. The space and weight requirements we have taken are those of the Titan III-C system with 777 satellites as the primary packages.

Since the deployment from the transtage will require a substantial period of time, it is necessary to consider the motions of the transtage itself. The purpose of this appendix is to consider the Titan III-C attitude control system and the implications it has for the deployment of the space array.

2.   Attitude Control System

The hydrazine tank and other features of the control system are shown schematically in Figure D-1. The rocket engine modules operate in an off-on mode for discrete intervals. Attitude control is maintained

FIGURE D-1 TITAN III-C ATTITUDE CONTROL SYSTEM

124

by a limit-cycle procedure; appropriate rockets are fired to maintain the desired angular position to a tolerance of half a degree. Since the rocket thrust is not reproducible, due to variation in fuel pressure and wear of the rocket and control valves, the rates of the three limit cycles can be described only statistically.

Table D-1 summarizes the pertinent attitude-control information; shown are the pitch, yaw, and roll rates at the 3σ limit, together with the limit-cycle tolerance. Since the deployment mechanism will not be located at the center of gravity, these angular rates and positions translate into linear displacements, which are also shown on the table. Available gyro information and the transtage orbital rate are also shown. It is important to note that the integrated rate or position ability of the gyro is considerably better than that indicated by the rate readout value, since the gyro drift rate is less than $\frac{1}{4}$ degree per hour.

Table D-1

ATTITUDE INFORMATION FOR TITAN III-C

	Angular Motion of Transtage	Linear Motion at Mechanism
Transtage control		
Pitch and yaw rate	$0.45°/s$ 3σ values	2.4 cm/s
Roll rate	$0.75°/s$	
Position	$0.5°$	2.6 cm
Control-System readout rate		
Analog	$0.01°/s$	0.017 cm/s
Digital	$0.005°/s$	0.0087 cm/s
Orbital Rate	$0.00417°/s$	

Three potential difficulties have been identified. First, the rate of change of the transtage attitude is large compared to the orbital rate; therefore, rate control cannot be used during the deployment. Second, and even more serious, the limit cycling during the deployment will introduce transverse motion to the beads that might cause the array to collapse as shown in Figure D-2. A third difficulty results from the fact that while the motors that control the roll operate in equal and opposite pairs, imparting torque only, the pitch and yaw rockets all fire aft, thereby accelerating the transtage forward. The implications of these problems are discussed in inverse order.

FIGURE D-2 EFFECT OF TRANSVERSE VELOCITY

3. Acceleration

The calculations in this section are based on the attitude information already given in Table D-1 and on the following data: the transtage will have a mass (m) of 4,200 lbs, and an inertia (I) of 2400 slugs/ft at the time of our deployment. The thrusters act with a moment arm (ℓ_t) of 62.6 inches. These figures come from the manufacturers' literature. Our assumptions and calculations will be given in metric units.

The forward thrust of each system can be calculated from the following equation:

$$\text{Force} = \frac{I}{\ell_t} \frac{\Delta \dot{\alpha}}{\Delta \alpha} \dot{\alpha} \qquad (D-1)$$

where α = transtage angle from set position.

If the mass of the transtage is known, the resultant acceleration can be computed. The results of these calculations are given in Table D-2, which shows the force from both the pitch and yaw systems operating at the same time at the 1σ, 2σ, and 3σ rate values. Also shown is the resulting acceleration, assuming there are no forces opposing the thrust. Although these accelerations have small values, their integration over reasonable deployment times results in significant displacements. Table D-3 shows these displacements as functions of deployment velocity. If the deployment takes place at 1 m/s, the time to deploy the 150-m active section plus the two pigtail ends amounts to 210 s. During this time the transtage, if it is yawing and pitching at the 3σ value, will move nearly 230 m. Since this translation is greater than the length of material deployed, the situation is unacceptable. At greater deployment velocities--for example, at 5 m/s--the time to deploy is considerably reduced, and even at the 3σ yaw and pitch rates, displacement during the deployment is less than 10 m.

127

Table D-2

FORWARD FORCE AND ACCELERATION
FROM COMBINED YAW AND PITCH THRUSTERS

	$\dot{\alpha}$ (deg/s)	Force (N)	Acceleration (m/s)
1 σ	0.15	3.21	5.8×10^{-4}
2 σ	0.30	12.86	2.3×10^{-3}
3 σ	0.45	28.93	5.2×10^{-3}

Table D-3

FREE 3σ ACCELERATION DISPLACEMENT
AT VARIOUS DEPLOYMENT RATES

V_d (m/s)	Time to Deploy (s)	$\iint Acc\, dt dt$ (m)
1	210	115
2	105	20.0
5	42	4.59
10	21	1.145

The foregoing calculations do not include the reaction force of
the deployment itself. Table D-4 shows these reaction forces versus
deployment velocity for arrays assumed to be made up of aluminum spheres
and uranium spheres. These two materials are selected for these sample
calculations because they represent the extremes of the range of density
available and are materials that have been considered for the array.

128

Table D-4

DEPLOYMENT REACTION FORCE[*]

V_d (m/s)	Force Using Aluminum Spheres (N)	Force Using Uranium Spheres (N)
1	0.0936	0.648
2	0.374	2.59
5	2.34	16.2
10	9.36	64.8

[*]Deployment velocity squared times linear density.

We note that at a deployment velocity of 5 m/s for the aluminum array we have a reaction force of 2.34 newtons (N), which is small compared to the 28.93-N thrust of the yaw and pitch jets when operating at the 3σ values. However, the 3σ value represents an extreme, and forces at the 1σ value occur nearly 70% of the time. The 1-G force is 3.21 N, comparable with the reaction force. In a deployment at these conditions it is likely that the transtage will not move at all. If uranium beads were used, the array tension at the deployment mechanism would be in the neighborhood of 13 N.

It can be seen that because of the forward acceleration of the transtage, it is necessary to deploy at rates in the m/s range. Increasing the velocity of deployment has two effects. The first is to decrease the time during which transtage motion can affect the deployment, and the second is to increase the reaction of the array against the transtage. A deployment velocity of about 5 ft/s with the aluminum array design can be expected to give a deployment in which the transtage moves less than a meter under normal conditions. Even under the worst conditions the transtage moves a distance that can be tolerated.

129

4. Transverse Velocity

The rotation rate of the array--one revolution per day--amounts to a velocity difference, between the ends normal to the direction of the array, of about 1 cm/s. As shown in Table D-1, the motion at the deployment mechanism due to transtage cycling amounts to 2.4 cm/s at the 3σ rate. While this number will probably average out to a much lower value over several cycles, the comparison between the two numbers shows that consideration must be given to the attitude motion of the transtage.

A better way of evaluating the effect of the transverse velocity is to compare the kinetic energy stored in the transverse velocity with the potentials capable of absorbing that energy. If the kinetic energy exceeds that of the potentials available, one must assume that the array will collapse.

a. Kinetic Energy

There are two sources of transverse velocity. If the beads are not ejected in the desired direction, they will have a transverse velocity proportional to the sine of the angle from the desired direction. The second source of transverse velocity is transverse velocity of the deployment mechanism itself. The second source is significant when the deployment mechanism is not located at the center of gravity of the vehicle. These two sources of transverse velocity are shown in Figure D-3.

We note that the two sources of transverse velocity are $90°$ out of phase. Therefore, the total transverse velocity in one plane is the sum of two orthogonal vectors:

$$V^2_{t_{max}} = (\alpha_{max} V_d)^2 + (\ell\dot{\alpha})^2 \quad . \qquad (D-2)$$

130

(a) ORIENTATION ERROR

(b) RATE ERROR
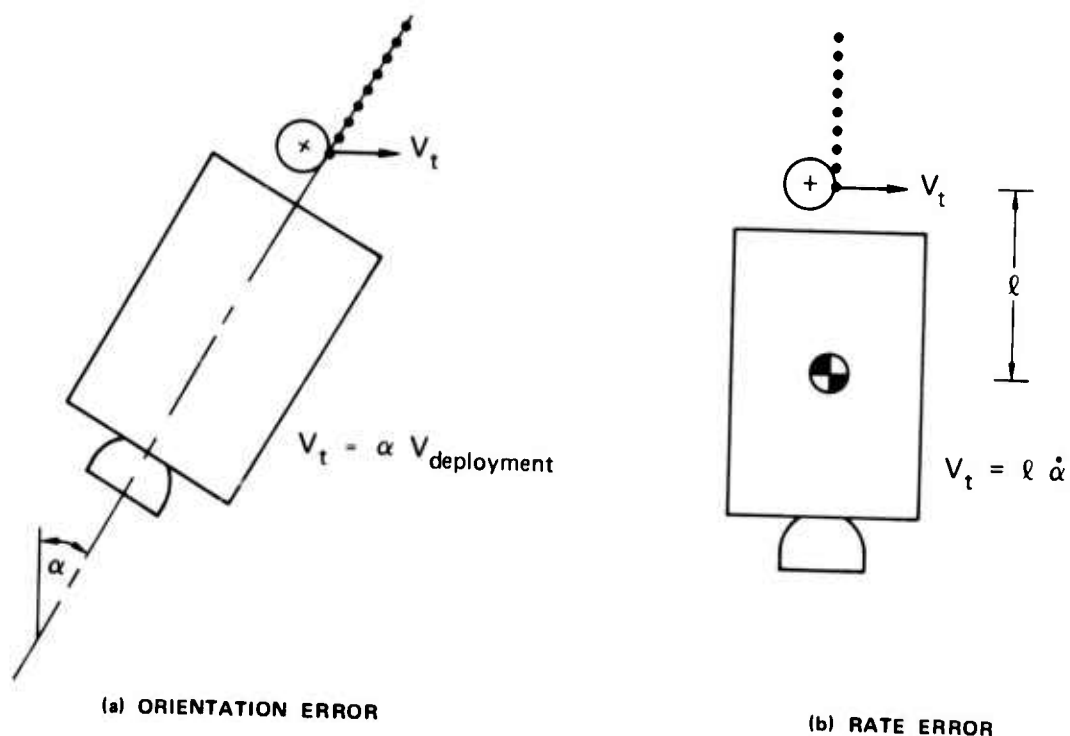
SA-3323-4

FIGURE D-3   SOURCES OF TRANSVERSE VELOCITY

The total kinetic energy (DE) can be written

$$\int_{-L/2}^{L/2} \sigma \, v_t^2 \, dx \tag{D-3}$$

or

$$KE = \frac{\sigma \, L \, v_t^2}{4} \quad . \tag{D-4}$$

Substitution of the 3σ rate and assumption of a deployment speed of 5 m/s gives a total kinetic energy of 9.31×3^{-3} N-m, about three quarters of which comes from the term with the deployment velocity. Use of a guide tube stabilized to cut the angular error to a maximum of

131

one-tenth of the limit-cycle error would cut the contribution due to the deployment velocity by a factor of 100, virtually eliminating that contribution to the kinetic energy. Reference to the attitude-control-system figures of Table D-1 shows that this should be easily possible. With this angular correction from the guide tube, the transverse kinetic energy is reduced to 2.00×10^{-3} N-m. The same attitude information shows that the undesired motion could be eliminated by mounting the deployment mechanism on a x-y table capable of 5 cm motion in both directions. In this case, the total kinetic energy would be reduced to 9.31×10^{-5} N-m.

Transverse velocities are also introduced by the deployment mechanism itself. These have been measured in laboratory tests on freely jointed arrays and were found to be of a random high-frequency nature with an amplitude about 1% of the deployment velocity. Because of the random nature of the disturbance, we suspect that the error is primarily due to mechanical tolerances in the test arrays that were deployed from the mechanism. In a completely flexible or freely jointed array this relatively large transverse velocity would be the dominant concern. Since the frequency is high, the energy is quickly dissipated. For an array with a stiff support, the energy is easily accommodated as beam loading. In any case, the smaller transverse velocities arising from transtage motion at the lower frequencies remains an important factor that we will work to reduce.

b. Gravity-Gradient Potential

The energy (PE) required to collapse the array from its gravity-gradient (GG) stable position to a point mass can be given by

$$PE_{GG} = \frac{n^2 \sigma L^3}{8} \tag{D-5}$$

We shall refer to this as the gravity-gradient potential energy.

132

Substitution of the values for an aluminum test array at synchronous orbit gives a value of the potential energy of 2.09×10^{-4} N-m. This value is smaller than the transverse kinetic energy even when guide tube control is assumed. Therefore, we conclude that it is not practical to deploy such an array by these means where the gravity gradient potential is the only sink for the energy. The transverse energy with x-y control to eliminate the motion of the deployment mechanism does yield a transverse kinetic energy that is smaller than the gravity gradient potential. The margin of safety, however, it not large, and the approximate nature of the calculations provides no great confidence in the results. It is prudent, therefore, to seek another source of potential energy.

C.   Bending Potential Energy

The energy involved in bending an elastic beam can be given as

$$PE_{Beam} = \int_{-L/2}^{L/2} \frac{EI}{2} \left(\frac{d^2 y}{dx^2} \right)^2 dx \tag{D-6}$$

where EI is the stiffness, x is the coordinate along the beam, and y is measured from the undeflected position. We assume that y is given as

$$y = A \sin \frac{\omega}{V_d} x \tag{D-7}$$

where ω is the frequency of the limit cycling. With this assumption the potential energy of bending a beam with a circular cross section can be given as

133

$$PE_{Beam} = \frac{\pi A^2 E r^4 L \omega^4}{16(1 - d/s) V_d^4} \qquad \text{(D-8)}$$

where r is the radius of the beam--i.e., wire running through the beads. The term in parentheses is a correction term corresponding to the fact that all bending takes place between the beads. A bending potential energy of 6.48×10^{-2} N-m is given by evaluation of Eq. (D-8) for the following conditions:

$$E = 2.07 \times 10^{11} \text{ N/m}^2 \quad \text{(steel)}$$

$$A = 5 \text{ m}$$

$$r = 0.0005 \text{ m} \quad \text{(0.001 m diam, 40 mil)}$$

$$L = 150 \text{ m}$$

$$\omega = 1.414 \text{ rad/s} \quad \text{(3 }\sigma\text{ value)}$$

$$d = 0.010 \text{ m}$$

$$s = 0.015 \text{ m}$$

$$V_d = 5 \text{ m/s} .$$

This figure is considerably larger than the kinetic energy, and the resulting deflections will be less than five meters.

If the transtage cycling occurs at the one-sigma rate, this bending potential energy has a considerably smaller value since the wavelength is much longer. At the same time, however, the transverse kinetic energy is also reduced.

It should be noted that Eq. (D-4) for kinetic energy and Eq. (D-5) for the gravity-gradient potential both contain the linear density of the array. Changing the density will not change the relative proportions of those two energies. The bending potential energy,

Eq. (D-8), does not contain the linear density of the array. To make this potential large compared with the kinetic energy, one should make the linear density small.

One should also note that the gravity gradient-potential energy is a strong function of the array length. This is to say that for very long arrays, the potential energy will eventually dominate. Hence, resistance to bending is not required for very long arrays, but is needed for the test array, because it is relatively short in terms of the gravity gradient.

Appendix E

RIGID-ROD MOTIONS, STRESSES, AND BUCKLING

Appendix E

RIGID-ROD MOTIONS, STRESSES, AND BUCKLING

1.   Introduction

The purpose of this appendix is to determine whether a flexible array will be subjected to compressive forces during capture from tumbling.

2.   Solution

To examine this question, consider a long, thin, rigid body tumbling in pitch. The incremental tension along the body can be written

$$dT = \sigma dx \, n^2 \left[3 \cos^2 \theta - 1 + \left(1 + \frac{\dot{\theta}}{n} \right)^2 \right] \tag{E-1}$$

where

dx = Incremental distance along the body

θ = Angle from the local vertical

σ = Linear density of the body

n = Orbital rate.

We are especially interested in the locus of points on the θ-$\dot{\theta}$ plane that describes the zero-tension condition, given by

$$3 \cos^2 \theta - 1 + \left(1 + \frac{\dot{\theta}}{n} \right)^2 = 0 \quad . \tag{E-2}$$

139

The equation of motion can be written by equating the rate of change of angular momentum to the restoring torque as follows:

$$\ddot{\theta} = -3n^2 \sin \theta \cos \theta \quad . \tag{E-3}$$

By noting that

$$\ddot{\theta} = \dot{\theta} \frac{d\dot{\theta}}{d\theta} \tag{E-4}$$

one can write Eq. (E-3) in the θ and $\dot{\theta}$ phase plane coordinates as

$$\dot{\theta} d\dot{\theta} = -\frac{3}{2} n^2 \sin 2\theta \, d\theta \quad . \tag{E-5}$$

Integration of this last equation yields

$$\frac{\dot{\theta}}{n} = \frac{3}{2} \cos 2\theta + C \tag{E-6}$$

where C is a constant. Closed curves in the phase plane are separated from unterminating ones by the solution of Eq. (E-6) that passes through $\theta = \frac{\pi}{2}$, $\dot{\theta} = 0$. For this solution the constant, C, equals 2/3, and the equation of the separatrix can be written

$$\left(\frac{\dot{\theta}}{n}\right)^2 = \frac{3}{2} (1 + \cos 2\theta) \quad . \tag{E-7}$$

This equation and Eq. (E-2) are plotted in Figure 5 of the main text. It should be noted that a reverse tumble will pass through the region of compression and finally coincide with the decay path of a decreasing positive tumble. An interesting point is that the positive tumble will also pass through a compressive region. This can be deduced from the separatrix of Eq. (E-7), which intersects the zero-tension line at $\theta = \frac{\pi}{2}$, $\dot{\theta} = 0$, and at $\theta = 54.74°$, $\frac{\dot{\theta}}{n} = -1$. Between these two locations the separatrix passes through a region that indicates compressive stresses in the array.

140

Maximum compression occurs at the point $\theta = 71.05°$, $\dfrac{\dot{\theta}}{n} = -0.5625$. The incremental tension here is

$$dT = \sigma dx \, n^2 \, (-0.49219) \quad . \tag{E-8}$$

The largest closed curve (labeled capture region) does not pass into the compression region. This curve corresponds to an array whose maximum libration amplitude is $66.344°$. A short portion of the closed curve is shown in the figure. The locus touches the zero-tension locus φ at the coordinates $\theta = 62.275°$, $\dfrac{\dot{\theta}}{n} = -0.4078$.

3. Buckling

The behavior of a flexible array in the phase-plane regions that correspond to compression is a complicated question that we have not addressed. In the case of stiff arrays, however, the behavior can be classified according to whether the array is buckled or not. It should be noted that "buckling" does not imply plastic behavior or a destruction of the array, but only that the array is not capable of remaining straight under the applied (body) forces. If the array is buckled, there is the question of the amplitude of the distortion. In the case of no buckling, there is no sudden change in the array behavior, and for practical purposes compression has no effect on the structure.

A simple, conservative estimate will be used to demonstrate that the test array will not buckle, even under the most severe gravity gradient compression. Assume that the central compression of the array, which occurs during recovery from a negative tumble,

$$\frac{n^2}{2}\left(Lm + \sigma \frac{L^2}{4}\right) \tag{E-9}$$

141

is applied to the ends of a free-free beam with the properties of the supporting stiff wire of the array. For the test array this central compression is 2.5×10^{-6} N. The simple Euler buckling load for end loading is

$$P = \frac{\pi^2 EI}{\ell^2} = \frac{\pi^3 r^4 E}{4\ell^2} \qquad (E-10)$$

which gives $P = 4.5 \times 10^{-6}$ N. Since the conservative buckling load for the test array is greater than the central compression, we are assured that buckling will not occur, and the test array will be uneffected by passing through the compressive region.

We note that buckling will occur for a sufficiently long array if all the other parameters are held constant. Further, we note that it is not feasible to prevent buckling for very long array lengths, because the thickness of the supporting wire would become prohibitive. Tumbling, however, is not a concern for the longer arrays. The gravity gradient effect increases with length, and the change in moment of inertia between undeployed and deployed states also increases with length, so that disturbances and errors before and during deployment become increasingly insignificant.

4. Conclusions

A gradual capture from tumble involves compressive forces that will affect the straightness of a flexible array. Capture from reverse tumble involves compressive forces twice those of capture from forward tumble. The test array will not buckle when subjected to the maximum compressive forces. Although this is not true for longer arrays, such arrays are not likely to be subjected to tumbling.

142

Appendix F

MUTUAL GRAVITATIONAL ATTRACTION OF THE BEADS

Appendix F

MUTUAL GRAVITATIONAL ATTRACTION OF THE BEADS

I. Introduction

The beads of the array will be attracted to one another by mutual gravitational forces. If these forces exceed the gravity-gradient force, then a completely flexible array will collapse. In the absence of a tip structure, the critical situation occurs at the end bead because this array element is subject to the gravity-gradient force but not to tension transmitted to it from beads farther out. At the same time, the mutual gravitation force on this bead is the greatest because all of the other beads pull together on this one bead in the opposite direction to the gravity-gradient force (see Figure F-1).

2. Formulation

The gravity-gradient force, F_g, can be written

$$F_g = 3n^2 \frac{L}{2} m \tag{F-1}$$

where

$$m = \rho \frac{\pi}{6} d^3 \tag{F-2}$$

and the variables are defined in Figure F-1.

145
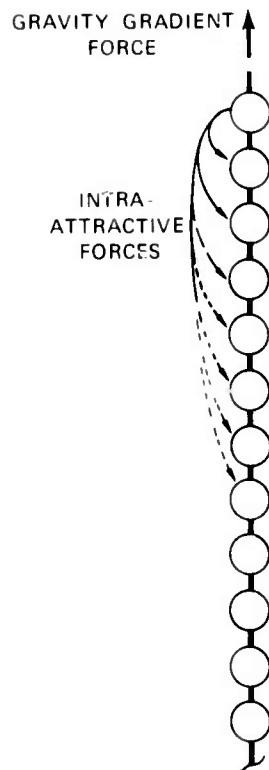
$$\frac{3L}{2}\,\omega^2\,\rho\,\frac{\pi}{6}\,d^3 \;>\; \frac{G\left(\rho\,\frac{\pi}{6}\,d^3\right)^2}{s^2}\sum_{n=1}^{\infty}\frac{1}{n^2}$$

$$\frac{L\,\omega^2\,s^2}{G\,d^3\,\rho} \;>\; 0.574$$

Al	502
Pb	120

L = LENGTH

ω = ORBIT RATE

ρ = DENSITY

d = BEAD DIAMETER

G = UNIVERSAL GRAVITATIONAL CONSTANT ($6.67 \times$ Nm^2/kg)

s = INTERELEMENT SPACING

$$\sum_{n=1}^{\infty}\frac{1}{n^2} = \frac{\pi^2}{6}$$

LA-3323-74

FIGURE F-1   BEAD MUTUAL-ATTRACTION STABILITY CRITERION

The mutual gravitation force, F_m, can be written

$$F_m \;=\; \frac{Gm^2}{s^2}\sum_{n=1}^{\infty}\frac{1}{n^2}\quad. \tag{F-3}$$

Because the forces contributed by beads at large distances from the end bead is small, the summation to infinity provides a very good approximation to F_m.

The gravity-gradient effect will dominate when

$$\frac{L\omega^2 s^2}{Gd^3} \;>\; 0.574\quad. \tag{F-4}$$

146

3. Conclusions

For aluminum beads and a 150-m array, the left-hand term of Eq. (F-4) exceeds the critical value by two orders of magnitude.

If end masses are added and if the array is made stiff, this criterion becomes extremely conservative.

Appendix G

TEMPERATURE DISTRIBUTION IN A SOLAR-IRRADIATED CYLINDER

Appendix G

TEMPERATURE DISTRIBUTION IN A SOLAR-IRRADIATED CYLINDER

1.   Introduction

The thermal bending of a solid cylinder (wire) will be a function of the temperature distribution existing within the structure.   To calculate this distribution, we assume that the temperature differences at the surface of the wire are small.   Consequently, reradiation from the cylinder is the same from all positions on its surface.   This assumption was checked, and proved valid, for the solution we obtained.

2.   Formulation

We take the heat flux at $r = a$ to be

$$
q = \begin{cases} q''' \left(\cos\theta - \dfrac{1}{\pi} \right), & -\dfrac{\pi}{2} < \theta < \dfrac{\pi}{2} \\[4mm] q'''/\pi, & \dfrac{\pi}{2} < \theta < \pi \end{cases} \tag{G-1}
$$

where the variables are defined in Figure G-1.

In terms of temperature, T, the steady-state problem is

$$
\nabla^2 T = 0 \tag{G-2}
$$

151
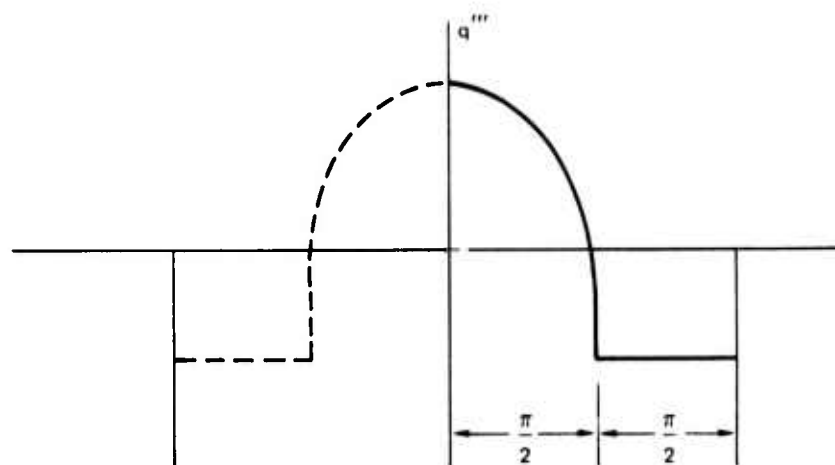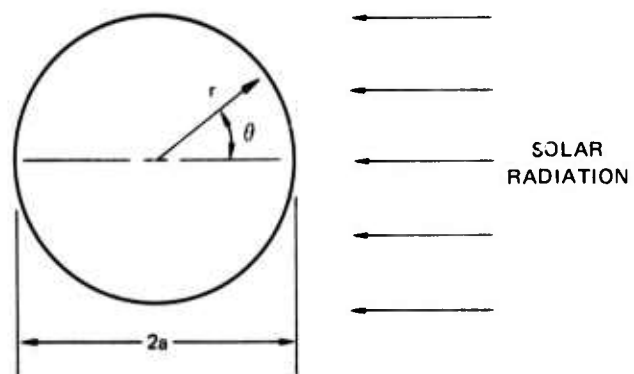
FIGURE G-1   SOLAR RADIATION ON CYLINDER

with the following boundary conditions:

$$\frac{\partial T}{\partial r} = \begin{cases} + \frac{q'''}{K}\left(\cos\theta - \frac{1}{\pi}\right) & -\frac{\pi}{2} < \theta < \frac{\pi}{2} \\[4mm] -\frac{q'''}{K\pi} & \begin{cases} -\pi < \theta < -\frac{\pi}{2} \\[3mm] \frac{\pi}{2} < \theta < \pi \end{cases} \end{cases} \qquad \text{(G-3)}$$

where K is the thermal conductivity. Assuming that the problem is length-independent, the solution of Eq. (G-3) is

$$T = \sum_{n=0}^{\infty} \left(A_n r^n + B_n r^{-n}\right)\left(C_n \sin n\theta + D_n \cos n\theta\right) . \qquad \text{(G-4)}$$

Because the temperature is limited,

$$B_n \equiv 0 \qquad \text{(G-5)}$$

And, from symmetry,

$$C_n \equiv 0 . \qquad \text{(G-6)}$$

Now, the product of H_n and D_n can be written as a single constant, A_n, and

$$T = \sum_{n=0}^{\infty} A_n r^n \cos n\theta . \qquad \text{(G-7)}$$

We then differentiate Eq. (G-7) with respect to r, multiply the result by $\cos p\theta$, and integrate. The A_n are thus selected to match the boundary conditions in Eq. (G-3):

153

$$\sum_{n=0}^{\infty} \int_{-\pi}^{\pi} n \, a^{n-1} \, A_n \, \cos n\theta \, \cos p\theta \, d\theta$$

$$= \int_{-\pi}^{\pi} - \frac{q'''}{K\pi} \, \cos p\theta \, d\theta$$

$$+ \int_{-\pi/2}^{\pi/2} \frac{q'''}{K} \, \cos p\theta \, \cos \theta \, d\theta \quad . \tag{G-8}$$

All the terms of the left-hand side are zero except when $p = n$. Hence we find that A_o is arbitrary, and, for $n \geq 1$,

$$A_n = \frac{q'''}{2Kn \, a^{n-1}} \quad . \tag{G-9}$$

The even terms make a negligible contribution to the thermal strain of the overall wire because they are symmetric. The higher-order odd terms are not as important as the $n = 1$ term (1) because they have stresses that create some compensating moments, and (2) because these terms have smaller amplitudes [Eq. (G-9)]. Hence we need consider only the first term, which yields a temperature profile of
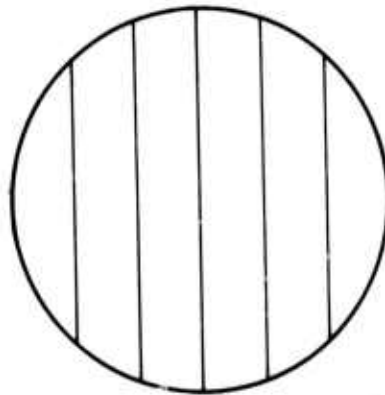
$$T = \frac{q'''}{2K} \, r \, \cos \theta \tag{G-10}$$

and is shown by the isotherms in Figure G-2.

The maximum temperature gradient from this dominant, $n = 1$ term is

$$\frac{dT}{dx} = \frac{q'''}{2K} \tag{G-11}$$

which is seen to be independent of the diameter of the rod.

154

LA-3323-76

FIGURE G-2   FIRST-ORDER ODD ISOTHERMS

3.   Conclusion

The temperature distribution calculated in Eq. (G-11) predicts that a copper rod will bend with a radius of curvature of 47 km when exposed to solar radiation broadside.   Such a curvature corresponds to a 6-cm displacement at the center of a 150-m wire.   This is more than desired for electromagnetic performance and raises questions of attitude excitation.   This effect, however, does not apply to the flexible cable or segmented array.

Appendix H

TEMPERATURE DISTRIBUTION IN A SOLAR-IRRADIATED SPHERE

Appendix H

TEMPERATURE DISTRIBUTION IN A SOLAR-IRRADIATED SPHERE

With arguments similar to those presented in the introduction to Appendix F, the governing equation for a solar irradiated sphere is

$$\nabla^2 T = 0 \tag{H-1}$$

with the boundary conditions

$$\frac{\partial T}{\partial r} = \begin{cases} \dfrac{q'''}{K}\left(\cos\theta - \dfrac{1}{4}\right) & 0 < \theta < \pi/2 \\[2ex] \dfrac{q'''}{4K} & \pi/2 < \theta < \pi \quad. \end{cases} \tag{H-2}$$

The general solution is

$$T = \sum_{n=0}^{\infty} \left[A_n r^n + B_n r^{-n-1} \right] \left[C_n P_n(X) + D_n Q_n(X) \right] \tag{H-3}$$

where $P_n(X)$ and $Q_n(X)$ are Legendre functions, and $X = \cos\theta$. Because of finite temperature and symmetry, Eq.(H-3) reduces to

$$T = \sum_{n=0}^{\infty} A_n r^n P_n(X) \tag{H-4}$$

where $A_n = H_n C_n$. The constants can now be evaluated by taking the derivative of Eq. (H-4) with respect to r and matching the boundary conditions given in Eq. (H-2). Multiplying by $P_s(S)$ and integrating gives

159

$$\sum_{n=0}^{\infty} nA_n a^n \int_{-1}^{1} P_n(X)P_s(X)dX$$

$$= \frac{q'''}{K} \int_{0}^{1} XP_s(X)dX - \frac{q'''}{4K} \int_{-1}^{1} P_s(X)dX \qquad . \qquad \text{(H-5)}$$

The left-hand side is zero except when $n = s$. Hence, the constant A_o is arbitrary and, for $n = 1$,

$$P_1(X) = X \qquad \text{(H-6)}$$

where

$$A_1 = \frac{q}{2aK} \qquad . \qquad \text{(H-7)}$$

For $n > 1$,

$$A_n = \frac{(n + 1/2)\ q'''}{na^n K} \int_{0}^{1} XP_n(X)dX$$

$$= \begin{cases} 0 & \text{for n odd} \\ \\ 2^{(n+1)} a^n n^2 (n-1) & \text{n even} \qquad . \qquad \text{(H-8)} \end{cases}$$

These results will be used during the detailed design phase of the project.

Appendix I

ORBITAL CHANGES DUE TO GRAVITATIONAL EFFECTS OF THE SUN AND MOON

Appendix I

ORBITAL CHANGES DUE TO GRAVITATIONAL EFFECTS OF THE SUN AND THE MOON

This appendix summarizes the effects of the gravitational fields of the sun and moon and of the earth's oblateness on an initially geostationary orbit. Greater detail is provided in the references given below.[2,3]

An equatorial orbit will drift due to the gravity-gradient effects of the sun and the moon. The nature of the drift can be understood by viewing the average gravitational forces of these bodies as applied torques that alter the orbital angular-momentum vector. The magnitude of this torque varies periodically depending on the angle that the radius vector from the sun or moon makes with the orbital plane. The fundamental period is half that of the radius vector from the relevant body.

As can be seen in Figure I-1, the torque applied on an equatorial orbit by the sun is periodic and is a maximum at the solstices and zero at the equinoxes. The average of this torque applied by the sun and that of the moon can be added. The total torque causes the angular-momentum vector to precess about the ecliptic pole.[*] The rate of

---

[2] A. Kamel and R. Tibbitts, "Some Useful Results on Initial Node Locations for Near-Equatorial Circular Satellite Orbits," Celestial Mechanics, Vol. 8, pp. 45-73 (1973).

[3] O. F. Graf, Jr., "Lunar and Solar Perturbations on the Orbit of a Geosynchronous Satellite," paper AAS 75/023, AAS/AIAA Astrodynamic Specialists Conference, Nassau, Bahamas, July 28, 1975.

[*] This precession is not exactly about the ecliptive pole because the moon's orbit is inclined about 5° to the ecliptic. This perturbation is of second order.
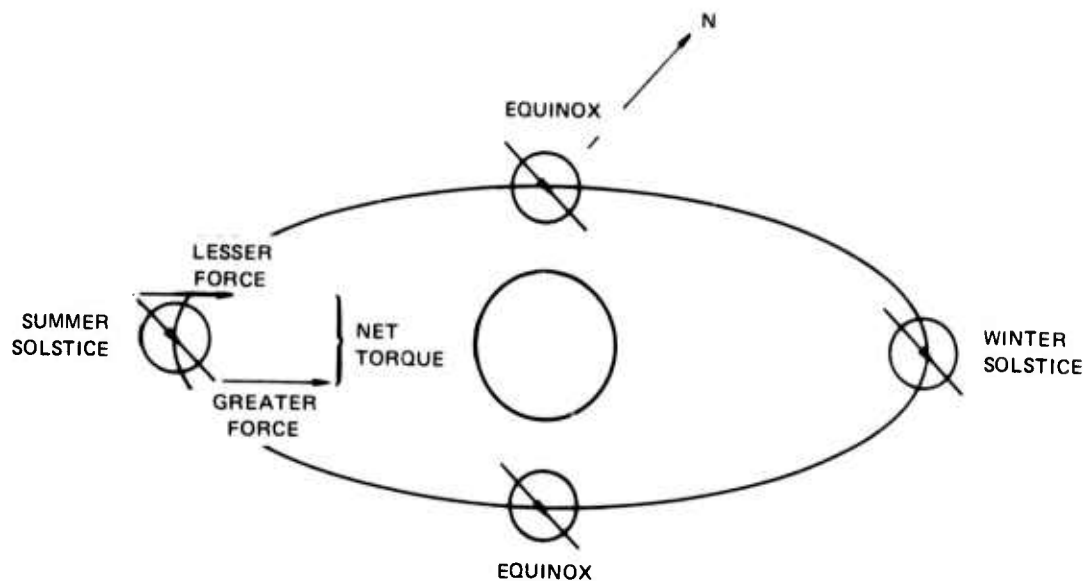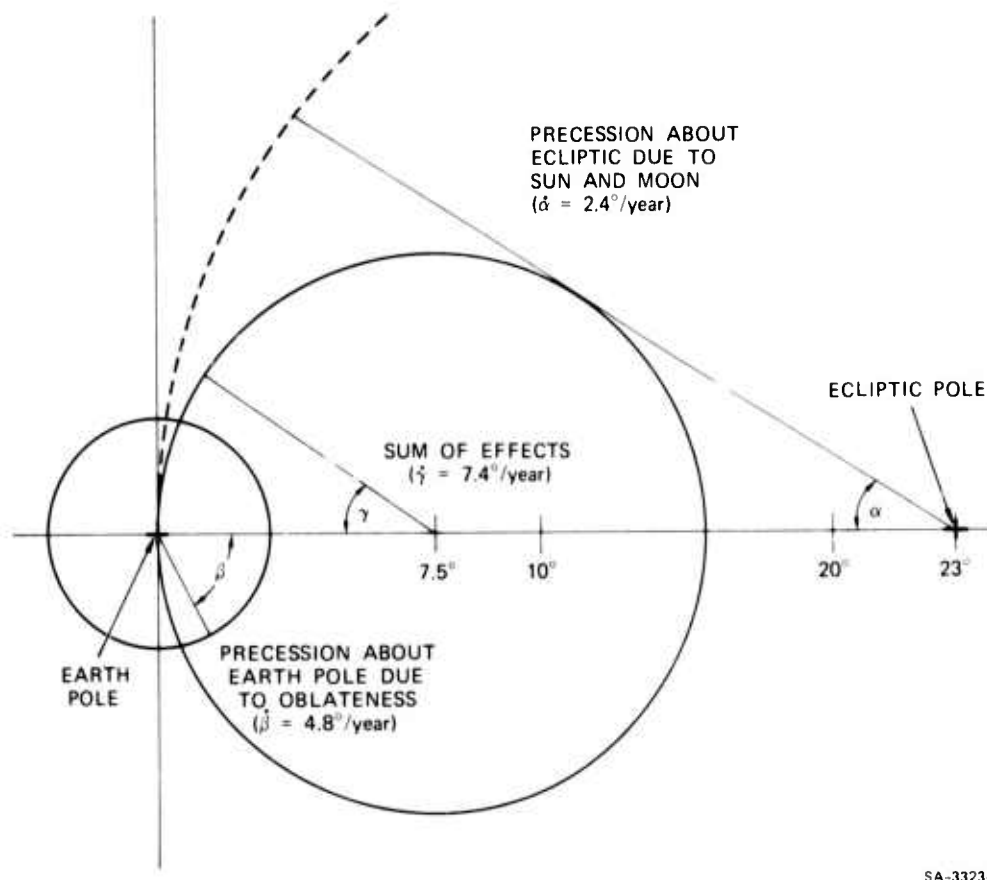
FIGURE I-1   EFFECTS OF THE SUN

precession for a synchronous orbit is about 2.4° per year (see Figure I-2), about two-thirds of which is due to the moon.

Oblateness of the earth contributes a torque that causes the angular-momentum vector to precess about the earth's pole. As soon as the orbit is perturbed from equatorial, oblateness precession occurs. For a synchronous orbit, this precession has a rate of about 4.8° per year (see Figure I-2). The sum of the two precessions results in a motion of the angular-momentum vector. This motion is circular, centered at about 7.5° from the pole of the earth in the direction of the ecliptic pole. The total motion occurs at a rate of 7.4° per year. The time to travel the circle is therefore about fifty years.

From the earth the satellite motion appears as a figure eight. The motion slowly grows from zero, for the equatorial orbit, to a maximum north-south displacement of $\pm15^\circ$ in twenty-five years and then decreases again for the next twenty-five years. In the first year, when the rate of growth is greatest, the displacement is less than $\pm1^\circ$ (0.841° according to Ref. 2).

164

PRECESSION ABOUT
ECLIPTIC DUE TO
SUN AND MOON
($\dot{\alpha}$ = 2.4°/year)

ECLIPTIC POLE

SUM OF EFFECTS
($\dot{\gamma}$ = 7.4°/year)

γ

7.5°   10°   20°   23°

α

β

EARTH
POLE

PRECESSION ABOUT
EARTH POLE DUE
TO OBLATENESS
($\dot{\beta}$ = 4.8°/year)

SA-3323-7

FIGURE I-2   SYNCHRONOUS-ALTITUDE EFFECTS

A few points should be noted:

(1)   The periodic torques and the departure of the moon from the
      ecliptic make the angular-momentum motion irregular and not
      circular as suggested by the average results presented.

(2)   A nearly-steady-state figure eight, as viewed from the earth,
      can be achieved by placing a satellite into an orbit inclined
      7.5° from the equatorial plane in the direction of the
      ecliptic.

(3)   The influence of the sun and the moon is greater with greater
      orbital radius, while the influence of oblateness is less.

(4)   The effects discussed are orbital considerations and have a
      negligible effect on array stability.

165

As a side comment, we note that there are at least two kinds of "solar-stable" orbits. The more common one is an orbit in which the rate of precession about the earth pole due to oblateness is the same as the rate of earth orbit about the sun, so that the orbit always has the same attitude with respect to the sun. The other kind of solar-stable orbit is one in which solar pressure is a dominant effect and gradually rotates the major axis of the orbital ellipse so that its orientation remains constant with respect to the sun.

Appendix J

CHANGE IN ARRAY SHAPE DUE TO NONUNIFORM SOLAR ILLUMINATION

Appendix J

CHANGE IN ARRAY SHAPE DUE TO NONUNIFORM SOLAR ILLUMINATION

We will consider a completely flexible cable with a point force, F, applied at its center and opposed by d'Alembert distributed force, $\mathfrak{J}$, as shown in Figure J-1. Deflection, y, is obtained as a function of the distance, x, from the center of gravity of the cable. The tension in the cable is assumed equal to the value it attains when the cable is in its stable gravity-gradient position. Small-angle approximations will be employed.
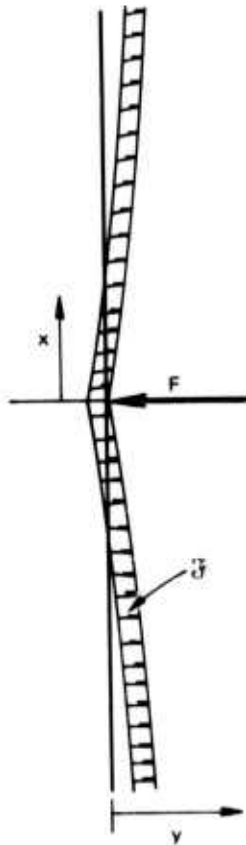
FIGURE J-1   FORCE APPLIED TO CENTER OF ARRAY

The differential tension, dT, in the cable is

$$dT = -3n^2 \sigma x dx \qquad (J-1)$$

where

n = Orbital rate $(2\pi/\text{day})$

σ = Linear density   (0.094 kg/m).

The tension at the ends of the array is determined by the mass, m, of the two identical tip inertias located at $L/_2 x = \pm L/2$ on the cable. Consequently,

$$T = \frac{3}{2} n^2 \left[Lm + \sigma\left(\frac{L^2}{4} - x^2\right) \right] \qquad (J-2a)$$

or

$$T = A^2 - B^2 x^2 \qquad (J-2b)$$

where A and B are constants. The relevant steady state cable equation is

$$\frac{d}{dx} T \frac{dy}{dx} = - \mathfrak{F} \qquad . \qquad (J-3)$$

The boundary condition is arbitrary. At the point of force application,

$$\frac{dy}{dx} = \frac{F\left(\frac{L}{2} + \frac{m}{\sigma} - x\right)}{\left(L + \frac{2m}{\sigma}\right) T} \qquad (J-4)$$

and we note that

$$\mathfrak{F} = \frac{F}{L + \frac{2m}{\sigma}} \qquad . \qquad (J-5)$$

The problem is now completely formulated.

Integration, expansion by partial fractions, and a further integration gives the general result. For a force applied at $x = 0$, the solution is

$$y = \frac{C_1 + \mathfrak{J}\frac{A}{B}}{2AB} \ln\left(1 + \frac{Bx}{A}\right) + \frac{C_1 - \mathfrak{J}\frac{A}{B}}{2AB} \ln\left(1 - \frac{Bx}{A}\right) + C_2 \quad . \qquad (J-6)$$

where we arbitrarily take the integration constant $C_2 = 0$, and find

$$C_1 = F/2 \quad . \qquad\qquad\qquad (J-7)$$

Substituting the following numerical values into Eq. (J-6):

$L = 150$ m

$m = 0.2 \ \sigma L$

$F = Pd^2/4$ (solar pressure force on one bead)

$\quad = 3.5 \times 10^{-10}$ N $\quad$ ($P = 4.5 \times 10^{-6}$ N/m^2, $\quad d = 1$ cm)

we obtain

x(m)	0.0	10	20	40	75
y(m)	0.1	2.129×10^{-4}	4.064×10^{-4}	7.454×10^{-4}	1.215×10^{-3}

The actual force that should be considered in a more rigorour analysis is the difference between the average momentum applied to each bead. This momentum variation can be due to a slightly different bead area and bead emissivity, and a difference in emissivity around each. Differences due to projected areas will be less than 0.1%.

The force calculated in the analysis is for blackbody absorption on the bead. Complete specular reflection gives the same result, neglecting the bead-to-bead effects. If the bead has a black surface facing the sun, and a zero emissivity on the back side, the momentum imparted is greater by 33%. Complete diffuse reflection momentum is greater than the blackbody case by 44%. Hence, the difference from the average will never approach the value used in the calculation.

Solar-pressure distortions are clearly important. Consideration will have to be given to tolerances in size and surface-degradation characteristics during the final design.

ACKNOWLEDGMENTS